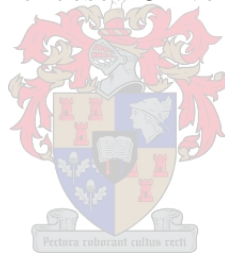


Density Functional Calculation of Simple Molecules

by

Olufemi Opeyemi Olaoye

*Thesis presented in partial fulfilment of the requirements for the degree
of Master of Science in Laser Physics in the Faculty of Science at
Stellenbosch University*



Department of Physics,
University of Stellenbosch,
Private Bag X1, Matieland 7602, South Africa.

Supervisors:

Prof. Heinrich PH Schwoerer

Prof. Erich G Rohwer

March 2012

Declaration

By submitting this thesis electronically, I declare that the entirety of the work contained therein is my own, original work, that I am the sole author thereof (save to the extent explicitly otherwise stated), that reproduction and publication thereof by Stellenbosch University will not infringe any third party rights and that I have not previously in its entirety or in part submitted it for obtaining any qualification.

Date: March, 2012.

Copyright © 2012 Stellenbosch University
All rights reserved.

Contents

Declaration	i
Contents	ii
List of Figures	iv
List of Tables	vi
Abstract	viii
Opsomming	ix
Acknowledgements	x
Dedications	xi
1 Introduction	1
2 Density Functional Theory and Applications	5
2.1 Why Density Functional?	5
2.2 DFT: Origin and Development	6
2.3 Exchange-Correlation Functional vs. Jacob's Ladder	16
2.4 Implementation of the Density Functional Model: Basis Sets vs. Exchange-Correlation Functional	18
2.5 Summary	21
3 Structural Optimisation of Formaldimine and Dithizonatophenylmercury II	23
3.1 Procedure	23
3.2 Geometry Optimisation	24
3.3 Ground State Energy	28
3.4 Summary	31
4 Isomerisation Reactions and Time-dependent Density Functional Calculation	32
4.1 Isomerisation Reactions in our Molecules: A Link to Potential Energy Surface	32
4.2 TD-DFT And UV-VIS Spectroscopy	36

<i>CONTENTS</i>	iii
4.3 Experimental Procedure	39
4.4 Summary	45
5 Structural Optimisation of Electronically-altered Mercury Dithi- zonates	48
5.1 Geometry Optimisation	48
5.2 Energetic Details	51
5.3 Summary	52
6 Absorption Spectra and Potential Energies of Electronically-altered Mercury Dithizonates	53
6.1 Electro-chemistry, Hammett Constants and Absorption Spectra of Substituted DPM Molecules	53
6.2 Broken Symmetry Calculation and Ground State Potential Energy Surface	60
6.3 Summary	66
7 Conclusion and Outlook	68
Appendices	70
A Photochromism and Geometrical Data of Substituted DPMs	71
A.1 Photochromic Effects	71
A.2 Geometrical Data of the Substituted DPM Isomers.	72
B Codes	75
B.1 Geometry Optimisation and Frequency Calculation	75
B.2 Singlet Excitation Calculation	76
B.3 Ground State Potential Energy Calculation	76
C Acronyms and Interchangeable Terms	78
C.1 Acronyms	78
C.2 Interchangeable Terms	78
D Calculated Ground State Potential Energies	80
D.1 Conversion of Units	80
List of References	83

List of Figures

1.1	Structures of (a) Formaldimine and (b) Orange and Blue Isomers of Dithizonatophenylmercury II. {Key: Orange: Hg; Yellow: S; Blue: N; Dark Gray: C; and Light Gray: H.}	3
1.2	Dithizonatophenylmercury (II) Showing Photochromic Effects and Absorption Spectra of the Orange (Reactant) and the Blue (Product) in Dichloromethane.	3
1.3	Schematic Structures of Substituted DPM Isomers. {Key: Orange: Hg; Yellow: S; Blue: N; and Dark Gray: C.}	4
2.1	Hartree-Fock Self Consistent Field Calculation	10
2.2	Jacob's Ladder of Approximate XC-Functionals.	18
2.3	Routes for the Implementation of our Density Functional Model.	18
3.1	Structures of (a) Formaldimine and (b) Orange and Blue Isomers of Dithizonatophenylmercury II. {Key: Orange: Hg; Yellow: S; Blue: N; Dark Gray: C; and Light Gray: H.}	24
3.2	Formaldimine molecule; showing geometrical details (a) L=bond length; θ =bond angle and (b) ϕ =dihedral angle.	25
3.3	Formadimine molecule: showing the atoms' labels	25
3.4	Structures of (a) Orange and (b) Blue Isomers of DPM showing the atoms' labels.	26
3.5	Optimised Structures of (a) Orange and (b) Blue Isomers of DPM.	27
3.6	B3LYP Formaldimine Energy Convergence.	29
3.7	B3LYP Energy Convergences of (a) Orange and (b) Blue Isomers of DPM.	29
4.1	Isomerisation Through (a) Inversion Path (θ), (b) Twisting Path (ϕ) and (c) Twisting (ϕ) and Inversion (θ) Paths in Formaldimine. Figure reprinted from Ref. [17].	33
4.2	Schematic Model of Photo-isomerisation of DPM Molecule.	34
4.3	Cis-Trans Dihedral Twisting Rotation in Formaldimine and DPM.	36
4.4	Ground State (S_0) Potential Energy Surfaces of Formaldimine and DPM.	37
4.5	Singlet-Singlet Excitation Energies of Formaldimine Using (a) PW91/6-31G(d), (b) OLYP/6-31G(d), (c) BLYP/6-31G(d) and (d) B3LYP/6-31G(d). Program: Gaussian 09.	41
4.6	UV-VIS (curves) and Calculated (lines) Absorption Spectra of DPM Isomers.	43

4.7	Steady State Absorption Spectra of DPM (a) Non-polar and Polar Aprotic and (b) Non-polar and Polar Protic Solvents.	45
4.8	Experimental (curves) and Calculated (lines) Electronic Spectra of DPM Orange Isomer in (a) Methanol, (b) Ethanol, (c) Acetone, (d) Acetonitrile, (e) Dimethylsulfoxide and (f) Cyclo-hexane.	46
5.1	Schematic Structures of Substituted DPM Isomers. {Key: Orange: Hg; Yellow: S; Blue: N; and Dark Gray: C.}	48
5.2	Structural Labelling of the Substituted Dithizonatophenylmercury II Isomers. {Key: Orange: Hg; Yellow: S; Blue: N; Gray: C.}	50
6.1	UV-Visible Absorption Spectra of (a) Orange and (b) Blue Isomers of the Para-substituted DPMS in Dichloromethane.	55
6.2	Experimental vs. Solvent (Dichloromethane) Phase TD-DFT Central Wavelengths of (a) Orange and (b) Blue Isomers of the Para-substituted DPM.	56
6.3	UV-Visible Absorption Spectra of (a) Orange and (b) Blue Isomers of the Meta-substituted DPMS in Dichloromethane.	57
6.4	Experimental vs. Solvent (Dichloromethane) Phase TD-DFT Central Wavelengths of (a) Orange and (b) Blue Isomers of the Meta-substituted DPMS.	58
6.5	UV-Visible Absorption Spectra of the (a) Orange and the (b) Blue Isomers of Ortho-substituted DPM in Dichloromethane	59
6.6	Experimental vs. Solvent (Dichloromethane) Phase TD-DFT Central Wavelengths of (a) Orange and (b) Blue Isomers of the Ortho-substituted DPMS.	60
6.7	Relaxed Ground State Potential Energy Surfaces of Para-substituted DPM. Method: G09/B3LYP/CEP-31G.	62
6.8	Relaxed Ground State Potential Energy Surfaces of Meta-substituted DPM. Method: G09/B3LYP/CEP-31G.	63
6.9	The Blue Isomers of o-F-DPM and o-OMe-DPM. {Key: Orange: Hg; Yellow: S; Blue: N; Dark Gray: C; Light Gray: H; Cyan: F; Red: O.}	64
6.10	Relaxed Ground State Potential Energy Surfaces of Ortho-substituted DPM. Method: G09/B3LYP/CEP-31G.	64
6.11	Ground State (S_0) Potential Energy Barrier Plots for the (a) Para-, (b) Meta- and (c) Ortho-Substituted DPMS.	66

List of Tables

3.1	Optimised Structures of Formaldimine. The last two columns were taken from Ref. [46].	26
3.2	Optimised Structures of Dithizonatophenylmercury II.	27
3.3	Bonding Energies of Formaldimine with DZP Basis Set. Software: ADF	30
3.4	Bonding Energies of DPM Isomers with TZP Basis Set. Software: ADF	30
3.5	Lowest Structural Energies of Optimised DPM Blue Isomeric Form in Polar Protic Solvent, Polar Aprotic Solvent and Gas Phase Relative to That of the DPM Orange Isomer. The last column is taken from Ref. [2].	31
4.1	Selected Singlet Excitations of Formaldimine; f is the oscillator strength and λ is the absorption wavelength. Solvent = Dichloromethane (DCM) ($\epsilon = 8.9$), G09 = Gaussian 09.	40
4.2	Selected Singlet Excitations of DPM Orange and Blue Isomers; A is the relative absorbance, f is the oscillator strength and λ is the absorption wavelength. Solvent = Dichloromethane (DCM) ($\epsilon = 8.9$), G09 = Gaussian 09.	42
4.3	Solvent Dependence of the Dithizonatophenylmercury II Orange Isomer Showing Absorption Central Wavelengths.	45
5.1	Ground State Energies of the Electronically-altered Blue Isomers Relative to Those of the Orange Isomers. R = Substituents.	52
6.1	Selected Singlet Excitations of the Para-substituted DPM Isomers. f: oscillator strength, λ : absorption wavelength, A: relative absorbance, Solvent: dichloromethane ($\epsilon = 8.9$), G09: Gaussian 09.	56
6.2	Selected Singlet Excitation Wavelengths of the Meta-substituted DPM Isomers. f: oscillator strength, λ : absorption wavelength, A: relative absorbance, Solvent: dichloromethane ($\epsilon = 8.9$), G09: Gaussian 09.	58
6.3	Selected Singlet Excitation Wavelengths of the Ortho-substituted DPM Isomers. f: oscillator strength, λ : absorption wavelength, A: relative absorbance, Solvent: dichloromethane ($\epsilon = 8.9$), G09: Gaussian 09.	60
6.4	Central Absorption Wavelengths and Hammett Constants [56] of the Electronically-altered DPMS.	61
6.5	Potential Energy Barriers of the Non-substituted and Substituted DPMS. O:Orange and B:Blue.	65
A.1	Colour Changes in our Molecules	71

A.2	Optimised Structures of Para-substituted Dithizonatophenylmercury II Isomers. R = Substituents.	72
A.3	Selected Optimised Structures of Meta-substituted Dithizonatophenylmercury II Isomers. R = Substituents.	73
A.4	Selected Optimised Structures of Ortho-substituted Dithizonatophenylmercury II Isomers. R = Substituents.	74
D.1	Ground State Potential Energies at Different Dihedral Angles for Formaldimine and DPM.	80
D.2	Ground State Relaxed Potential Energies at Different Dihedral Angles for the Para-substituted DPM.	81
D.3	Ground State Relaxed Potential Energies at Different Dihedral Angles for the Meta-substituted DPM.	81
D.4	Ground State Relaxed Potential Energies at Different Dihedral Angles for the Ortho-substituted DPM.	82

Abstract

Density functional theory is a useful computational tool in the understanding of molecular dynamics on potential energy surfaces. Starting with a prototype molecule *formaldimine*, the *photochromic* molecule *dithizonatophenylmercury II* (DPM) and a set of its photochromic derivatives, (involving substitutions of electron donating and electron withdrawing substituents at ortho, meta and para positions of the dithizonato phenyl rings), are studied through *density functional calculation* in comparison with steady state absorption spectra obtained from UV-Visible and femto second spectroscopy experiments. In polar aprotic, polar protic and non-polar solvents these molecules isomerise around C=N double bond chromophore, from *orange* electronic ground states to *blue* electronic ground states upon photo-excitation. We investigate the structural optimisations, the absorption spectra, the solvent dependence and the potential energy surface (PES) of these molecules. The strong (weak) interactions exhibited by the polar protic (aprotic) solvents used are revealed through high (low) absorbance in the secondary bands of these molecules. The absorption spectra of DPM are found to be bathochromic in solvents with high dielectric constants. For the ground state PES calculation we make use of rigid and relaxed methods, and the latter is obtained through broken symmetry calculation. Of all the methods used in calculation, B3LYP/CEP-31G method gives the best approximation to the experimental data. All calculations are done using the two renowned software, Amsterdam Density Functional (ADF) and Gaussian, availing their different density functional methods.

Opsomming

Berekeninge met Density Functional Theory (DFT) is 'n nuttige tegniek om die dinamika van molekules op potensiële energievlakke te verstaan. Beginnende met 'n prototipe molekule formaldehid, wat die kern vorm van die groter fotochromiese molekule dithizonatophenyl kwik (DPM), word die modellering van die molekule meer ingewikkeld tot laasgenoemde bestudeer kan word asook sy fotochromiese afgeleides wat vervanging van elektronryk en elektronarm radikale by orto, meta en para posisies van die phenyl ringe insluit. DFT berekeninge word met spektra van Absorpsiespektroskopie met UV en sigbare lig asook tyd opgeloste spektra, verkry dmv femtosekondespektroskopie, vergelyk. In polêre aprotiese, polêre protiese en nie-polêre oplosmiddels, isomereer die molekule om die C=N dubbelbinding. Daar kan tussen die twee isomere onderskei word deur dat die een in oplossing in sy grondtoestand blou en die ander een oranje voorkom. Die isomerisering is 'n foto-geïnduseerde proses. Die optimering van die molekulêre struktuur, absorpsiespektra, oplosmiddel-afhanklikheid, en potensiële energievlak metings van die molekule word bestudeer. Die sterk/swak wisselwerking wat in polêre protiese/aprotiese oplosmiddels verskyn word geopenbaar deur die hoe/lae absorpsie van die sekondêre bande van die molekules. Daar is gevind dat die absorpsiespektra van DPM bathochromies in oplosmiddels met hoë diëlektriese konstantes is. Vir die potensiële energievlak berekeninge van die grondtoestand word rigiede en ontspanne metodes gebruik waar laasgenoemde met gebroke simmetrie berekeninge verkry word. Van alle metodes wat vir berekeninge gebruik was, gee die B3LYP/CEP-31G metode die beste benadering aan eksperimentele data. Alle berekeninge word gedoen met twee bekende sagteware pakkette; Amsterdam Density Functional (ADF) en Gaussian, wat op twee verskillende DFT metodes gebaseer is.

Acknowledgements

And God said, "Let there be light," and there was light. I give all glory to the Father of light who gives me strength and wisdom to handle this project successfully.

My profound gratitude goes to my supervisor, Professor Heinrich Schwoerer, who is more of a father to me. Thank you for the great challenges you posed from time to time and for the always present constructive corrections throughout my study. I sincerely appreciate the efforts rendered by my co-supervisor, Professor Erich Rohwer, who is also my HOD.

I sincerely appreciate the African Institute for Mathematical Sciences, Stellenbosch University, and the Laser Research Institute, Physics Department for funding my Master's study.

I appreciate the time to time discussions with Dr. Catharine Esterhuysen of the Chemistry Department, Stellenbosch University. A big thank you to a friend and co-worker, Gurthwin Bosman, who rigorously searched and drilled the talents I possess. I appreciate Egmont Rohwer for taking time to translate the abstract to Afrikaans.

I thank Professor Jeanet Conradie, Dr. Karel von Eschwege and the students of the Chemistry Department of the Free State University, Bloemfontein, for the useful discussions we had and the suggestions during the course of my study.

To the Laser Research Institute students and lecturers, I say thank you for allowing me to do research with you.

To my parents, Mr. and Mrs Timothy Kolawole Olaoye, I say a very big thank you for the best legacy you set for me. To my siblings and in-law, I say thank you for the cooperation you gave. Dare Abiola and Funso Areola, you are great friends and treasures to me.

To Pastor Funlola Olojede and Pastor Blessing Oyekanmi, thank you for your continued prayers for the success I now relish.

To a friend and sister, Fadina T. R., thanks a million! Akinlotan M. D., thanks for your advice and friendship. Lamidi E. O. is a wonderful sister to me, I appreciate you. Tomilola, thank you for your love, continued prayers, friendship, and inspirational advice.

Now to Him who is able to do exceedingly greater things, be all glory, honour and adoration!

"...still pressing on to take hold of that for which Christ took hold of me." Philippians 3:12.

Dedications

To the Giver of life...He who lives forever more; and whose glory fills the whole earth!

To my mother; a great labourer who sets an excellent legacy for her seeds.

Chapter 1

Introduction

The quest to probe and understand molecular dynamics in its entirety using time-resolved spectroscopy has been at the heart of the study of *ultra-fast molecular spectroscopy* [1, 2, 5]. At the core of the study of spectroscopy, many interesting properties of molecules are being investigated to understand their behaviour as a result of excitations. Central to these properties is the *energy landscape* – both of the electronic ground states and the electronic photo-excited states. Through these electronic states, the internal and external properties regarding electronic configurations, orbital energies, absorption and/or emission spectra in terms of wavelengths, vibrational frequencies, excitation energies and lots more could be studied, and the treatment of molecular dynamics on potential energy surfaces are often the most employed methods [1, 9, 17].

Every molecule is unique in that each has an associated electromagnetic spectrum which characterizes its absorption regions. In order to explain experimental observations of molecular dynamics on potential energy surfaces, some theories have to be put in place. At the root of these theories are the celebrated Schrödinger wave equations (1925) and the subsequent Dirac equation (1929)¹ which introduced the concept of spin. Their solutions paved ways for exciting new areas of research and instinctively explained experimental observations of these molecular dynamics [6, 7, 22]. The solutions to these equations could be used to describe the spectra of the hydrogen atom; extending to other atoms in the periodic table. Diatomic molecules are usually treated as harmonic oscillators and its potential energies as harmonic or with the additions of correction terms as the non-trivial Morse potential [7, 11].

Solving these equations for a polyatomic molecule, or even for atoms with more than one electron, is not trivial due to the now prominent electron-electron couplings and the electron-nucleus (external potential) interactions in the general Hamiltonian. In addition, the exchange-correlation effects associated with electrons in a polyatomic molecule are somewhat difficult to account for [6, 18, 20, 21].

As a result, the accurate theoretical description of what was observed experimentally for heavy atoms and polyatomic molecules remained a mystery until the 1960s when Hohenberg and Kohn put forward an observation based on the use of *electron density* to obtain the energetic details and other ground state properties of these molecules [18, 20, 25].

¹Dirac equation was introduced to incorporate relativistic effects into Schrödinger equation.

This concept of electron density, as implemented by Walter Kohn² and Sham (1965), serves as a unique quantity describing the potential wells of the core orbitals of these molecules [6, 18, 20, 21]. This seemingly simple observation became a revolutionary idea and it led to the birth of a new field which today is known as **Density Functional Theory (DFT)**.

The photochemical isomerisation processes of organic molecules involving C=C double bonds such as stilbene, olefin and rhodopsin have been extensively investigated [1, 3, 4]. In the same spirit, isomerisation reactions around N=N double bonds (azo groups), for example azobenzene (PhN=NPh), have also been investigated in recent years [5]. Of special interest to this study are the isomerisation reactions around C=N double bonds (an intermediate *chromophore*³ between C=C and N=N double bonds); examples of which are *formaldimine* (H₂C=NH) and *dithizonatophenylmercury (II)* (DPM) (See Figure 1.2). Formaldimine is similar to DPM in that both have carbon-nitrogen double bonds (C=N) in their chromophore and it has been reported that cis-trans isomerisation reactions occur around these bonds [2, 16, 17, 28, 61].

In an on-going experiment in our laboratory we investigate the steady state absorption, femto second transient absorption and the dynamics of the transition states of DPM and some of its electronically altered derivatives⁴: Para substituents: {Fluorine (F), Chlorine (Cl), Methyl (CH₃), Sulphur-Methyl (SCH₃)}; Meta substituents: {Fluorine (F), Methyl (CH₃), Methoxyl (OCH₃), Dimethyl ((CH₃)₂)} and Ortho substituents: {Fluorine (F), Methyl (CH₃), Methoxyl (OCH₃) and Sulphur-Methyl (SCH₃)} (See Figures 1.3).

DPM and its derivatives show interesting photochromic effects⁵, especially in polar protic solvent like dichloromethane (DCM) and a non-polar solvent like cyclohexane, when illuminated by light. These molecules isomerise from *orange* isomers (absorption in the blue spectral range) into *blue* isomers (absorption in the orange spectral range). The initial characterisation of the absorption spectra of DPM isomers by UV-VIS spectroscopy is shown in Figure 1.2.

The major concern of this project shall be on the study of the structural optimisations, vertical excitation energies and the ground state potential energies along the reaction coordinates of all these molecules in the orange and blue isomers. To achieve these, some software were used. We employed the two renown packages: Amsterdam Density Functional (ADF; adf 2010.01 version) [12, 13, 14] {www.scm.com} and Gaussian (G09 version) [15] {www.gaussian.com} software for all our calculations.

We made use of a supercomputer available through the Center for High Performance Computing (CHPC) (www.chpc.sun.ac.za) to access the Gaussian software. Molden package and Gauss View were used to analyse the results obtained from

²Walter Kohn won the 1965 Nobel Prize in Chemistry for his discovery on Density Functional theories and applications.

³Chromophore refers to an atom or a group of atoms in a molecule responsible for the colour changes in molecules.

⁴In dithizonates, electrons could be donated or withdrawn through para-, meta- and ortho-positions of their phenyl rings. Para-, Meta- and Ortho- refer to the positions where hydrogen atoms are substituted in the phenyl rings of these molecules (See Figures 1.3).

⁵The photochromic effects of these molecules generally have orange and blue isomers, except for p-SMe-DPM and o-OMe-DPM which are red in ground states and blue when excited in dichloromethane solution. For uniformity, we would keep to the orange and blue isomers throughout this study.

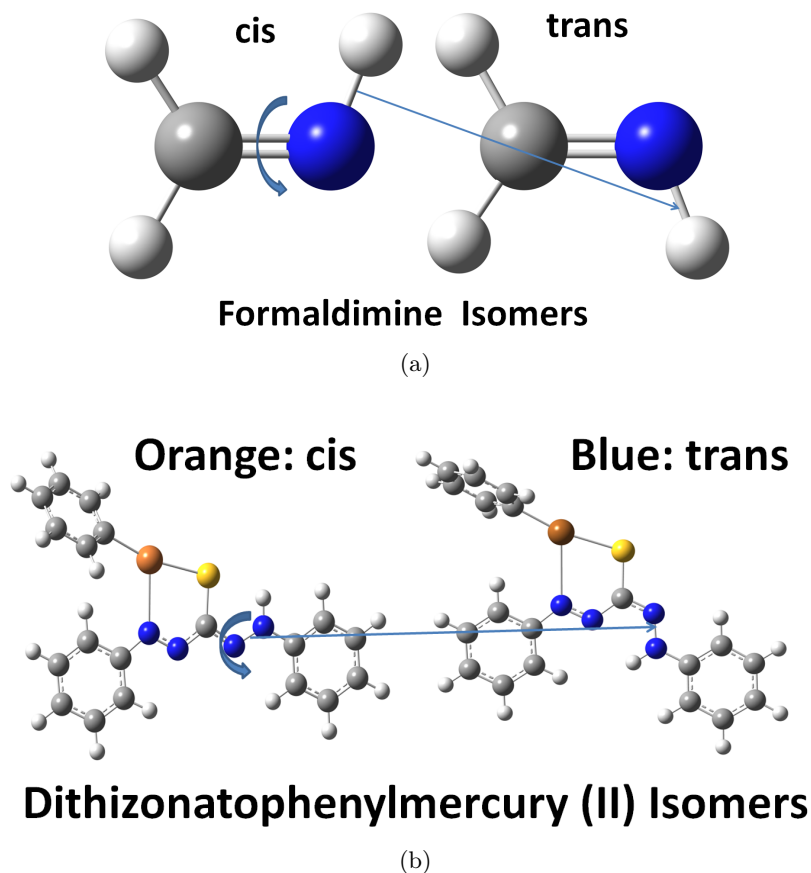


Figure 1.1: Structures of (a) Formaldimine and (b) Orange and Blue Isomers of Dithizonatophenylmercury II. {Key: Orange: Hg; Yellow: S; Blue: N; Dark Gray: C; and Light Gray: H.}

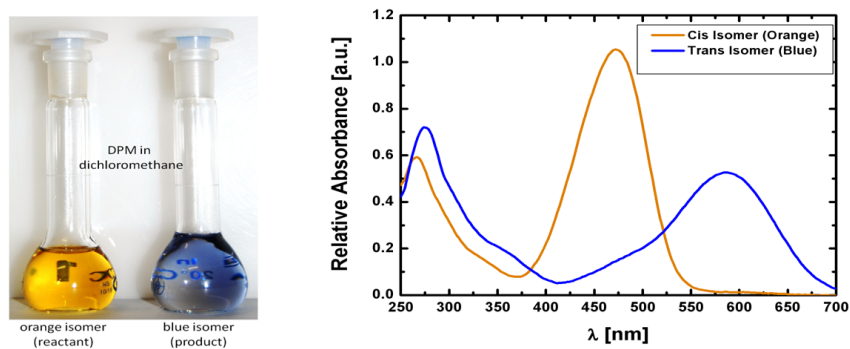


Figure 1.2: Dithizonatophenylmercury (II) Showing Photochromic Effects and Absorption Spectra of the Orange (Reactant) and the Blue (Product) in Dichloromethane.

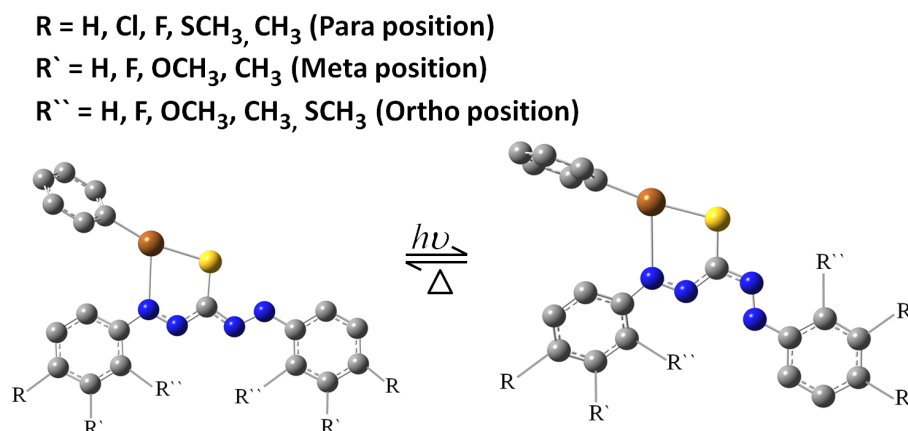


Figure 1.3: Schematic Structures of Substituted DPM Isomers. {Key: Orange: Hg; Yellow: S; Blue: N; and Dark Gray: C.}

Gaussian (09) calculations, and in the conversion of Z-matrix format of our molecular structure to the Cartesian coordinates format and vice-versa. The results obtained are also visualised and interpreted through the Chemcraft package, especially in the comparisons of the optimised geometrical data and visualisation of the orbitals and absorption spectra of our molecules.

The energy conformations of our molecules would be the first milestone and these readily emerged from the *Optimisation* of the molecules. The optimised orientations of the molecules usually give rise to the ground state energy. We will treat the vertical excitation energies (leading to absorption spectrum) of our molecules with time-dependent Density Functional Theory (TD-DFT). Then, the absorption spectra for all the molecules will be compared to their respective steady state measurements we obtained from UV-VIS (Ultraviolet-Visible) spectroscopy. We will also do some studies on solvent dependence of the DPM orange spectra, using polar and non-polar solvents. Finally, we will study isomerisation reactions of the cis-trans configurations of our molecules and these will be related to their corresponding potential energy surfaces.

Chapter 2

Density Functional Theory and Applications

2.1 Why Density Functional?

In this section, we shall develop a motivation for the basis of the Density Functional model. The stage was set in Chapter 1 in relation to the study of molecular dynamics. Going back to the famous Schrödinger wave equations, we can write an approximate, non-relativistic Schrödinger Hamiltonian (electron-nucleus interaction) as [6, 18, 20, 21]:

$$\hat{H}_{e-n} = \hat{T}_n + \hat{V}_{n-n} + \hat{T}_e + \hat{V}_{e-e} + \hat{V}_{e-n}, \quad (2.1)$$

where \hat{V}_{e-n} is the electron-nucleus interaction energy operator (otherwise known as the external potential energy), \hat{V}_{e-e} is the electron-electron interaction energy operator, \hat{V}_{n-n} is the nucleus-nucleus interaction energy operator, \hat{T}_n is the kinetic energy of the nucleus and \hat{T}_e is the kinetic energy of the electron. The pragmatic problem is evident in Equation (2.1) which is a second-order differential equation. The kinetic energy terms are universally known¹ while potential energy terms are not. Even if by providence we know all the terms in Equation (2.1), it is still a non-trivial equation to solve analytically and/or numerically. As a matter of fact, we could have thrown away the useful Equation (2.1) altogether for the inadequate treatments of the potential wells of molecules. The suggestion put forward by Born-Oppenheimer, however, partially solved the problem. This suggestion was based on the difference in the masses of electrons and nucleus: the electronic degree of freedom is far swifter than that of the nucleus [21, 22]. This then gave us the permission to regard the coordinates of the nucleus to be fixed in space and we can write Equation (2.1), according to Born-Oppenheimer Approximation as [6, 18, 20, 21, 22]:

$$\hat{H}_e = \hat{T}_e + \hat{V}_{e-e} + \hat{V}_{e-n} \quad (2.2)$$

where \hat{V}_{n-n} and \hat{T}_n have been set to zero. Equation (2.2) is now the partially decoupled version of Equation (2.1) in that we are only left to solve the Schrödinger

¹Kinetic energy of all systems is known to be unique; all emerging from $K.E. = \frac{p^2}{2m}$, where m is the mass and p is the momentum.

wave equation for electrons. Hereto, our problem would have been solved completely if not for the presence of the last term in Equation (2.2), viz: \hat{V}_{e-n} .

Our first-hand interest is to obtain an accurate energy spectrum of our molecules and from this obtain some desirable properties of the ground state of the molecules. To do this, we would need to know the exact forms of the terms in the RHS of Equation (2.2). Since the external potential energy depends on the system that consists of a molecule we are considering, we have to know the behaviour of the electron-electron and electron-nucleus interactions.

More so, the interaction energy, \hat{V}_{e-e} , contains the Coulomb repulsion energy that is well known and the exchange-correlation energy (XC term) of electrons that is unknown. Early efforts put forward to solve this problem only treated the exchange effect but completely neglected the correlation part. To obtain an accurate expression for this XC term has been throughout the ages a challenging task in the world of Physicists and Chemists alike.

At the turn of the 1960s, a new method was born and this was rooted in the concept of electron density – using electron density to fetch the exact behaviour of the external potential energy. Of a particular interest to Density Functional Theories (DFT) is the presence of the exchange-correlation term and the explicit form of the external potential energy. This external potential energy is usually determined through the positions (coordinates) and charges of all nuclei in a molecule [18, 21]. Up to date, the best treatment of these molecular dynamics are via Density Functional models and this is why we are considering DFT in this project.

2.2 DFT: Origin and Development

The original concept of the Density Functional Theory was put forward by Thomas (1927) and Fermi (1928) [23]. They introduced the concept of electron density, $\rho(\mathbf{r})$, in estimating the kinetic energy and the potential energy of electrons. Herein, it was assumed that the motion of electrons are uncorrelated; emphasizing the possibility of obtaining the kinetic energy and the potential energy through local approximation based on free electrons [23]. This approach could not however describe real systems. According to this electron density concept, the wave function, ψ , is best determined in a probability equation [18, 20, 21, 23]:

$$\rho(\mathbf{r}) = N \int d\mathbf{r}_2 \dots \int d\mathbf{r}_N \psi^*(\mathbf{r}, \mathbf{r}_2 \dots \mathbf{r}_N) \psi(\mathbf{r}, \mathbf{r}_2 \dots \mathbf{r}_N). \quad (2.3)$$

In line with Fermi and Thomas's approach, Dirac suggested that the exchange effects can be catered for, via the exchange energy density in a homogeneous system given by [23]:

$$E_X = -\frac{3}{4} \left(\frac{3}{\pi} \right)^{\frac{1}{3}} \rho^{\frac{1}{3}} = \frac{0.458}{r_s} \text{au}, \quad (2.4)$$

where $r_s = (3/(4\pi\rho))^{\frac{1}{3}}$ is a measure of the average inter-electronic distance. This description is obviously limited to a homogeneous system and the effect of electron correlation and the description of external potential are difficult. The external potential energy does include the influences of the positional external forces such as

electric field and magnetic field forces on atoms or molecules, and other external factors affecting their dynamics [21]. If we know these terms, we could use them in the electronic Hamiltonian and as such, obtain the wave function that describes the eigenstates of our molecules. But this trend cannot be followed and thus, we have to devise another means.

Another fallible attempt would be to determine the wave function directly from factors other than the external potential energy. One of the oldest approaches to solving many electron-Hamiltonian wave functions was put forward by Hartree [24]. According to him, a many-electron wave function can be written as the product of the wave functions of every individual electron present in a molecule [6, 18, 20, 21, 23, 24]:

$$\psi(\mathbf{r}_1, \mathbf{r}_2, \dots, \mathbf{r}_N) = \psi_1(\mathbf{r}_1)\psi_2(\mathbf{r}_2) \dots \psi_N(\mathbf{r}_N). \quad (2.5)$$

This equation in itself holds that each electron responsible for the building of any particular molecule can be isolated and their respective wave functions calculated without having to interfere with one another, and finally, the product of these wave functions would give us the total wave function of the molecule in question. Generally, wave functions are known to represent atomic and/or molecular orbitals. These include both the inner and the outer core shells. Applying the electronic Hamiltonian operator of Equation (2.2) to the many-electron wave function in Equation (2.5), we have

$$\hat{H}_e\psi(\mathbf{r}_1, \mathbf{r}_2, \dots, \mathbf{r}_N) = E\psi(\mathbf{r}_1, \mathbf{r}_2, \dots, \mathbf{r}_N), \quad (2.6)$$

where E is the eigenvalue of the orbital wave functions and it represents the total energy of the electronic ground state. Apart from the hydrogen atom, H, the method of variable separable cannot be applied to solve Equation (2.6) due to the existence of an inter-electronic repulsion term in the electronic Hamiltonian of Equation (2.2) [6, 18]. Electrons are known to be associated with an intrinsic angular momentum, s , and a magnetic quantum number m_s ² so that a complete representation of the many-electron wave function would include the incorporation of the two electron spins along with their coordinates. We can write this as [18, 20, 21]:

$$\hat{H}_e\psi(\mathbf{r}_1\sigma_1, \mathbf{r}_2\sigma_2, \dots, \mathbf{r}_N\sigma_N) = E\psi(\mathbf{r}_1\sigma_1, \mathbf{r}_2\sigma_2, \dots, \mathbf{r}_N\sigma_N) \quad (2.7)$$

where the σ_s represents the compressed form of the electron spins. This obviously complicates the problem at hand and we have to devise a way of writing these orbital wave functions in a manner that they would not violate Pauli exclusion principle. Of course, the dynamics, or loosely stated, the chemical interaction of these orbitals, are greatly affected by electron spins and their symmetries. Electrons are known as fermions and as such, their wave functions exhibit antisymmetry properties, i.e.

$$\psi(\mathbf{r}_1\sigma_1, \mathbf{r}_2\sigma_2, \mathbf{r}_3\sigma_3, \dots, \mathbf{r}_N\sigma_N) = -\psi(\mathbf{r}_1\sigma_1, \mathbf{r}_3\sigma_3, \mathbf{r}_2\sigma_2, \dots, \mathbf{r}_N\sigma_N), \quad (2.8)$$

where the negative sign is introduced to account for interchanging coordinates $\mathbf{r}_2\sigma_2$ and $\mathbf{r}_3\sigma_3$ in the RHS. This property is fully embedded in the Pauli exclusion principle. Slater proposed that this orbital wave function can be fully expressed in a determinant form, respecting the fact that electrons are indistinguishable [18, 21, 26]:

²The electronic spin states are often represented by the Greek labels α and β and given as: $\alpha = |\frac{1}{2} \frac{1}{2}\rangle$ and $\beta = |\frac{1}{2} -\frac{1}{2}\rangle$.

$$\psi_0 \approx \Phi_{SD} = \frac{1}{\sqrt{N!}} \begin{vmatrix} \phi_1(\sigma_1 r_1) & \phi_2(\sigma_1 r_1) & \cdots & \phi_N(\sigma_1 r_1) \\ \phi_1(\sigma_2 r_2) & \phi_2(\sigma_2 r_2) & \cdots & \phi_N(\sigma_2 r_2) \\ \vdots & \ddots & \ddots & \vdots \\ \phi_1(\sigma_N r_N) & \phi_2(\sigma_N r_N) & \cdots & \phi_N(\sigma_N r_N) \end{vmatrix},$$

where the ground state wave function is expanded approximately as Slater orbital wave functions with the incorporation of electron spins and the coefficient, $\frac{1}{\sqrt{N!}}$, compensates for the double counting of electrons. It should be noted here that these Slater orbital wave functions have associated the effects of an exchange term with them [23]. Now that we have been able to represent our orbital wave function as the determinant of Slater orbitals, the next question is: "What is the exact representation or expression of these Slater orbitals?" Even if we can easily diagonalize the determinant, we would need to know the final expression of the wave functions in explicit form. This leads us to the formulation given by Hartree and Fock.

2.2.1 Hartree-Fock Proposition

To obtain the Slater orbitals, Hartree and Fock proposed an approximate orbital wave function. This theory is a rigorous calculation and it was believed to be the best approximate method to estimate the ground state wave function [26]. With reference to Equation (2.5), the ground state wave function can be written in terms of the spherical harmonics, $Y_{lm}(\theta_i, \phi_i)$, as given in [6]:

$$\varphi_i(\mathbf{r}_i) = \varphi_i(r, \theta, \phi) = Y_{lm}(\theta_i, \phi_i)g(r_i), \quad (2.9)$$

where $g(r_i)$ is some sort of basis function that will be fully analysed later in this chapter. If we are able to isolate these wave functions and solve each separately, the interactions among the electrons cannot be neglected and this is where the exchange-correlation functional comes in. The first electron isolated would still be affected by other electrons in our system of molecules. Thus, each electronic wave function has associated with it an effective Hamiltonian which would be an average of the other electrons' Hamiltonians. This is given in [6, 18, 20, 21] as:

$$\hat{h}_1^{eff} = \frac{-\nabla_1^2}{2} - \frac{Z}{r_1} + \sum_{j \neq 1} \int \frac{|\varphi_j(r_j)|^2}{r_{j1}} d\tau_j, \quad (2.10)$$

where \hat{h}_1^{eff} gives us the one-electron Hamiltonian; on the right hand side, the first and second terms represent the kinetic energy and the potential energy of the first electron, and the third term is the Coulomb attraction induced by the presence of the other electrons. Moreover, the third term introduces the concept of charge density which is simply the distribution of electronic charges over a region of space and this is given as the product of the electronic charge and its corresponding spatial wave function. In particular, an electronic charge density is a key factor in describing wave functions in Density Functional Theory. This charge density is often expressed as [6, 18, 21]:

$$\begin{aligned} \rho(\mathbf{r}_j) &= e|\varphi_j(\mathbf{r}_j)|^2 \\ &= |\varphi_j(\mathbf{r}_j)|^2 \end{aligned} \quad (2.11)$$

where the electronic charge, e , has been set to 1 (in atomic units. Atomic units are used throughout in this work). Inserting Equation (2.11) into (2.10), we have

$$\hat{h}_1^{eff} = \frac{-\nabla_1^2}{2} - \frac{Z}{r_1} + \sum_{j \neq 1} \int \frac{\rho(r_j)}{r_{j1}} d\tau_j. \quad (2.12)$$

The last term on the right hand side (RHS) can be expressed in terms of the coulomb operator, J_j , as [6]:

$$J_j(1) = \int \frac{\rho(r_j)}{r_{j1}} d\tau_j. \quad (2.13)$$

Equation (2.13) shows that the average Coulomb repulsion, which should include the exchange-correlation functional, is related to the charge density of the electrons in the system of our molecules. Now, to obtain the electronic wave function for the first electron, we apply the Hamiltonian of Equation (2.10) to its corresponding spatial orbital in the form:

$$\hat{h}_1^{eff}(r_1)\varphi_1(r_1) = \varepsilon_1\varphi_1(r_1). \quad (2.14)$$

This looks like a benchmark success. However, according to the effective Hamiltonian analysed in Equation (2.10), we will need to know every other spatial orbitals explicitly in order to solve Equation (2.14) for the first electron. We may well decide to write for each and every electrons their corresponding Equation (2.14). This requires an iteration solution since any electron we choose is affected by every other electron [6, 18, 21].

For this iteration, an ansatz for the expressions of the wave functions, φ_i , other than the first electrons are taken and plugged into Equation (2.14) and this is repeated in a cycle format, each stage being marked with a tolerance (error), until the energy of a molecule converges. This is known as a self consistent field (SCF) approximation and it constitutes the Hartree theory. This SCF represents the total energy in density functional calculation. The total energy for the Hartree-Fock formulation is given by [6]:

$$E_{total} = 2 \sum_{i=1}^N \varepsilon_i - \sum_{i,j=1}^N (2J_{ij} - K_{ij}), \quad (2.15)$$

where K_{ij} is called the exchange energy operator, as defined in [6]. We noticed in this last equation that the exchange energy is subtracted from the Coulomb repulsion energy and the remaining part is in turn subtracted from the eigenvalues, ε_i . This tells us an important truth of the true minimum energy of any molecule. The energy sum includes some errors and these are what we categorize as electron-correlation energy. In a situation whereby there are many electrons in a molecule, this exchange energy tends to be double-counted since electrons are indistinguishable. As a result, there is a correction term ($2J_{ij} - K_{ij}$) to the total energy of the system.

The Hartree-Fock equation given in Equation (2.15) form matrices and these are used to obtain an ansatz for the spatial orbitals to be used in the Slater determinant. The flowchart diagram of the SCF calculation is given in Figure 2.1.

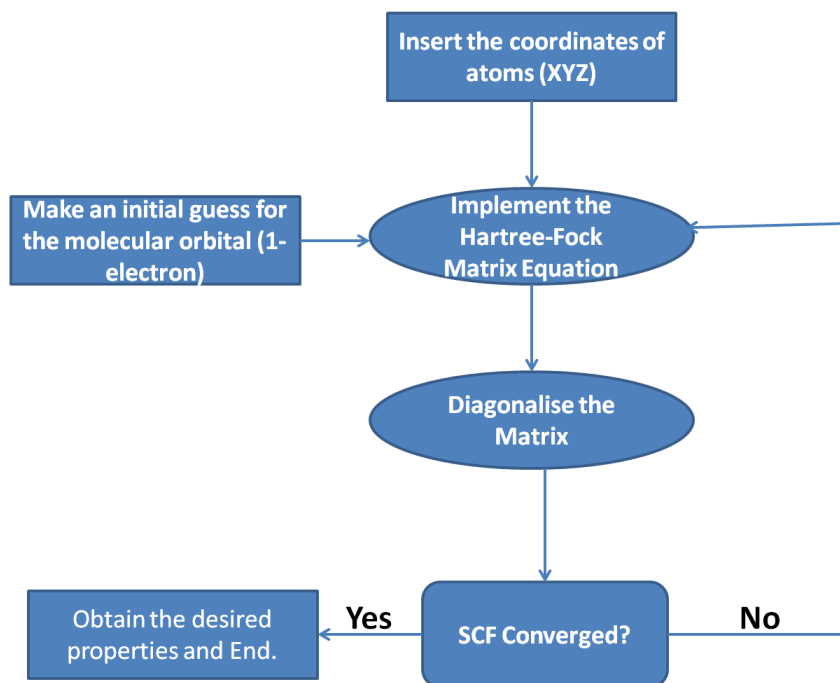


Figure 2.1: Hartree-Fock Self Consistent Field Calculation

2.2.2 Just Before DFT

The Hartree-Fock formulation just described neglects electron-correlation effects. This correlation energy involves two forms, viz: dynamical and non-dynamical electron correlations [18]. The dynamical part is proportional to the repulsion energy between two electrons while the non-dynamical is connected to the fact that the Slater determinant does not produce a true minimum energy. Electron correlation energy is often expressed as [6, 18, 21]:

$$E_{\text{correlation}} = E_{\text{minimum}} - E_{\text{H-F}}. \quad (2.16)$$

One of the efforts put forward to calculate the correlation energy was based on the Moller-Plesset (MP) time-independent perturbation theory, which involves orders of expansion depending on the number of electrons to be excited [6, 18, 21]. The common orders associated with the Moller-Plesset method are MP2 (order two, involving the excitation of two electrons) and MP4 (order 4, involving the excitation of four electrons). Expectedly, MP4 requires a greater deal of computational effort but it gives better results than MP2. In performing this calculation, the perturbation Hamiltonian is the difference between the minimum (or exact) and the Hartree-Fock Hamiltonians. However, this effort does not lead to a satisfactory energy minimum; though it is better than the results obtained from Hartree-Fock.

Then came the configuration interaction (CI), which assumes that the wave function can be written as a sum of many Slater determinants,

$$\psi = \sum_i c_i D_i, \quad (2.17)$$

where c_i are the coefficients determined via variational optimisation and D_i represent the Slater determinants [6]. The famous means of calculating eigenfunctions and their corresponding eigenvalues involves diagonalising a matrix equation of the form

$$|\mathbf{H} - E\mathbf{S}| = 0$$

where \mathbf{H} represents the Hamiltonian matrix, E is the eigenvalue and \mathbf{S} , the identity matrix [6]. To diagonalize this matrix requires a great deal of effort and its applications are limited to molecules with a few number of electrons. Moreover, they do not ultimately give rise to an exact energy. Other methods which we will not develop here include Multi-configuration SCF (MCSCF), MCSCF-CI and the Coupled-Cluster (CC) methods.

All these preliminaries make it easier for us to understand the concept of Density Functional Theory.

2.2.3 Electron Density Concept by Hohenberg and Kohn

Concerning the explicit expression of Equation (2.2),

$$\hat{H}_e = \hat{T}_e + \hat{V}_{e-e} + \hat{V}_{e-n},$$

a landmark success was recorded at the turn of the 1960's when Hohenberg and Kohn proposed and proved two important theorems based on using the concept of electron density to fetch the wave functions of the electrons in a system under study [25]. This was in line with the proposition that Thomas and Fermi made earlier. Hohenberg-Kohn's theories formed the foundation of what is today known as *density functional theory*. Density functional refers to any operator or quantity which is a function of the electron density.

Hohenberg and Kohn in their 1964 paper titled: "Inhomogeneous Electron Gas", define the terms on the RHS of Equation (2.2) as follow [25]:

$$\hat{T} \equiv \frac{1}{2} \int \nabla\varphi^*(r)\nabla\varphi(r)dr; \quad (2.18)$$

$$\hat{V}_{e-e} \equiv \frac{1}{2} \int \frac{1}{|r-r'|} \varphi^*(r)\varphi^*(r')\varphi(r')\varphi(r)drdr' \quad \text{and}, \quad (2.19)$$

$$\hat{V}_{e-n} \equiv \int v(r)\varphi^*(r)\varphi(r)dr. \quad (2.20)$$

In Equation (2.11), we defined the electron density as the square of the spatial orbital. A careful observation into Equations (2.20) and (2.19) readily reveals that these energies are functionals of the electron density which in terms of the wave function can be expressed as [6, 18, 20, 21, 25]:

$$\rho(\mathbf{r}) = \int \varphi^*(\mathbf{r})\varphi(\mathbf{r})dr. \quad (2.21)$$

We already see now that the interaction energy, \hat{V}_{e-e} and the external potential, \hat{V}_{ext} , are functionals of the electron density. As we know, we do not have problem in

expressing the Coulomb repulsion energy explicitly; what would be of interest to us is to know the exact representation of the external potential and the expressions for the exchange-correlation functional.

Hohenberg and Kohn showed that electron density uniquely determines the external potential energy [25]. This is best shown through their existence theorem which was developed in [25]. Their first theorem assumes a non-degenerate state [25]. They stated that no two external potentials can deliver a single electron density. Moreover, an accurate expression of the external potential gives rise to an accurate Hamiltonian. Thus, the many-electron Hamiltonian is also a functional of the electron density. The universal functions; the kinetic and the inter-electronic potential energies, are often expressed as the Hohenberg-Kohn functional given as [25]:

$$F_{HK}[\rho(\mathbf{r})] = T_e[\rho(\mathbf{r})] + V_{e-e}[\rho(\mathbf{r})] \quad (2.22)$$

so that the total energy becomes,

$$E[\rho(\mathbf{r})] = V_{e-n}[\rho(\mathbf{r})] + F_{HK}[\rho(\mathbf{r})]. \quad (2.23)$$

Another fascinating property of the ground state electron density is that it integrates to the total number of electrons, N , in a given system of molecules and it is often written as [18, 20, 21, 25]:

$$\int \rho(\mathbf{r}) d\mathbf{r} = N. \quad (2.24)$$

Expectedly, N is also a functional of the electron density. So, a correct ground state electron density leads to an accurate expression of the external potential which in turn yields the correct ground state wave function. From this, we could obtain the true energy minimum and all other properties we might want. Schematically, we can represent this trend as follows [21, 18, 20]:

$$\rho_o \rightarrow \{N, Z, R\} \rightarrow \hat{V}_{ext} \rightarrow \hat{H} \rightarrow \psi_o \rightarrow E_o \quad \{\text{and all other properties}\}.$$

Now that we have fixed the problem with the external potential, we are left with the exact description of the interaction energy, \hat{V}_{e-e} . The Hohenberg-Kohn functional can be expanded further as [18, 21, 25]:

$$F_{HK}[\rho(\mathbf{r})] = T_e[\rho(\mathbf{r})] + \frac{1}{2} \int \frac{\rho(\mathbf{r}')\rho(\mathbf{r})}{|\mathbf{r} - \mathbf{r}'|} d\mathbf{r}d\mathbf{r}' + \epsilon[\rho(\mathbf{r})]. \quad (2.25)$$

Here, $\epsilon[\rho(\mathbf{r})]$, which represents a non-classical energy contribution due to the self interaction of electrons, Coulomb correlation and the exchange effect, is a functional similar to $F_{HK}[\rho(\mathbf{r})]$. A particular interest in this third term is the inclusion of the exchange-correlation functional effect. The second term on the RHS represents the explicit form of Classical Coulomb energy. What we need now would then be a way of expressing the kinetic energy, $T_e[\rho(\mathbf{r})]$ and the non-classical contribution energy, $\epsilon[\rho(\mathbf{r})]$. This is a major challenge in Density Functional Theory. The key problem to this is: "How do we know the true ground state density that will deliver the true energy minimum?" This question is taken care of by the second theorem by Hohenberg and Kohn and it states that *the functional that delivers the true energy*

minimum delivers the lowest energy if, and only if, it is fed by the true ground state density [18, 21, 25]. This is based on the variational principle and it reads as [18]:

$$E_{min} \leq E[\rho'] = T_e[\rho'] + V_{ee}[\rho'] + V_{ext}[\rho']; \quad (2.26)$$

where ρ' is a trial electron density. It should be noted that while the first theorem only applies to non-degenerate systems, the second theorem generalizes Hohenberg-Kohn propositions to degenerate systems [18, 20, 25]. The conditions imposed for the search of the true ground state density are clearly seen in the expression,

$$\rho'(\mathbf{r}) \geq 0 \quad \text{and} \quad \int \rho'(\mathbf{r}) d\mathbf{r} = N.$$

Inasmuch as a particular density associates itself with a unique Hamiltonian and wave function, we tend to return to our formal approach to solving a twisted problem: iteration. The electron density is somewhat associated with the external potential as we saw it in the first theorem by Hohenberg and Kohn [25].

In fact, the search for the true ground state electron density often displays two modes of representable, viz: N -representable and V_{e-n} -representable [18, 20, 21, 25]. This is to make sure that we have the true external potential and the true energy minimum. Unfortunately, the search for an electron density that is V_{e-n} -representable still remains a mystery and as such, a weaker N -representable is commonly used [18]. In effect, this search affords two series of iterations as introduced by Lévy (1979), a phenomenon often known as the *Lévy constrained-search*. This is also based on minimisation and we can write the expression as [18, 20]:

$$E_{min} = \min_{\rho \rightarrow N} \left[\min_{\psi \rightarrow \rho} \langle \psi | \hat{T}_e + \hat{V}_{e-e} + \hat{V}_{e-n} | \psi \rangle \right], \quad (2.27)$$

where the outer minimisation is mapped over N -electron antisymmetric wave functions and the inner minimisation mapped over all the available densities, out of which only one delivers the true ground state wave function. Since the external potential depends only on the electron density, we can rewrite Equation (2.27), after a slight rearrangement, as:

$$E_{min} = \min_{\rho \rightarrow N} \left[F[\rho] + \int \rho(\mathbf{r}) V_{e-n} d\mathbf{r} \right];$$

where,

$$F[\rho] = \min_{\psi \rightarrow \rho} \langle \psi | \hat{T}_e + \hat{V}_{e-e} | \psi \rangle.$$

The last two equations combined tells us that a given density delivers a corresponding energy which upon minimisation leads us to the ground state energy and ground state density.

The key question now is: "How do we map over N -electron antisymmetric wave functions to search for the true ground state wave function?" If indeed we know how to identify exactly the ground state wave function out of all the available ones, we could use it to obtain all the information we need. The truth is [18],

there is no exact wave function in Density Functional Theory.

Do we then conclude that Hohenberg-Kohn's proposition is useless, after all? No. This leads us to Kohn-Sham's proposition.

2.2.4 Kohn-Sham Non-interacting Particle Scheme

The following year, after Hohenberg-Kohn's paper was published [25] in 1964, Kohn and Sham set forth to put Hohenberg-Kohn theories into practical applications [27]. We made mention earlier that most formulations of many-electron wave function problems arise from Hartree-Fock proposition. The Kohn-Sham formulation also takes the same form and this is what we shall look at in this section.

Our main problem lies in the expression for electronic wave function, and Hartree-Fock proposed that this can be expanded as Slater orbitals; a method that allows us to "isolate" each electron, find their wave function and take the total wave function as the product of these orbitals. In Hohenberg-Kohn's paper [25], the wave function was taken to be a functional of the electron density such that the associated total energy of the system is expressed as [18]:

$$\begin{aligned} E[\rho(\mathbf{r})] &= T[\rho(\mathbf{r})] + V_{e-e}[\rho(\mathbf{r})] + V_{ext}[\rho(\mathbf{r})] \\ &= T[\rho(\mathbf{r})] + J[\rho(\mathbf{r})] + V_{ncl}[\rho(\mathbf{r})] + V_{ext}[\rho(\mathbf{r})], \end{aligned} \quad (2.28)$$

where the interacting potential, V_{e-e} , is split into the classical and non-classical energies, J and V_{ncl} , respectively. Of these, only the Coulomb repulsion, J , is known. The Kohn-Sham formulation first assumed that a non-interacting reference system, in which electrons are isolated, could be mapped onto a real interacting reference system [18, 20, 27]. An exact expression for the kinetic energy of non-interacting fermions (electrons) as implemented by Hartree and Fock can be written here as:

$$T_{HF} = -\frac{1}{2} \sum_i^N \langle \phi_i | \nabla^2 | \phi_i \rangle$$

where ϕ_i are orthonormal spin orbitals [6, 18, 20]. Moreover, a Hamiltonian representing a non-interacting reference system has an associated local external potential and this often leads to an expression devoid of any electron-electron interaction,

$$\hat{H}_{local} = -\frac{1}{2} \sum_i^N \nabla_i^2 + \sum_i^N \hat{V}_{local}(\mathbf{r}_i).$$

In a complete analogy of what we did for the Hartree-Fock model, this also involves expanding the wave function as the determinant of spin orbitals, which in this regard refers to Kohn-Sham orbitals,

$$\psi_0 \approx \Phi_{local} = \frac{1}{\sqrt{N!}} \begin{vmatrix} \varphi_1(\sigma_1 r_1) & \varphi_2(\sigma_1 r_1) & \cdots & \varphi_N(\sigma_1 r_1) \\ \varphi_1(\sigma_2 r_2) & \varphi_2(\sigma_2 r_2) & \cdots & \varphi_N(\sigma_2 r_2) \\ \vdots & \ddots & \ddots & \vdots \\ \vdots & \ddots & \ddots & \vdots \\ \varphi_1(\sigma_N r_N) & \varphi_2(\sigma_N r_N) & \cdots & \varphi_N(\sigma_N r_N) \end{vmatrix},$$

with an associated eigenvalue equation,

$$\hat{f}^{KS} \varphi_i = \varepsilon_i \varphi_i, \quad (2.29)$$

and the Kohn-Sham operator \hat{f}^{KS} given by

$$\hat{f}^{\text{KS}} = -\frac{1}{2}\nabla^2 + \hat{V}_{\text{local}}(\mathbf{r}).$$

The associated local kinetic energy of the non-interacting reference system, in analogy to what was obtained in the Hartree-Fock model (see Equation for T_{HF} above), can be written as:

$$T_{\text{local}} = -\frac{1}{2} \sum_i^N \left\langle \varphi_i \left| \nabla^2 \right| \varphi_i \right\rangle, \quad (2.30)$$

where $T_{\text{local}} \leq T_e$. If we ask for less than an exact energy, we can write the total local energy of the system (non-interacting) as [18]:

$$E_{\text{local}} = T_{\text{local}} + V_{\text{local}}.$$

Mapping the energy of this non-interacting system onto the real interacting system offers a residual energy³ and this is often introduced through the expression,

$$E_{XC} = (T_e[\rho(\mathbf{r})] - T_{\text{local}}[\rho(\mathbf{r})]) + (V_{e-e}[\rho(\mathbf{r})] - J[\rho(\mathbf{r})]), \quad (2.31)$$

so that the total energy of the system of our molecules is given by,

$$E[\rho(\mathbf{r})] = T_{\text{local}}[\rho(\mathbf{r})] + J[\rho(\mathbf{r})] + V_{\text{ext}}[\rho(\mathbf{r})] + E_{XC}[\rho(\mathbf{r})]. \quad (2.32)$$

E_{XC} is known as the exchange-correlation energy and it is the dumping site for all the unknowns. Before we go on to analyse this exchange-correlation energy, let us write the total energy of Equation (2.32) as each term appears [18, 20]:

$$E[\rho(\mathbf{r})] = -\frac{1}{2} \sum_i^N \left\langle \varphi_i \left| \nabla^2 \right| \varphi_i \right\rangle + \frac{1}{2} \int \frac{\rho(\mathbf{r}')\rho(\mathbf{r})}{|\mathbf{r} - \mathbf{r}'|} d\mathbf{r}d\mathbf{r}' + \int \frac{\rho(\mathbf{r})}{\mathbf{r}} d\mathbf{r} + E_{XC}[\rho(\mathbf{r})]. \quad (2.33)$$

We are getting close to the main expression for the total energy of molecules. The only unknown now is the exchange-correlation energy. Just as we performed iterations, (through a variational principle), in the Hartree-Fock model to determine the Slater orbitals, we use the same approach here to determine the Kohn-Sham orbitals, φ_i . In fact, the actual Kohn-Sham orbitals are usually described as *basis sets* (to be discussed in Section 2.4). The potential energy associated with the exchange-correlation functional is obtained via,

$$V_{XC} = \frac{\delta E_{XC}}{\delta \rho}.$$

The implementation of Equation (2.33) is a tricky process in density functional calculation. In the next two sections, we shall demonstrate how this is tackled in our model, starting with the last term – exchange-correlation energy.

³Residual energy in this context includes contributions from the kinetic and the inter-electronic repulsion energies.

2.3 Exchange-Correlation Functional vs. Jacob's Ladder

After Kohn-Sham's contributions, some efforts have been put forward to express the XC term explicitly. It should be noted that no exact approach is known and all the following will be approximations of the true expression of the XC term. More so, there are a large number of functionals today; we shall pay more attention to the ones peculiar to this work.

Exchange-correlation energy is a functional of electron density and as a result, depends on its behaviour across the shells and/or orbitals of an atom or molecule. Kohn and Sham specifically pointed out that the XC term for a slowly varying electron density⁴ could be expressed as [27]:

$$E_{XC}[\rho] = \int \rho(\mathbf{r})\epsilon_{xc}(\rho(\mathbf{r}))d\mathbf{r}, \quad (2.34)$$

where ϵ_{xc} is the exchange-correlation energy per electron in a system of uniform electron gas. This equation was introduced and treated as the first and foremost approximation of the XC energy, and it is famously referred to as the *local density approximation* (LDA) (spin-restricted) [20]. It is called LDA because it makes use of a local density, as clearly seen in the integral of Equation (2.34). A slowly varying or a constant electron density satisfies the Dirac's exchange energy of Equation (2.4) for homogeneous systems, and we can write [23, 25],

$$\begin{aligned} E_{XC}[\rho] &= E_X[\rho] + E_C[\rho] \\ &= -\frac{3}{4} \left(\frac{3}{\pi} \right)^{\frac{1}{3}} \rho^{\frac{1}{3}} + E_C[\rho]. \end{aligned} \quad (2.35)$$

Much of the problem with the XC term lies within the expression for the correlation energy. Of course, there are also errors associated with Dirac's exchange energy for it can only account for a homogeneous system. Most heavy atoms and molecules are inhomogeneous and, as such, are associated with high density near the regions of the nucleus (especially for atoms) [27]. The Kohn-Sham approximation caters for regions with low and high density but could not account for the region associated with the surface of atoms and the overlapping regions in molecules. They proposed that this is where the major error in the XC term comes from [27].

Local density approximation takes on Dirac's exchange energy popularly known as Slater's exchange (S) and its mostly used correlation energy are the works of Vosko, Wilk and Nusair (VWN)(1980), so that in DFT notations what we see is the acronym, "SVWN" [18]. A more accurate LDA functional was presented by Perdew and Wang (1992) (PW92) [18]. Local density approximation generally results in an underestimation of the minimum energy and this in turn affects other properties of interest.

Then came the unrestricted *local spin density approximation* (LSDA) for which Equation (2.34) simply includes the effect of spin density [20, 18, 21],

$$E_{XC}^{LSDA}[\rho_\alpha, \rho_\beta] = \int \rho(\mathbf{r})\epsilon_{xc}(\rho_\alpha(\mathbf{r}), \rho_\beta(\mathbf{r}))d\mathbf{r} \quad (2.36)$$

⁴The electron density could either be a slowly varying or a high density. If it is slowly varying around a region, we could assume that it is constant near that region [27].

with

$$\rho(\mathbf{r}) = \rho_\alpha(\mathbf{r}) + \rho_\beta(\mathbf{r}), \quad (2.37)$$

where α and β represent spin up and spin down, respectively. LSDA also does not fare better in the prediction of minimum energy [18, 20, 21].

An improvement came with the notion of using the gradient of the electron density instead of simply the electron density. This often takes the form of expressing the total energy as the functional of the gradient of the electron density. This is known as a *generalized gradient approximation* (GGA). Many functionals, more than we can mention and analyse here, have been proposed for GGA from different authors over the years. In this piece of work, we used ⁵

1. Perdew and Wang 91 (both exchange and correlation functional) (PW91);
2. Becke (exchange functional) and Lee, Yang and Parr (correlation functional) (BLYP) and;
3. Handy's OPTX modification of Becke's exchange functional and Lee, Yang and Parr correlation functional (OLYP).

GGA tends to overestimate the minimum energy. The introduction of *hybrid functional* gives more accuracy to the prediction of the minimum energy in that it balances the exchange and correlation functional used. This is achieved through the mixture of the Hartree-Fock exchange and the Becke exchange functional (Becke 3 parameter). We only used B3LYP in this work and this requires a non-local correlation functional from LYP (Lee, Yang and Parr) and a local correlation from VWN. The LYP functional generally provides local and non-local correlation functionals. To satisfy the requirement of B3LYP, the local exchange energy expression in the LYP correlation is subtracted from the Hartree-Fock exchange energy so that the expression for B3LYP is often given as ⁶

$$E_{XC}^{hybrid} = A * E_X^{Slater} + (1 - A) * E_X^{HF} + B * \Delta E_X^{Becke} + E_C^{VWN} + C * \Delta E_C^{non-local}.$$

Other functionals associated with this equation are B3P86 and B3PW91 in the same format as B3LYP. Exchange-correlation functionals can also take the form of meta-GGA (square of the gradient of the electron density), kinetic energy functional (hyper-GGA) and random phase approximation (RPA) [18, 21, 23]. The order of increasing accuracy is often explained through Jacob's ladder [21, 23] (See Fig.2.2). The general expression for the exchange-correlation functional for the first five rungs of Jacob's ladder can be written as [18, 20, 21]⁷:

$$E_{XC}[\rho_\alpha, \rho_\beta] = \int f(\rho_\alpha, \rho_\beta, \nabla\rho_\alpha, \nabla\rho_\beta, \nabla^2\rho_\alpha, \nabla^2\rho_\beta, \tau_\alpha, \tau_\beta, \varepsilon_\alpha, \varepsilon_\beta) d^3r. \quad (2.38)$$

⁵The description of these functional was taken from the Gaussian 03 manual.

⁶The description of these functional was taken from the Gaussian 03 manual.

⁷In this integral, a single approximation can only be used at a time; by simply dropping other approximations in the function f .

RPA unoccupied Ψ_i
Hyper-Meta-GGA \mathcal{E}_x
Meta-GGA $\tau / \nabla^2 \rho(r)$
GGA $\nabla \rho(r)$
LDA $\rho(r)$

Figure 2.2: Jacob's Ladder of Approximate XC-Functionals.

2.4 Implementation of the Density Functional Model: Basis Sets vs. Exchange-Correlation Functional

The model we shall present here does not exhaust what DFT could do; we are only interested in the calculations of some dynamical properties. The routes of our calculations are shown in Figure 2.3. As shown, the *ground state energy* is often

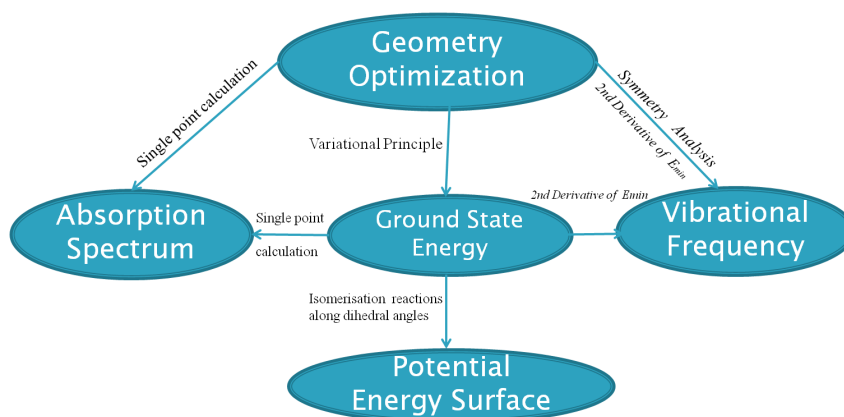


Figure 2.3: Routes for the Implementation of our Density Functional Model.

the central point of every quantum mechanical calculation. The general solutions to the Schrödinger wave equations are usually in terms of the eigenvalues (energies) through which all properties of interest could be calculated. The DFT model is also based on this ground state energy. In the expression of the electron density (see Equation (2.21)), we see that it depends on the *Cartesian coordinates*,⁸ $\mathbf{r}(x, y, z)$, of each of the atoms in the systems of molecules we are considering. The starting

⁸Cartesian coordinates are mostly used as inputs of the initial and the final positions (or orientations) of each atom in molecules in DFT calculations. Alternatively, Z-matrix format could also be used.

point, as shown in Figure 2.3, of these calculations is the geometry optimisation. Geometry optimisation depends on the atomic coordinates, often represented as Cartesian coordinates or in Z-matrix format. The optimised structures distinctly give rise to the minimum energy and all other properties of interest.

Kohn-Sham orbitals are directly connected to the *local kinetic energy* of the system of our molecules; other terms in the Hamiltonian depend solely on the electron density (See Equations (2.30) & (2.33)). In addition, the electron density depends on these orbitals, as it was defined in Equation (2.21). The expression of the kinetic energy is a second order differential operator. Most computer algorithms and/or codes usually require linear equations and as such, we need to expand our Kohn-Sham orbitals in a linear form. Thus, the Kohn-Sham (KS) orbitals, φ_i , in the expression of the kinetic energy are circumvented through the introduction of *basis sets* which are defined as the linear combination of atomic orbitals (LCAO) [6, 18, 20, 38, 40],

$$\varphi_i = \sum_{k=1}^M c_{ki} \eta_k, \quad (2.39)$$

where c_{ki} are variable coefficients. An infinite (complete) set of the KS orbitals approaches exactness as $M \rightarrow \infty$. At least for our molecules, and in many real applications, M is finite. Substituting Equation (2.39) into the KS operator of Equation (2.29), we have

$$\hat{f}^{\text{KS}}(\mathbf{r}_1) \sum_{k=1}^M c_{ki} \eta_k(\mathbf{r}_1) = \varepsilon_i \sum_{k=1}^M c_{ki} \eta_k(\mathbf{r}_1). \quad (2.40)$$

A general trick in Quantum Mechanics for this kind of equation is to find the completeness of the basis functions and this could be obtained by multiplying with arbitrary basis functions, η_μ , from the left and integrate over space to get M equations [18]

$$\sum_{k=1}^M c_{ki} \int \eta_\mu(\mathbf{r}_1) \hat{f}^{\text{KS}}(\mathbf{r}_1) \eta_k(\mathbf{r}_1) d\mathbf{r}_1 = \varepsilon_i \sum_{k=1}^M c_{ki} \int \eta_\mu(\mathbf{r}_1) \eta_k(\mathbf{r}_1) d\mathbf{r}_1 \quad (2.41)$$

satisfying the range, $1 \leq i \leq M$. This equation gives rise to a matrix equation of the form [18]

$$\mathbf{F}^{\text{KS}} \mathbf{C} = \mathbf{S} \mathbf{C} \varepsilon, \quad (2.42)$$

where,

$$\mathbf{F}_{\mu k}^{\text{KS}} = \int \eta_\mu(\mathbf{r}_1) \hat{f}^{\text{KS}}(\mathbf{r}_1) \eta_k(\mathbf{r}_1) d\mathbf{r}_1 \quad \text{and} \quad \mathbf{S}_{\mu k} = \int \eta_\mu(\mathbf{r}_1) \eta_k(\mathbf{r}_1) d\mathbf{r}_1 \quad (2.43)$$

and

$$\mathbf{C} = \begin{bmatrix} c_{11} & c_{12} & \cdots & c_{1M} \\ c_{21} & c_{22} & \cdots & c_{2M} \\ \vdots & \vdots & & \vdots \\ c_{M1} & c_{M2} & \cdots & c_{MM} \end{bmatrix}.$$

The eigenvalues, ε_i , are given by the diagonal matrix,

$$\varepsilon = \begin{bmatrix} \varepsilon_1 & 0 & \cdots & 0 \\ 0 & \varepsilon_2 & \cdots & 0 \\ \vdots & \vdots & & \vdots \\ 0 & 0 & \cdots & \varepsilon_M \end{bmatrix}.$$

Through the matrix equation (2.42), the Kohn-Sham orbitals could be determined and the charge density for the other terms in the total energy can be written in LCAO format [18],

$$\rho(\mathbf{r}) = \sum_i^N |\varphi_i(\mathbf{r})|^2 = \sum_i^N \sum_{\mu}^M \sum_k^M c_{\mu i} c_{k i} \eta_{\mu}(\mathbf{r}) \eta_k(\mathbf{r}). \quad (2.44)$$

Just as the Hartree-Fock formulation for the exchange-correlation functional is problematic, their orbitals are also difficult for evaluating integrals. The Slater orbitals that go into the Hartree-Fock formulation closely describe a cusp-like shape of true atomic orbitals near the nucleus and are often expressed in the form [6, 18]

$$\eta^{\text{STO}} = B e^{-\zeta r} r^{n-1} Y_{lm}(\theta, \phi), \quad (2.45)$$

where B is a normalization factor, n is the principal quantum number, ζ is the orbital exponent, and $Y_{lm}(\theta, \phi)$ are the spherical harmonics. Equation (2.45) is linked to Equation (2.5). Since these atomic orbitals could not be used effectively for molecules, an improvement occurred through the introduction of Gaussian orbitals, usually of the form

$$\eta^{\text{GTO}} = B x^a y^b z^c e^{-\alpha r^2} Y_{lm}(\theta, \phi), \quad (2.46)$$

where the sum of a , b and c determines atomic orbitals (s, p, d, f), α is the orbital exponent and it describes how compact (large α) or diffuse (small α) a basis function is [18]. However, Gaussian-type orbitals (GTO) are reported to be poor in predicting the actual shape of the atomic orbitals and superimposed or contracted Gaussian functions, often denoted as STO-nG, are mostly used in DFT calculations [6, 18, 40]. This means that multiple Gaussian basis functions correspond to one Slater-type orbital with a value of $n = 3, 4, \dots, 10$ [6, 18]. The contracted Gaussian-type orbitals (STO-nG) can be written as [6, 18]:

$$\eta_s = \sum_{\tau}^N d_{s\tau} \eta_{\tau}^{\text{GTO}}, \quad (2.47)$$

where $d_{s\tau}$ are coefficients for normalizing the GTOs to look like the STOs. For the two programs we used in this study, they employed different forms of basis functions. Amsterdam Density Functional (ADF) software usually makes use of the Slater-type orbitals while Gaussian makes use of the Contracted Gaussian-type orbitals. This accounts for the different ground state energy conformations usually reported by ADF and Gaussian; Gaussian calculations usually generate higher negative bonding energies. The addition of *polarisation functions*⁹ further improves these sets of basis functions [6, 18]. The following basis functions are used in this work, with their specifications:

⁹Polarisation functions have a higher angular momentum, l , than the Gaussian orbitals.

- Double Zeta with one polarisation (DZP) in the domain of Amsterdam Density Functional (ADF).
- In Gaussian, 6-31G(d) [41, 42] which corresponds to DZP in ADF. This notation in Gaussian is explicitly described in terms of the *split-valence*: "6-31G(d)" means that 6 Gaussian functions were used for the inner-shell orbitals and a split-valence set of four Gaussians, with subsets of 3 and 1, for the valence orbitals, and "d" represents a diffuse function for non-hydrogen atoms [6]. DZP and 6-31G(d) are mainly used for small molecules and we used the two for *formaldehyde* in this work.
- In ADF, Triple Zeta with one polarisation (TZP) was used for the *mercury dithizonates* because it is more accurate for molecules containing metal atoms.
- We used CEP-31G in Gaussian because 6-31G(d) cannot handle molecules with metals. CEP-31G is the effective core potential triple split-valence put forward by Stevens, Barch and Krauss [43, 44, 45].

Choosing an exchange-correlation functional and a compatible basis set for a specific DFT calculation is of great importance. Almost every functional could work for all calculations, depending on the level of accuracy we desire, but not all basis sets can be used for all calculations. ADF and Gaussian have different specifications.

2.5 Summary

1. The theoretical preliminaries leading to density functional calculation (DFT) were founded by Hartree-Fock formulation and Slater determinants.
2. DFT theories are based on Hohenberg-Kohn propositions. They particularly made a difference in treating the external potential and the exchange-correlation energy fully (based on electron density).
3. The main theme of DFT calculations is that *the ground state energy is a functional of the electron density*.
4. The *local kinetic energy* is calculated through the expansion of the Kohn-Sham orbitals into sets of *basis functions*. (See Equation (2.39)).
5. The *electron density*, on which the other terms in the Hamiltonian depend, is calculated through the sum of the absolute squares of the Kohn-Sham orbitals. Thus, the electron density inherently depends on the basis functions. (See Equation (2.44)).
6. The integro-differential equation of Equation (2.33) was transformed into a linear matrix equation (2.42), which could be easily coded through the introduction of basis functions.
7. ADF makes use of Slater-type orbitals (STOs) while Gaussian makes use of Gaussian-type orbitals or the Contracted Gaussian Functions (STO-nG).

8. Basis sets and exchange-correlation functionals that are compatible with molecules under study have to be chosen carefully to avoid errors in DFT calculations.
9. The methods followed for the DFT procedure are defined in Figure 2.3.

Let us now see how this ground state energy equation is applied in the DFT model.

Chapter 3

Structural Optimisation of Formaldimine and Dithizonatophenylmercury II

3.1 Procedure

We will follow the properties as shown in Figure 2.3. Some of the screen shots of our codes will be shown and explained in Appendix B. For a quick reminder, the structures of formaldimine and DPM isomers (orange and blue in dichloromethane solution) are shown in Figure 3.1.

In order to obtain the best orientations of these molecules, their structures were first optimised in all calculations. These optimisations led to minimum energies (ground state) and other desirable electronic properties.

In the Amsterdam Density Functional (ADF) program, the coordinates of the atoms in our molecules were artificially generated, resulting in Cartesian coordinates, which were pre-optimised using ADF input's interface. On this interface we specified the exchange-correlation functional, the basis sets, number of iterations, integration accuracy, relativistic effects (we used scalar form throughout), excitations, symmetries and the solvents.

We gained access to Gaussian 09 program through the Centre for High Performance Computing, Cape Town (www.chpc.ac.za), free of charge for academic purposes. Since I submitted the jobs to a cluster at CHPC, the calculations were faster than in ADF wherein we used a single PC system.

Molden package {www.cmbi.ru.nl/molden} as well as Gauss View were used along with the Gaussian (09) package to analyse the results obtained, and in the conversion of Z-matrix format of our molecular structure to the Cartesian coordinates format and vice-versa. The results obtained from ADF and Gaussian are also visualised and interpreted through the Chemcraft package, especially in the comparisons of the optimised geometrical data of the molecules, the orbitals and the absorption spectra.

We optimised our molecules using different combinations of XC functional and basis functions and with two major DFT programs, Gaussian (G09) and Amsterdam Density Functional (ADF).

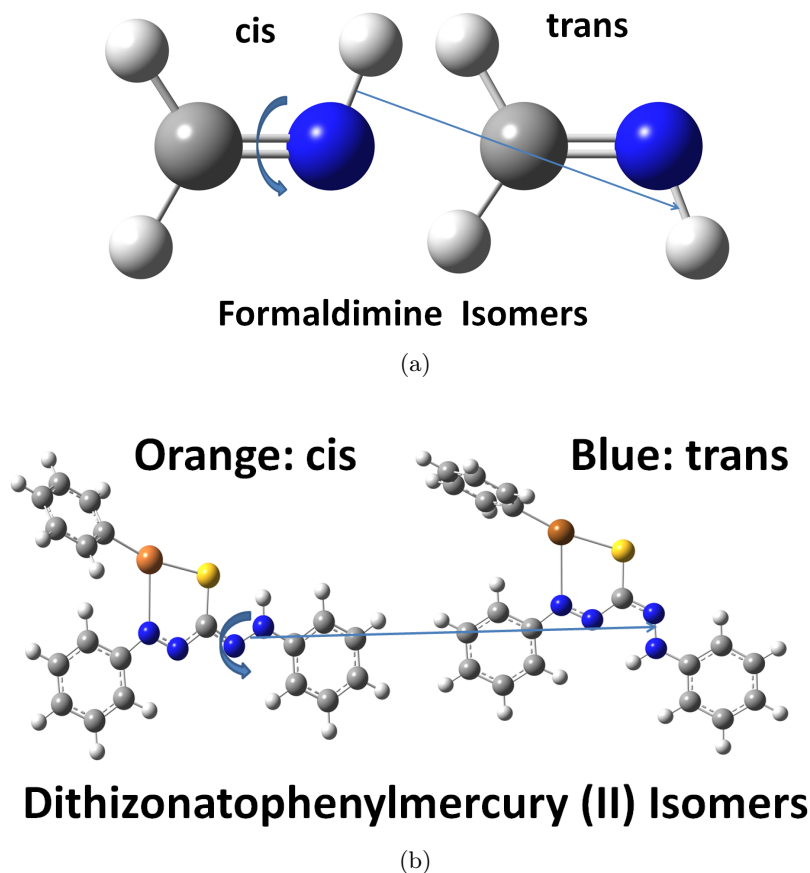


Figure 3.1: Structures of (a) Formaldimine and (b) Orange and Blue Isomers of Dithizonatophenylmercury II. {Key: Orange: Hg; Yellow: S; Blue: N; Dark Gray: C; and Light Gray: H.}

3.2 Geometry Optimisation

Geometry optimisation is usually treated in terms of *bond length*, *bond angle* and *dihedral (torsion) angle*. Bond length is the distance between two atoms, bond angle is the angle formed by three atoms (or angle formed by two bond lengths), and the dihedral angle is the angle between the planes formed by the first three atoms and the last three atoms in a four-atom conformation (see Figure 3.2).

In Table 3.1, we present the geometry optimisation of formaldimine. Since the X-ray crystal data of formaldimine is not available in literature, we compared our measurements with a previous calculation [46]. Here they basically used the second order Møller-Plesset perturbation theory (MP2) and the configuration interaction with single and double substitutions (CISD) to calculate the optimised structures of formaldimine; (see the last two columns of Table 3.1). We found out that all the combinations that we used gave bond lengths and bond angles in the same range as those found in literature [46], with a slight deviation, of the order of 0.001 – 0.010 Å in the bond lengths and 0.1 – 2° in the bond angles.

Since formaldimine isomerises around C=N double bonds, the most important

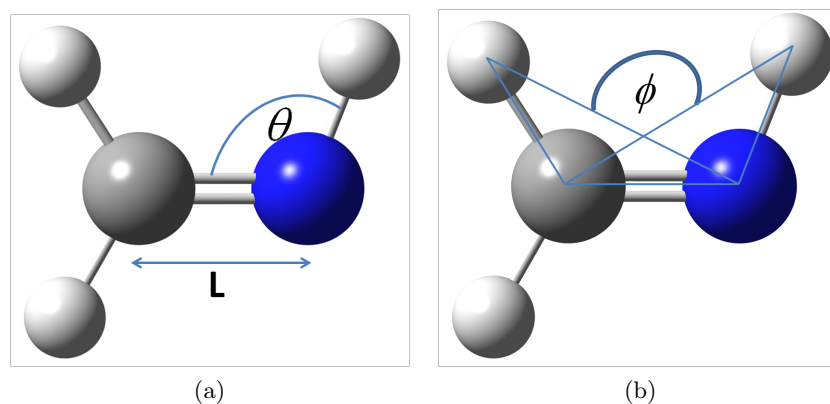


Figure 3.2: Formaldimine molecule; showing geometrical details (a) L =bond length; θ =bond angle and (b) ϕ =dihedral angle.

bond parameter in it is the bond length between carbon and nitrogen atoms which are in the same range when compared to the typical values recorded in Ref. [2]. The results of calculations done using the two DFT software (ADF and G09) approaches gave the same range of values. The structure of formaldimine, showing the labelling of the atoms, is given in Figure 3.3.

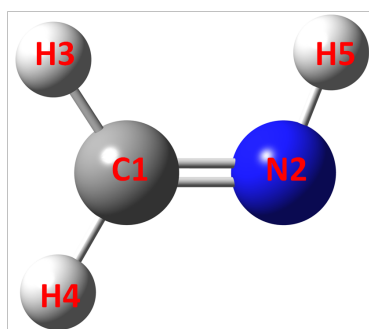


Figure 3.3: Formaldimine molecule: showing the atoms' labels

Table 3.1: Optimised Structures of Formaldimine. The last two columns were taken from Ref. [46].

Program: ADF								
Bond Lengths Å								
Methods	Hartree	LDA	BLYP	PW91	OLYP	B3LYP	CISD	MP2
Basis Sets	DZP	DZP	DZP	DZP	DZP	DZP	6-31G	6-31G
N2-H5	1.020	1.046	1.035	1.034	1.027	1.027	1.022	1.026
C1-N2	1.270	1.278	1.277	1.271	1.273	1.269	1.271	1.281
C1-H3	1.099	1.107	1.101	1.101	1.101	1.097	1.093	1.094
C1-H4	1.096	1.099	1.097	1.097	1.096	1.093	1.088	1.089
Bond Angles (°)								
C1-N2-H5	112.2	111.0	110.6	110.3	109.9	111.2	110.3	109.8
H4-C1-N2	119.5	118.5	118.5	118.4	118.5	118.8	118.8	118.4
N2-C1-H3	123.7	125.0	125.2	125.1	125.2	124.8	125.2	125.5

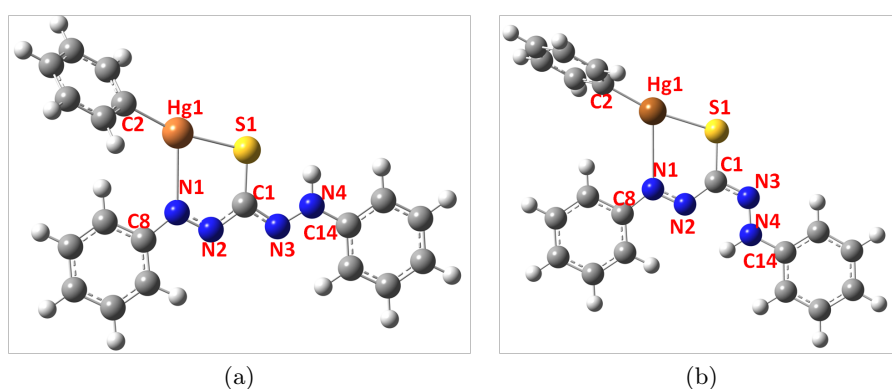


Figure 3.4: Structures of (a) Orange and (b) Blue Isomers of DPM showing the atoms' labels.

As was already described in Chapter 1, dithizonatophenylmercury (II) (DPM) has a photochromic effect in a polar aprotic solvent, dichloromethane, when illuminated with light and it isomerises from an orange reactant into a blue product. The isomers (orange and blue) of a DPM molecule, showing the labelling of the atoms in accordance with our optimisations, are given in Figure 3.4. These isomers were optimised using PW91/TZP and OLYP/TZP in the ADF program and B3LYP/CEP-31G in the Gaussian (09) program. Many optimised orientations were taken in this regard but we only present the most accurate in comparison with the X-ray crystal data. For example, PW91 and OLYP functional were also used in Gaussian but the results were pretty similar to the ones obtained in ADF. ADF results, however, gave the best geometrical orientations when compared to the X-ray crystal data. With regard to absorption spectra calculations, the B3LYP method was excellent in Gaussian. Table 3.2 shows these measurements.

We compared our calculations with X-ray crystal data (Cambridge Crystallo-

Table 3.2: Optimised Structures of Dithizonatophenylmercury II.

Bond Lengths Å							
	Orange Isomer				Blue Isomer		
Program	Crystal Data	ADF	ADF	G 09	ADF	ADF	G 09
Methods	X-RAY	PW91	OLYP	B3LYP	PW91	OLYP	B3LYP
Basis Sets		TZP	TZP	CEP-31G	TZP	TZP	CEP-31G
rmsd	-	0.11	0.12	0.34	-	-	-
Hg1-S1	2.372	2.425	2.418	2.498	2.403	2.401	2.468
Hg1-C2	2.101	2.099	2.101	2.125	2.100	2.102	2.125
Hg1-N1	2.651	2.604	2.753	2.592	2.662	2.787	2.672
N1-N2	1.277	1.276	1.271	1.307	1.283	1.279	1.311
N1-C8	1.432	1.412	1.419	1.444	1.405	1.410	1.438
N2-C1	1.416	1.369	1.375	1.400	1.367	1.369	1.399
C1-S1	1.731	1.785	1.785	1.857	1.782	1.785	1.849
C1-N3	1.301	1.326	1.324	1.341	1.330	1.330	1.343
N3-N4	1.337	1.318	1.315	1.353	1.319	1.318	1.356
N4-C14	1.401	1.396	1.399	1.425	1.392	1.394	1.422
Bond Angles (°)							
Hg1-S1-C1	104.8	102.5	104.4	100.9	102.8	104.5	101.6
S1-Hg1-N1	73.8	74.9	73.5	76.0	75.2	73.9	76.2
N1-Hg1-C2	118.4	118.9	118.9	120.7	114.8	113.6	115.5
Hg1-N1-N2	115.1	117.3	114.2	118.5	114.9	112.9	115.7
N1-N2-C1	117.7	118.2	119.1	118.6	118.6	119.3	119.2
N2-C1-S1	124.8	127.0	128.0	125.9	128.4	129.1	127.3
S1-C1-N3	127.5	121.1	121.6	122.2	113.8	113.1	114.9
C1-N3-N4	116.0	117.3	119.4	118.6	118.3	118.7	119.7
S1-C1-N3-N4		0.1	1.2	0.07	177.4	177.2	179.99

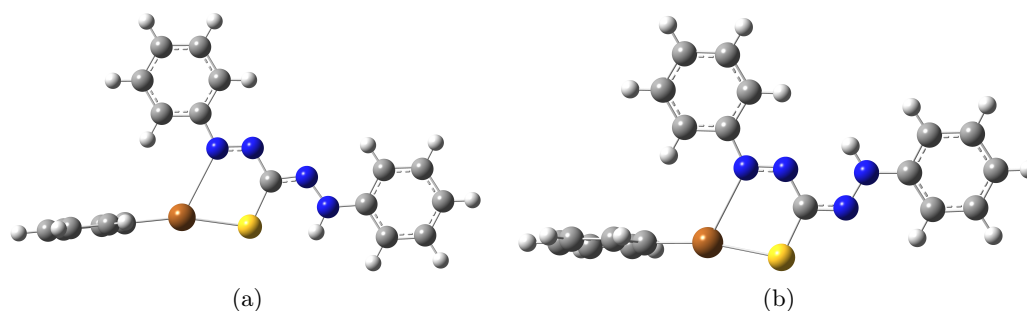


Figure 3.5: Optimised Structures of (a) Orange and (b) Blue Isomers of DPM.

graphic Database Centre) [48] and the results obtained in Ref. [2] (not shown in Table 3.2). The X-ray crystal data is for the orange isomer of DPM; the blue isomer is yet to be crystallized due to the fast back reaction from the blue excited state into the orange ground state. The optimised geometries of DPM isomers are given in Figure 3.5. In both optimised structures, the phenyl ring attached to the mercury atom shows a planar geometry. Our calculations show little or no geometrical deviation from what was obtained in Ref. [2]. The root mean square deviations (rmsd)¹ of the DPM orange isomer from the X-ray crystal data are 0.11, 0.12 and 0.34 for PW91, OLYP and B3LYP, respectively, as shown in Table 3.2. The detailed analysis of these bond lengths and angles are given in Chapter 5.

It is known that the starting geometries of the molecules should be realistic in order to obtain a sensible minimum during optimisation and to obtain good approximations of the experimentally observed data. As such, one would expect that the most deviated, in terms of structural optimisation, of these methods (B3LYP) from the X-ray crystal data would give the worst approximation in terms of all the properties we are investigating. Due to the fact that gas phase calculations, as we have in DFT methods, usually tend to overestimate the bond lengths and bond angles [2, 47], close attention must be paid to the combination of the methods being used. Surprisingly, as we will see in the absorption spectra calculations and the potential energy surface scans, B3LYP functional convincingly gave the overall best approximation. However, treating only the structural optimisations, ADF/PW91 gave the best reliable geometry orientations.

In DPM, dihedral angles are recorded since we considered isomerisation of the DPM orange ground state to its blue ground state. As shown in Table 3.2, it was found that the dihedral angles along S1–C1–N3–N4 increased from 0° to approximately 180° as the DPM orange isomer transforms to the blue isomer.

3.3 Ground State Energy

The smoothness of energy convergence obtained from using B3LYP functional for formaldimine and DPM isomers are shown in Figures 3.6 and 3.7, respectively. The energy convergence sharply decreased from the first point of iteration and started to converge at the fifth point of iteration for formaldimine and DPM isomers, (see Figures 3.6 and 3.7). The convergences were not easily achieved, especially for DPM isomers, and the blue isomer took a longer route to converge.

The bonding energy fragments (energy terms in Equation (2.33)) obtained for formaldimine and the DPM isomers using ADF software are given in Tables 3.3 and 3.4. These conform to the terms expressed in the total energy in Equation (2.33). Due to the differences in the basis sets (as analysed under the basis set discussed in Chapter 2), implementation by the two software we used, the ground state energies obtained for these molecules were strikingly far apart. For example, the energies calculated by the combinations, PW91/DZP (in ADF) and PW91/6-31G(d) (in Gaussian) gave -27.2 eV and -2574.1 eV, respectively. This gives a difference of about a factor of 100. Other combinations implemented in ADF and Gaussian

¹The root mean square deviations are calculated through the "RMS Compare Structures" available in Chemcraft package.

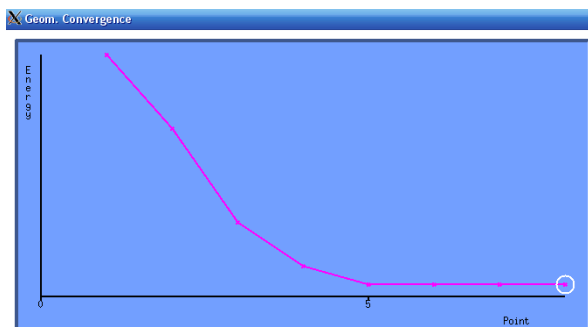
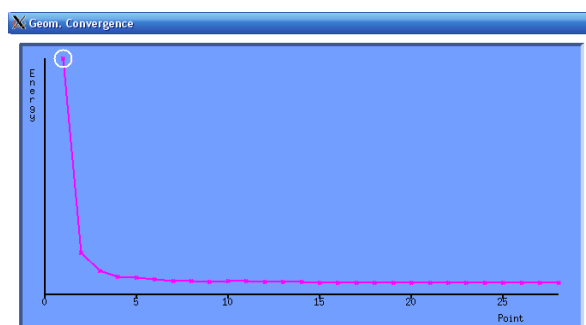
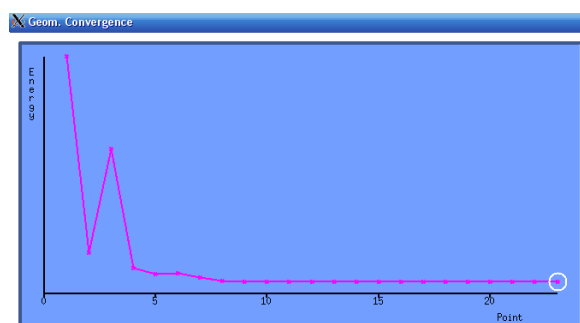


Figure 3.6: B3LYP Formaldimine Energy Convergence.



(a)



(b)

Figure 3.7: B3LYP Energy Convergences of (a) Orange and (b) Blue Isomers of DPM.

for these molecules ranked in the same way. We only implemented B3LYP/6-31G(d) and B3LYP/CEP31-G combinations for formaldimine and DPM isomers in Gaussian. These gave -2575.3 eV, -8712.8 eV and -8712.6 eV for formaldimine, the orange and the blue isomers of DPM, respectively. This difference was fully expected and it was not a problem as long as the energy band gaps (during excitation) presented by these different software were in the same range.

Early work on the photochromism and the existence of the orange isomer of metal dithizonates was done by L.S. Meriwether and co-workers [34], Irving and co-workers

Table 3.3: Bonding Energies of Formaldimine with DZP Basis Set. Software: ADF

Fragments	LDA:VWN (eV)	GGA:BLYP (eV)	GGA:PW91 (eV)	GGA:OLYP (eV)
Electrostatic	-16.6704	-16.2909	-16.4115	-16.8260
Kinetic	26.2618	23.0853	22.8145	25.3154
Coulomb	-12.4773	-10.3351	-9.7934	-11.8598
XC	-25.6587	-22.5222	-23.8365	-23.2193
Total	-28.5447	-26.0628	-27.2269	-26.5898

Table 3.4: Bonding Energies of DPM Isomers with TZP Basis Set. Software: ADF

Fragments	Orange Isomer		Blue Isomer	
	GGA:PW91 (eV)	GGA:OLYP (eV)	GGA:PW91 (eV)	GGA:OLYP (eV)
Electrostatic	-230.7958	-230.5623	-230.5155	-230.4007
Kinetic	231.2149	231.8317	230.9302	231.7108
Coulomb	-19.8995	-19.0508	-19.7909	-18.9176
XC	-244.0945	-234.4925	-243.9432	-234.4280
Total	-263.5749	-252.2739	-263.3194	-252.0356

[36] and Reith and co-worker [37], over five decades ago. The *blue isomeric form* of the mercury dithizonates was proposed and studied by von Eschwege and co-workers [2].

However, they did not consider any solvent effect in contrast to what we have in this study. Thus, we have herewith investigated the validity of the prediction of the blue isomeric structural form, using a polar protic solvent, methanol, and a polar aprotic solvent, dichloromethane ². In Ref. [2], three possible structures of the blue isomer were studied: N4-H, which is favoured over S1-H and N2-H structures. S1-H and N2-H structures involve a proton (hydrogen) transfer from the N4 to the S1 and N2, respectively (See Figure 3.4).

As shown in Table 3.5, it is interesting to note that regardless of solvents or no solvents, the N4-H blue isomeric form gives the lowest structural energy (being 37 kJ/mol and 90 kJ/mol less than N2-H and S1-H blue isomeric forms in methanol, respectively. It was 54 kJ/mol and 133 kJ/mol less in dichloromethane) compared to that of the orange isomer. This shows that N4-H structures have the greatest tendency of being formed during isomerisation reactions of all the molecules considered. We shall, therefore, use this N4-H structure throughout this work.

²Protic solvents are solvents which can donate a hydrogen ion (proton) while aprotic solvents cannot [See <http://en.wikipedia.org/wiki/Solvent> and <http://en.wikipedia.org/wiki/Aprotic>].

Table 3.5: Lowest Structural Energies of Optimised DPM Blue Isomeric Form in Polar Protic Solvent, Polar Aprotic Solvent and Gas Phase Relative to That of the DPM Orange Isomer. The last column is taken from Ref. [2].

Method	G09/B3LYP/CEP-31G				G03/B3LYP/CEP-31G
Solvent	Methanol		Dichloromethane		Gas Phase
	Relative Energies		Relative Energies		Relative Energies
Structures	(eV)	(kJ/mol)	(eV)	(kJ/mol)	(kJ/mol)
N4-H	0.18	17.84	0.18	17.67	20.5
N2-H	0.57	54.57	0.74	71.65	68.0
S1-H	1.12	108.33	1.57	151.47	166.7

3.4 Summary

In this chapter, we have presented the structural optimisation of formaldimine and DPM. These optimisations have led to their respective ground state energy minima. We also confirmed that the N4-H blue isomeric form has the greatest tendency of being formed during isomerisation of the DPM orange isomer.

We shall now calculate their absorption spectra and ground state potential energy surfaces. This leads us to the next chapter.

Chapter 4

Isomerisation Reactions and Time-dependent Density Functional Calculation

4.1 Isomerisation Reactions in our Molecules: A Link to Potential Energy Surface

Isomerisation is a phenomenon whereby a molecule undergoes a structural change without changing its molecular formula (stoichiometry). This process is often associated with a change in the physical and chemical properties of molecules. The on-going investigation of photo-isomerisation reactions of the retina chromophore along C=C double bonds as rhodopsin isomerises to bathorhodopsin showed fascinating properties (in terms of vibrational modes, cis-trans isomerisation and absorption spectra) [1, 30]. Herein, we want to study the isomerisation reactions in our molecules starting with our kernel molecule, *formaldimine*. Some studies have been done on this kernel molecule: a study of its singlet and triplet states in relation to its potential energy surface [16, 17].

Formaldimine is the simplest form of *imine group*¹ and it undergoes a *cis-trans* isomerisation around its C=N double bond. This isomerisation process had been reported to favour two forms: *in-plane inversion motion*, when it is thermally induced and *twisting motion*, when it is photochemically induced [16, 17]; (see Fig.4.1). In our case, we will focus on the photochemically induced isomerisation since our ultra-fast spectroscopy experiments are based on laser-induced reactions. However, in some cases, isomerisation around *π -conjugated systems* could favour the combination of the twisting rotation and the in-plane inversion motion [16, 17].

Conjugated systems are associated with a region of overlapping π -orbitals with delocalized π -electrons distributed along adjacent σ -orbitals [35]. Due to the π -orbitals interaction between the $2p_C$ orbital of the carbon atom and the sp^x of the nitrogen atom, formaldimine has often been described as a *protonated Schiff base* with a C_s symmetry [16, 30]. This involves excitation of $\pi - \pi^*$ as the twisting angle is varied around the orthogonal geometry (90°). Some properties associated

¹Imines are associated with the functional group, C=N (carbon-nitrogen double bond).

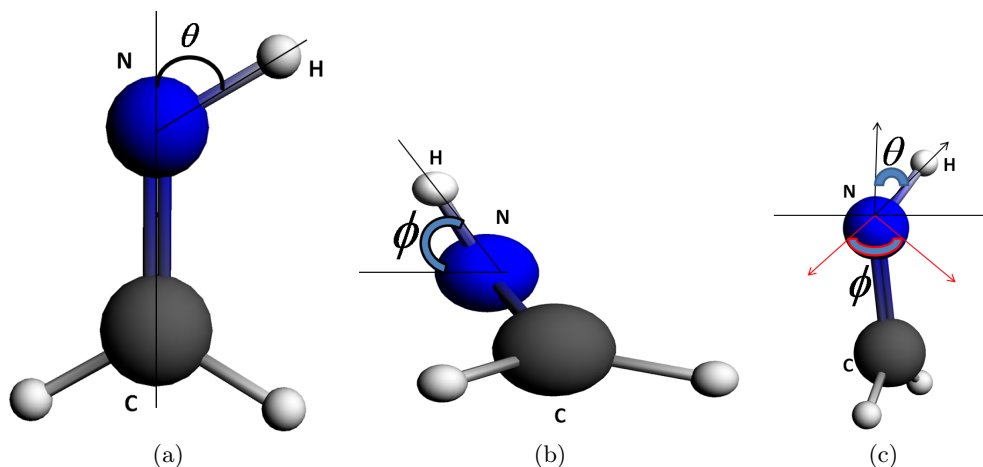


Figure 4.1: Isomerisation Through (a) Inversion Path (θ), (b) Twisting Path (ϕ) and (c) Twisting (ϕ) and Inversion (θ) Paths in Formaldimine. Figure reprinted from Ref. [17].

with formaldimine could be extended to the mercury dithizonates since the molecules also possess C=N (double bonds) chromophore in the core of their ligands' backbone.

The schematic diagram of the focus of this study is shown in Figure 4.2. Essentially, the wave-packet² of our molecules are excited from a singlet ground state, S_0 , to the first singlet excited state, S_1 . From here, the wave-packet may flow over via point "a" to the other side of the S_1 surface, or flow down through the bifurcation presented by point "b" or "c" at the orthogonal geometry of S_0 surface. If it does bifurcate, the model shows that it can either repopulate the ground state isomer via point "b", or move on to the ground state of the blue isomer through point "c". There can also be an intermediate absorption (labelled as "INT" in Figure 4.2) from the minimum of the S_1 surface [61].

Isomerisation reactions in these molecules can be followed by the calculation of energy for different geometrical orientations of molecules and these give rise to potential energy curves. This has a link with the optimisation of the geometries of our molecules; the minimum energy is calculated at each twisting rotation. However, this has only been done successfully for the ground state conformations. The photo-excited states potential energy calculation is as difficult to access through quantum mechanical simulation as it is experimentally. Though the excited state calculations have been linked to a *conical intersection*³ between the ground state potential energy surface and that of the excited state, especially in formaldimine [16, 17, 30, 50], the corresponding calculations for metal dithizonate complexes are still much in the dark and there is on-going active research in this line. We shall only present the potential energy surfaces of the ground states of our molecules.

The regions around the ground state potential energy surface (PES) maxima are usually degenerate. These are usually characterised by pronounced sharp peaks (artefacts). This is because the de-excitation of these molecules from some electronic

²Wave-packets are defined as the linear combination of stationary eigenstates.

³Conical intersection is a region through which an ultra fast transfer occurs; from an excited to the ground state potential energy surface. This is indicated by dashed lines in Figure 4.2.

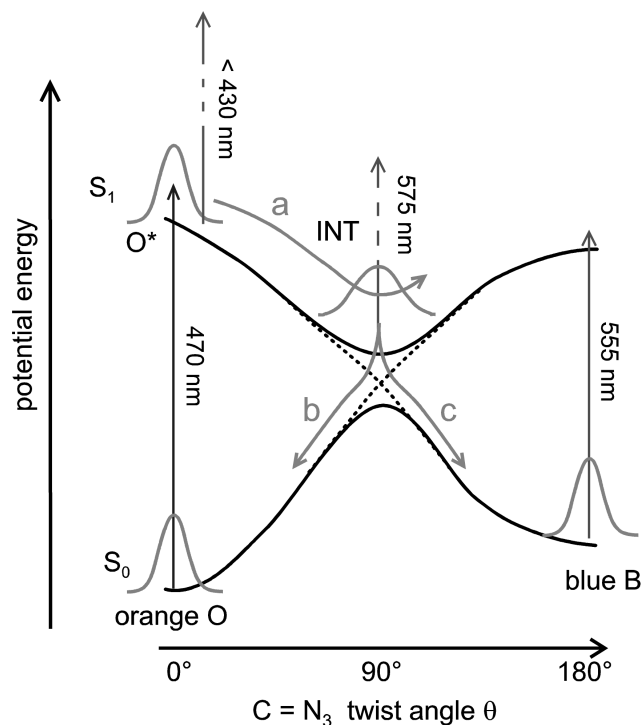


Figure 4.2: Schematic Model of Photo-isomerisation of DPM Molecule.

excited states (orange isomer) can either repopulate the electronic ground states (orange isomers) or populate the electronic ground states of the blue isomers. In both cases, the molecule has to flip over via its *transition state* which is sometimes located at the orthogonal geometry (90°).

To do this, the polarities (alpha and beta) of the spin density (see Equation (2.37)) tend to interact with one another due to the redistribution of electrons during excitations. As a result, we end up getting local energy minima around the orthogonal geometry of the PES. The solution to these sharp peaks came in the form of *broken symmetry calculations*⁴ which ensure the separation of the spin densities around the maxima of PES. Broken symmetry involves a rearrangement of the electrons in a molecular orbital in order to flip from one isomer to the other. Broken symmetry calculations change the mode of our calculations from a restricted closed shell to an unrestricted open shell. However, this broken symmetry calculation is usually only effective from 70 – 120°. Other angles proved stabilised (stable eigenmodes) when checked. (More on these broken symmetry calculations will be discussed in Chapter 6.)

In Figure 4.4, the first singlet potential energy surfaces of formalimine and DPM corresponding to S₀ are presented. The energy values plotted are relative to the ground state energy minima (−2574.90 eV and −8711.83 eV for formalimine and DPM, respectively). We used two potential energy surface scan methods: rigid and relaxed scans. In rigid scans, the SCF (minimum) energy is calculated at each

⁴The order for broken symmetry calculation is: Optimised Geometry → Stable Restricted Hartree Fock (RHF) → Unrestricted Hartree Fock.

dihedral (or torsion) angles, but only using the optimised geometry of the ground state (at 0°). In relaxed scans, however, the geometries of our molecules are optimised at each dihedral angle and the minimum energy is calculated. These scans are often done from $0 - 180^\circ$. Broken symmetry calculations can only be used in the relaxed PES mode.

For formalimine, we employed the rigid scan method. There is an initial slight difference (0.06 eV) between the ground and the excited state minimum energies. The two energy minima depicting ground and excited states of formalimine should be the same because its structure does not change before and after excitation. Thus, the energy minimum at 180° was relaxed to obtain the true minimum energy. The singlet potential energy surface of formalimine corresponding to S_0 had been previously calculated by Hirai et. al [17] via the Semi-classical approach, and which gave a potential barrier of about 2.3 eV. It is interesting to note that we got a barrier of 2.32 eV for the rigid scan using the B3LYP/6-31G(d) method, with a smooth maximum at the orthogonal geometry (90°).

Since the geometries corresponding to each dihedral angles are optimised in the relaxed scans, the true minimum energies are obtained. However, formalimine combined twisting and inversion motions when we used the relaxed scan method. This led to a flat PES surface at its orthogonal geometry. The energies around this region proved stable when calculated and so broken symmetry analysis could not be used. The overall results show that formalimine is stable in its excited state, as much as it was in its ground state.

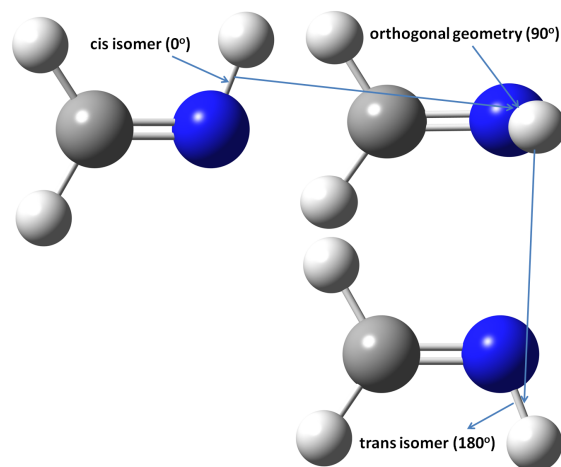
The potential energy surface of DPM is much in the same fashion as that of formalimine since they rotate around the same kind of chromophore (C=N) (see Figure 4.3). However, DPM has two isomers with different ground state energies for which the orange isomer has a lower energy than the blue isomer. This influences their absorption wavelengths, as we shall see shortly. The structure of the orange isomer of DPM is optimised in a polar protic solvent, methanol, and a polar aprotic solvent, dichloromethane, to investigate the effects that these would have on the rotation. It was found that the solvents do not have any effect on the relaxed potential energy barrier obtained for DPM, (which in both cases is 1.20 eV). Comparing this to that of formalimine, we found that the barrier of DPM is about half of that of formalimine. This tells us that the longer the delocalised π -electrons are in molecules, the lower the energy and vice versa. The famous example of this is *the-particle-in-the-box model*.

We used the broken symmetry method to get to the true energy maxima of the $70 - 120^\circ$ dihedral angles in DPM. The SCF energies and their corresponding angles for formalimine and DPM are given in Table D.1. The dihedral angle at 100° for DPM did not converge; we used 105° instead. The energy gap between the two isomers of DPM connotes their stability; the orange form is much more stable than the blue form. The difference in energies between two minima relates to their relative stability (i.e. the thermodynamics of the system); while the barrier height affects the kinetics, i.e. rate of conversion.

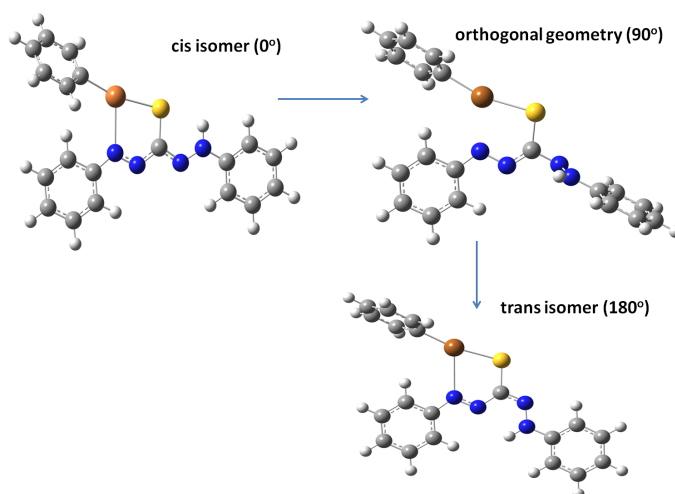
The energy values presented in Table D.1 are relative in nature; different methods would give rise to different energies at different dihedral angles. However, the barriers obtained from different effective methods should be in the same range of values.

We shall look into this in more detail in Chapter 6, where we present the potential

energy barrier results for the electronically altered DPMs. The B3LYP functional combined with the CEP-31G basis set again gave the best results for these scans as broken symmetry calculations were more effective using B3LYP than PW91 and OLYP.



(a) Dihedral Twisting Rotation in Formaldimine (0 – 180°).



(b) Dihedral Twisting Rotation in DPM (0 – 180°).

Figure 4.3: Cis-Trans Dihedral Twisting Rotation in Formaldimine and DPM.

4.2 TD-DFT And UV-VIS Spectroscopy

We shall herewith explore the use of the *time-dependent density functional calculation* to characterise the *absorption spectra* of the molecules under study. Excitations in organic molecules are usually associated with a transition between the

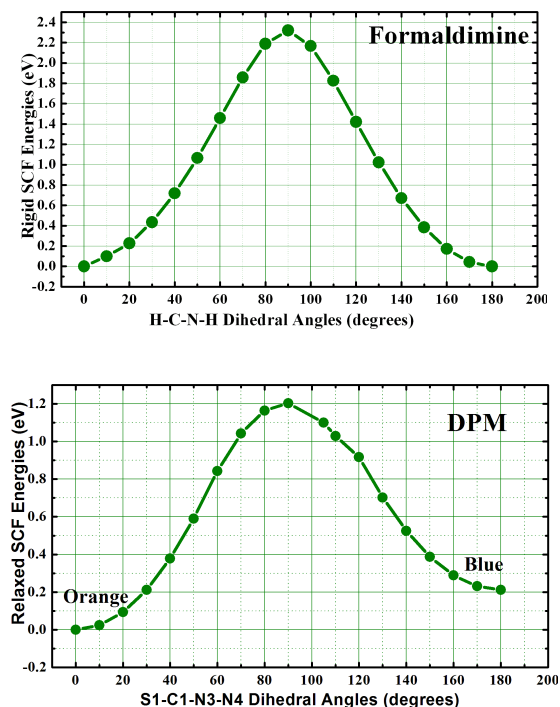


Figure 4.4: Ground State (S_0) Potential Energy Surfaces of Formaldimine and DPM.

Highest Occupied Molecular Orbital (HOMO) and the Lowest Unoccupied Molecular Orbital (LUMO)⁵. Regarding the HOMO–LUMO transition associated with the π -conjugated systems of the *cis-trans* photo-isomerisation of the retina chromophore, a transfer of proton was involved [1, 30]. These molecules undergo a similar *cis-trans* isomerisation but a recent study shows that the most stable conformation of the blue isomers of DPM molecules involve no proton transfer; the hydrogen atom attached to the nitrogen (N4) (see Figure 3.1 and Table 3.5), stayed on it before and after isomerisation [2].

Excitation energy calculations of fairly large molecules could be obtained through the restricted open shell Hartree-Fock (HF) model [29, 30], the Ziegler-Rauk-Baerends sum method [31], which could be implemented in the Amsterdam Density Functional program (ADF), the restricted and the non-restricted configuration interaction with single substitution (RCIS & CIS), and the random phase approximation (RPA) with some slight deviations from experimental data [6, 28].

Alternative methods for the computation of excitation energies include the restricted open-shell Kohn-Sham method (ROKS) [32], which was basically used in describing isomerisation reactions in the retina; Quantum Monte Carlo (QMC) [28], that was recently proposed for excitations in photo-active molecules, and the time-dependent density functional theory (TD-DFT model) which has been extensively used in the description of excitation spectrum for large molecules [1, 2, 28, 30].

Every method has limitations. Of these methods, the TD-DFT model works

⁵HOMO is to organic molecules what a valence band is to inorganic molecules. Similarly, LUMO is to organic molecules what a conduction band is to inorganic molecules.

better in the regime of molecules with many atoms and it incorporates correlation energy which was neglected by earlier methods. Other approaches also implemented in the software we used are the configuration interaction methods (CIS and RCIS), which gave poor results; far deviated from the experimental data (see Tables 4.1 and 4.2). More so, we tend to be satisfied with the TD-DFT model since this research is in the domain of density functional calculations in this work.

Now, how do we incorporate *time* into the domain of pseudo-wave functions and the exchange-correlation functional? Let us go back to the root – the Schrödinger time-dependent wave equation:

$$\hat{H}\psi(\mathbf{r}, t) = i\frac{\partial}{\partial t}\psi(\mathbf{r}, t) \quad (4.1)$$

with an associated general solution of the form

$$\Psi(\mathbf{r}, t) = \sum_n c_n(t)\varphi_n(\mathbf{r}) \exp(-iE_n t), \quad (4.2)$$

where $c_n(t)$ are coefficients often expressed in terms of pulse spectrum and the Franck-Condon factors [8]. This solution holds only for the regime of small atoms and diatomic molecules and it cannot be used to describe polyatomic molecules, as we have in this work. However, we could gain insight into how the excited state wave functions should behave.

According to the original density functional theory (DFT) by Hohenberg and Kohn, there exists a mapping between the electron density, $\rho(\mathbf{r})$, and the external potential energy, $V_{e-n}(\mathbf{r})$. Can we also have a mapping of a time-dependent electron density, $\rho(\mathbf{r}, t)$, to a corresponding time-dependent external potential, $V_{e-n}(\mathbf{r}, t)$? The answer lies in the rigorous theorems and proofs of existence of this mapping by Runge and Gross in the early 1980s [33]. In line with Equation (4.1), Runge and Gross showed that we can write [33],

$$i\frac{\partial}{\partial t}\psi(\mathbf{r}, t) = \hat{H}(t)\psi(\mathbf{r}, t), \quad (4.3)$$

subject to the initial condition, $\psi(t_0) = \psi_0$. This equation is as difficult to solve as its time-independent counterpart. The problem again lies with the existence of the external potential energy for there is no known way to solve the resulting second-order differential equation.

The conspicuous difference in the time-dependent Hamiltonian from the its time-independent counterpart is seen in the expression for the external potential [33],

$$\hat{H}(t) = \hat{T} + \hat{V}_{e-e} + \hat{V}_{e-n}(t). \quad (4.4)$$

How do we express these terms as a functional of the time-dependent electron density? A quick way would be to insert the time factor in the terms as:

$$i\frac{\partial}{\partial t}\psi(\mathbf{r}, t) = \left[-\frac{1}{2}\nabla^2 + \frac{1}{2} \int \frac{\rho(\mathbf{r}', t)\rho(\mathbf{r}, t)}{|\mathbf{r} - \mathbf{r}'|} d\mathbf{r}d\mathbf{r}' - \int \frac{\rho(\mathbf{r}, t)}{\mathbf{r}} d\mathbf{r} + E_{XC}[\rho(\mathbf{r}, t)] \right] \psi(\mathbf{r}, t). \quad (4.5)$$

According to Runge and Gross [33], this is not valid. They suggested that within a time frame, there exists a time-dependent electron density that uniquely determines

a corresponding external potential. Within this time interval, the electron density is obtained and this is used to calculate the external potential and, subsequently, the total energy of the system. This external potential could be expanded in Taylor's series up to an additive constant, $c(t)$ [33]:

$$V'_{e-n}(r, t) = V_{e-n}(r, t) + c(t), \quad (4.6)$$

so that for a fixed initial state, $\psi(t_o) = \psi_o$ and $\rho(\mathbf{r}, t)$, we can write [33]:

$$\psi(t) = \psi'[\rho(\mathbf{r})](t) \exp\{i\gamma(t)\} \quad (4.7)$$

subject to the condition that,

$$\frac{d}{dt}\gamma(t) = c(t). \quad (4.8)$$

Runge-Gross theorems stated that the XC energy which is a functional of the electron density and the initial wave function, ψ_o , could only be calculated within a time frame such that [33]

$$i\frac{\partial}{\partial t}\psi(\mathbf{r}, t) = \left[-\frac{1}{2}\nabla^2 + \frac{1}{2} \int \frac{\rho(\mathbf{r}', t)\rho(\mathbf{r}, t)}{|\mathbf{r} - \mathbf{r}'|} d\mathbf{r}d\mathbf{r}' - \int \frac{\rho(\mathbf{r}, t)}{\mathbf{r}} d\mathbf{r} + E_{XC}[\rho, \psi_o](t) \right] \psi(\mathbf{r}, t). \quad (4.9)$$

Often, a vertical excitation computation in TD-DFT is basically treated with the linear response theory that makes use of a linear expansion of the external potential energy [49]. This treatment is subject to limitations, usually on the number of excitations that could be accessed through the use of Equation (4.9). There is also a memory problem from the time evolution of the electron density that has to be suppressed [33]. Moreover, the problem with double excitations' implementation in DFT remains unclear [30].

Furthermore, the treatments of excitation spectra often depend on the number of delocalised π -electrons, and these determine the active absorption wavelengths of molecules in the electromagnetic (EM) spectrum. This usually ranges between the ultraviolet to the visible region of the EM spectrum. The longer the conjugated π -electrons in a molecular orbital are, the longer the absorption wavelengths and vice-versa [51]. As first examples, we shall now turn to the treatment of the absorption spectra of formalimine and the DPM isomers.

4.3 Experimental Procedure

The synthesis of all the molecules we considered in this work was performed according to the procedure published in Ref. [2] by von Eschwege *et al.* Apart from the solvent dependence study wherein we used different solvents, all the samples (molecules in crystalline form) were dissolved in dichloromethane (DCM). We dissolved 10 mg of each of the samples in 10 ml of DCM. The initial concentrations of each of the samples in DCM were diluted 8 times. The baseline of the reference sample (DCM) was first measured in order to set a background measurement of the solvent. The orange isomers were each placed in the light beams to measure their respective absorption spectra. Blue light (with a spectrum range between 360 – 520 nm) was then used to excite the molecules diluted in DCM. After excitations, one by one, the resulting blue

isomers were placed in the light beams of a spectrophotometer and the absorption spectra were measured for each of the samples.

The spectrophotometer (Type: Evolution 600 UV-VIS) with a VISIONpro software was used to analyse the UV-VIS steady state absorption spectra with the following specifications: Bandwidth = 2.0 nm; Scan speed = 240 nm/min; Data Interval = 1.0 nm and Lamp = Tungsten (for UV wavelengths) & Deuterium (for visible wavelengths).

The length of time, (a few minutes), it took to scan over a range of 250 – 700 nm was greater than the time, (also a few minutes), of de-excitations from *blue* to *orange*. This return time depends on temperature and nature of the substituents on the phenyl rings and the solvent used. For instance, the DPM molecule returned to its *orange* form faster in methanol than in DCM. As a result of these fast reversible reactions, we observed three bands, (the middle band is due to the quick orange build up), in all the substituted DPM blue isomers presented in Chapter 6.

4.3.1 Absorption Spectra of Formaldimine and Dithizonatophenylmercury II

Formaldimine has a double bond which is composed of sigma (σ) and pi (π) electrons at its chromophore. Thus, we expect all its absorption wavelengths to be in the ultraviolet spectra region. Table 4.1 and Figure 4.5 agree with this observation, and both compare so well with the lowest excitation energies in previous calculations [17, 28]. We used five different DFT methods. To maintain uniformity in the basis sets and the number excitations obtained, we chose to present the results obtained from the Gaussian (09) program.

The excitation/absorption spectra are treated in terms of *absorption wavelength*, λ , measured in nano meter (nm) and *oscillator strength*, f , in atomic unit (au). Oscillator strength is a measure of *relative absorbance*, A . In Table 4.1, the first wavelengths of these five methods represent the lowest singlet excitation wavelengths (ranging from 216 – 238 nm; approximately 5.7 – 5.2 eV) of formaldimine and we can see that they have very weak oscillator strengths. Of these methods, the lowest excitation energy calculated for RCIS/6-31G(d) gives a poor result (about 0.3 eV higher) compared to the range of values given in literature [17]. The absorption wavelengths

Table 4.1: Selected Singlet Excitations of Formaldimine; f is the oscillator strength and λ is the absorption wavelength. Solvent = Dichloromethane (DCM) ($\epsilon = 8.9$), G09 = Gaussian 09.

G09/B3LYP/6-31G(d)		G09/PW91/6-31G(d)		G09/OLYP/6-31G(d)		G09/BLYP/6-31G(d)		G09/RCIS/6-31G(d)	
λ (nm)	f (au)	λ (nm)	f (au)	λ (nm)	f (au)	λ (nm)	f (au)	λ (nm)	f (au)
230	0.005	237	0.005	232	0.005	238	0.005	216	0.072
137	0.311	137	0.253	137	0.253	140	0.251	168	0.363
124	0.130	133	0.109	133	0.102	136	0.096	122	0.082
105	0.446	111	0.432	110	0.429	112	0.417	105	0.181
87	0.340	91	0.354	91	0.340	92	0.344	101	0.061
86	0.160	83	0.652	83	0.668	84	0.651	97	0.060
80	0.574	82	0.100	82	0.082	83	0.078		

and the oscillator strengths obtained from PW91/6-31G(d) and OLYP/6-31G(d) are

pretty similar, and BLYP/6-31G(d) follows suite. These three methods are based on the generalised gradient approximation (GGA) to the exchange-correlation energies and they all give maximum oscillator strengths around 83 – 84 nm absorption wavelength. B3LYP, which is a hybrid functional, gives a lower absorption wavelength of 80 nm at a maximum. These maximum wavelengths usually represent a HOMO-LUMO transition with a yield contribution of about 70%. In some other cases, the first maximum may represent HOMO-LUMO+ n or HOMO- n -LUMO transitions.

Moreover, each of these absorption wavelengths and oscillator strengths represent superposition of multiple transitions in the excitation spectra. However, the

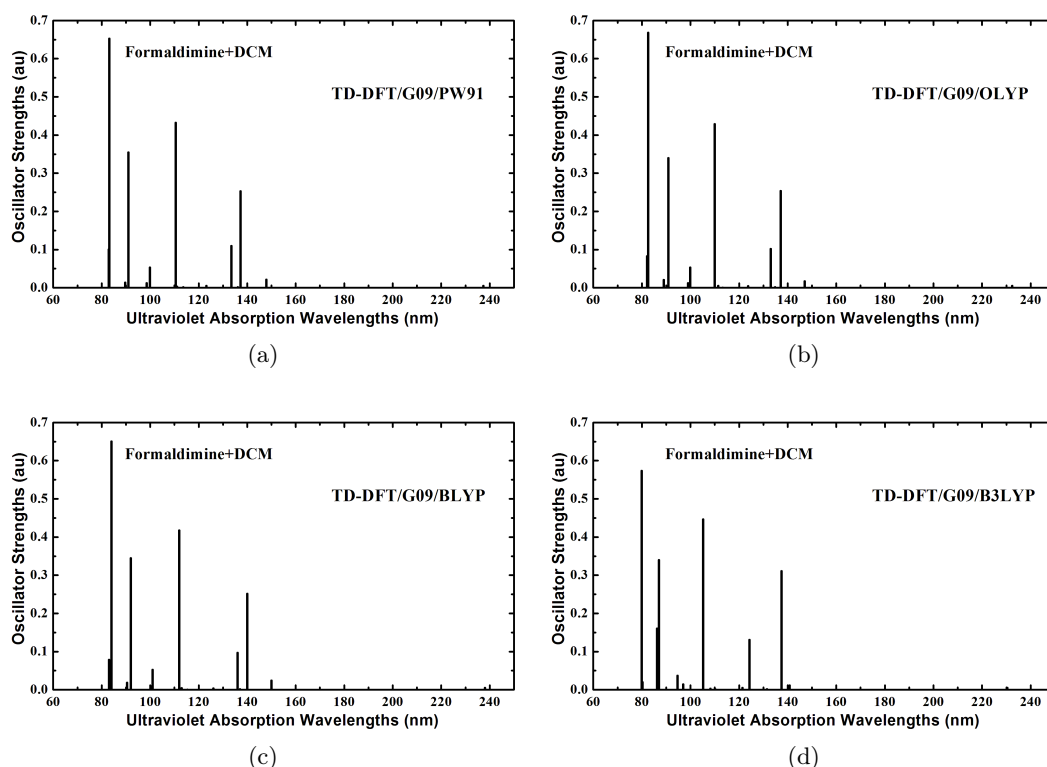


Figure 4.5: Singlet-Singlet Excitation Energies of Formaldimine Using (a) PW91/6-31G(d), (b) OLYP/6-31G(d), (c) BLYP/6-31G(d) and (d) B3LYP/6-31G(d). Program: Gaussian 09.

interesting photo-excited state properties of formaldimine could unfortunately not be followed with femto second spectroscopy due to its absorption spectra in the ultraviolet region of the electromagnetic spectrum.

In contrast to formaldimine, there is an increased delocalised system of π -electrons in a DPM molecule and this makes the excitation energy become lower and lower so that the absorption wavelengths of DPM are accessible through femto second spectroscopy.

We present the singlet excitation energies of DPM isomers in Tables 4.2 for four different functionals, using ADF and Gaussian. Figure 4.6 gives the plots of the singlet-singlet excitations done by the three methods we used and the overlays of the steady state absorption measurement obtained from UV/Visible spectroscopy.

In the orange isomer, two major steady state absorption bands are observed. The first (primary band) is at 266 nm near the UV region and the second (secondary band) at 472 nm in the blue spectra range. Of these, the secondary band represents the central wavelength, which is usually used for *pump wavelength* in femto second spectroscopy analysis. For the blue isomer, the first peak (primary band) is around 276 nm and is both *bathochromic* and *hyperchromic* (an increase in the absorption wavelength and intensity, respectively) compared to the orange's. The secondary band of the blue isomer is around 588 nm.

Comparing these with the DFT calculated spectra, the B3LYP method gave the best approximation of the experimental absorption spectra. It was so accurate that it gave exactly the same maximum absorption wavelength of 472 nm as was observed experimentally for the orange isomer, and the blue isomer only deviated by 10 nm. There is also a close agreement between the calculation and experiment in the primary band of the blue isomer. In all the methods, there are spectral matching between the calculated and experimental observations, especially at the troughs (shoulders) around 350 – 410 nm for the orange isomer and 350 – 450 nm for the blue isomer. Again, the RCIS/CEP-31G method gives the worst result when compared to the experimental data in Table 4.2

Table 4.2: Selected Singlet Excitations of DPM Orange and Blue Isomers; A is the relative absorbance, f is the oscillator strength and λ is the absorption wavelength. Solvent = Dichloromethane (DCM) ($\epsilon = 8.9$), G09 = Gaussian 09.

Experiment		G09/B3LYP/CEP-31G		ADF/PW91/TZP		ADF/OLYP/TZP		G09/RCIS/CEP-31G/	
Orange Isomer									
λ (nm)	A	λ (nm)	f (au)	λ (nm)	f (au)	λ (nm)	f (au)	λ (nm)	f (au)
472	1.056	472	0.893	513	0.427	495	0.406		
				507	0.144	494	0.165		
				412	0.145	405	0.257		
ca. 350	0.114	358	0.182	352	0.086	391	0.050	319	1.524
						371	0.032		
ca. 306	0.271	306	0.074	292	0.121	344	0.088	224	0.123
266	0.599	261	0.186	283	0.157	223	0.111		
Blue Isomer									
λ (nm)	A	λ (nm)	f (au)	λ (nm)	f (au)	λ (nm)	f (au)	λ (nm)	f (au)
588	0.526	598	0.475	669	0.259	637	0.288		
				452	0.194	441	0.240		
ca. 390	0.094	390	0.268	368	0.142	362	0.147	383	0.355
ca. 322	0.301	321	0.171	310	0.150	306	0.171	366	0.607
276	0.727	271	0.487	296	0.388	293	0.390	239	0.214

4.3.2 Solvent Dependence of the DPM Orange Isomer

For a better study of the photochromic effects of DPM in solutions, we carried out some solvent dependence of the absorption wavelengths of the orange isomer using

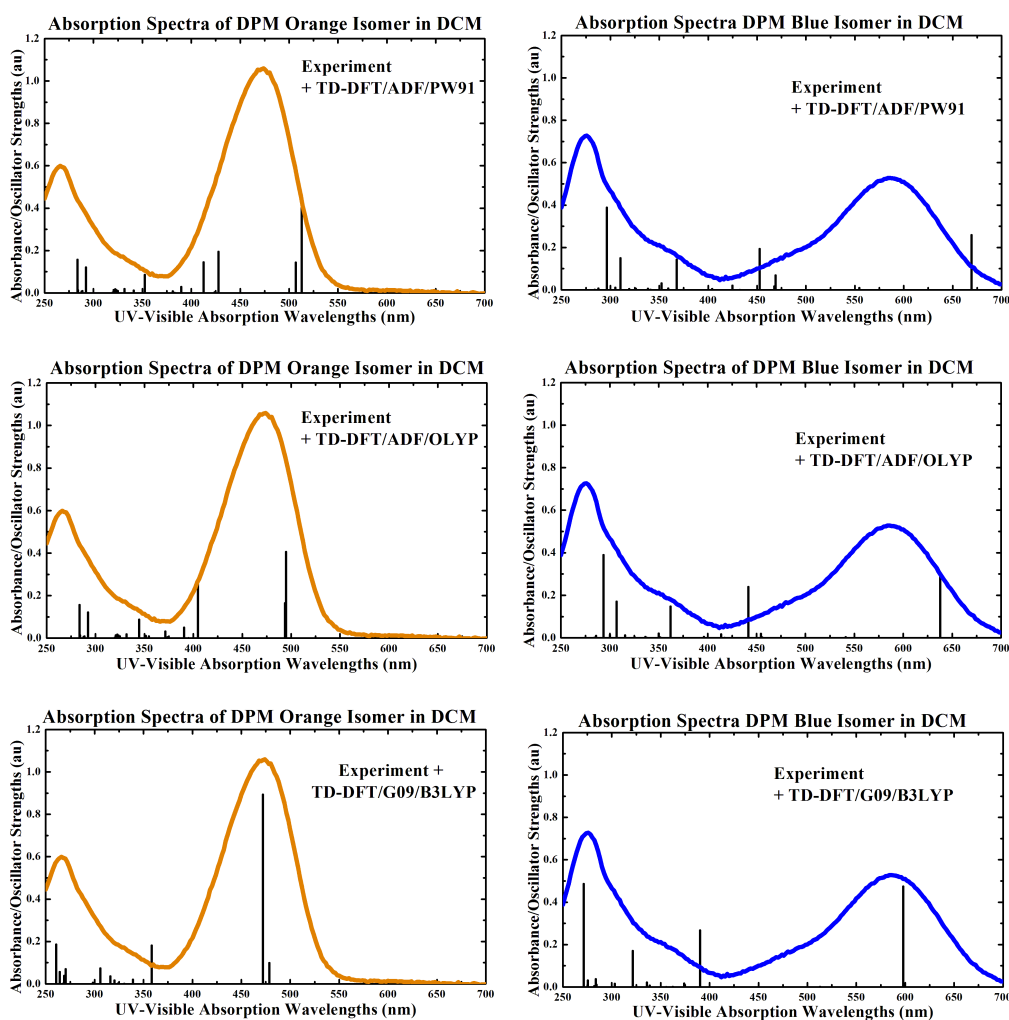


Figure 4.6: UV-VIS (curves) and Calculated (lines) Absorption Spectra of DPM Isomers.

the B3LYP functional and UV-VIS spectroscopy experiments. This is to investigate the best environment (choice of solvent in both calculation and experiment) in which the molecules respond most accurately when illuminated with light. We chose a non-polar solvent: cyclo-hexane; four polar aprotic solvents: dichloromethane (DCM), acetone, acetonitrile (MeCN), dimethylsulfoxide (DMSO) and two polar protic solvents: methanol and ethanol. All these solvents are available in Gaussian. We also calculated the DPM orange spectra in water but not experimentally because DPM would not dissolve in water.

The table of values for the experimental versus calculated secondary band, along with their dielectric constants, is presented in Table 4.3. Considering the values (experiment and calculation) presented in this table, DCM proves to be the best environment for the DPM orange isomer. More so, it is easier to convert the DPM orange isomer in DCM into its blue counterpart than in any other solvents we con-

sidered here. Therefore, our reference solvent for comparison shall be DCM. The solvents dependence of the orange isomer of DPM is illustrated in bathochromic or hypsochromic effects ⁶.

In water, the calculated orange isomer secondary band is 470 nm, about a 2 nm deviation from that of dichloromethane. In the blue isomer, this is 593 nm against the experimental value of 588 nm.

The experimental secondary band of DPM in cyclo-hexane (non-polar) is centered at (473 nm) against a calculated (495 nm). These are both bathochromic with respect to DCM.

In the polar protic solvents, starting with methanol, no shift was observed in the experimental secondary band (472 nm) of DPM, but the calculation (470 nm) shows a slight blue shift. In ethanol, the secondary bands obtained from calculation (495 nm) and experiment (476 nm) are both red-shifted.

Considering the polar aprotic solvents, the secondary band in both acetone and acetonitrile is centered at 470 nm, against the same calculated value of 495 nm. This shows that they have roughly the same external influence on DPM. Finally, in dimethylsulfoxide (DMSO), the secondary band is red-shifted in experiment (485 nm) and calculation (497 nm).

The plots for the spectra obtained for these solvents are given in Figures 4.7 and 4.8. Using the same concentrations, polar protic solvents showed an increased absorbance as against the non-polar solvent. This indicates that there is a stronger interaction between the functional groups of the solvents and that of DPM, and agrees with literature study on solvents' effect [52]. For the aprotic solvents, their absorbance ranked roughly the same with that of the non-polar solvent, except for DMSO that shows a high absorbance, relative to the protic solvents. The strong interaction exhibited by DMSO could be attributed to its high dielectric constant and dipole moment. Hence, DPM in DMSO was the most red-shifted (bathochromic), about 20 nm from that of DCM or methanol. In the overall analysis, DPM in DCM is the most promising with regards to the agreement between the experiment and calculation.

⁶Bathochromic effect refers to red-shift (longer wavelength) while hypsochromic effect refers to blue-shift (shorter wavelength).

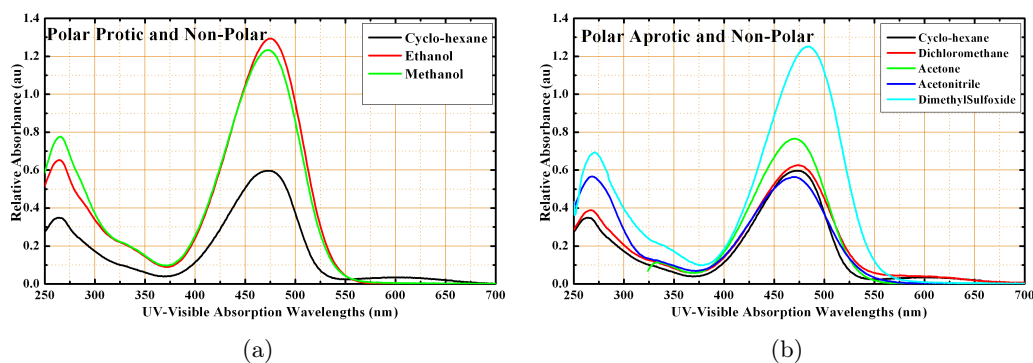


Figure 4.7: Steady State Absorption Spectra of DPM (a) Non-polar and Polar Aprotic and (b) Non-polar and Polar Protic Solvents.

Table 4.3: Solvent Dependence of the Dithizonatophenylmercury II Orange Isomer Showing Absorption Central Wavelengths.

Methods	G09/B3LYP/CEP-31G	UV/Visible	
Solvents	Calculated λ (nm)	Experimental λ (nm)	Dielectric Constant (ϵ)
Non-Polar			
Cyclo-hexane	495	473	2.023
Polar Protic			
Ethanol	495	476	24.55
Methanol	470	472	32.63
Polar Aprotic			
Dichloromethane	472	472	8.93
Acetone	494	470	20.7
Acetonitrile	494	470	36.64
Dimethylsulfoxide	497	485	46.7

4.4 Summary

1. The photo-isomerisation reactions of our molecules lead to a twisting motion around their chromophores (C=N), causing a dihedral rotation of 180° . This leads to the calculation of potential energy surface scans.
2. The potential energy barrier of 2.32 eV, using the rigid scan method, was obtained for the formalimine molecule. This is in the range of the previously calculated results [17]. The relaxed potential barrier obtained for DPM was 1.20 eV. The broken symmetry method was applied in estimating the true minima energies for the region around the DPM PES maxima.
3. The absorption wavelengths of formalimine are in the ultraviolet region of the EM spectrum with a maximum between 80 – 84 nm. The absorption spectra of DPM isomers extend from UV to visible, with two major absorption bands (primary and secondary). The secondary bands are at 472 nm for the orange (matching exactly with experiment), and 598 nm for the blue (with a deviation of 10 nm from the experiment).

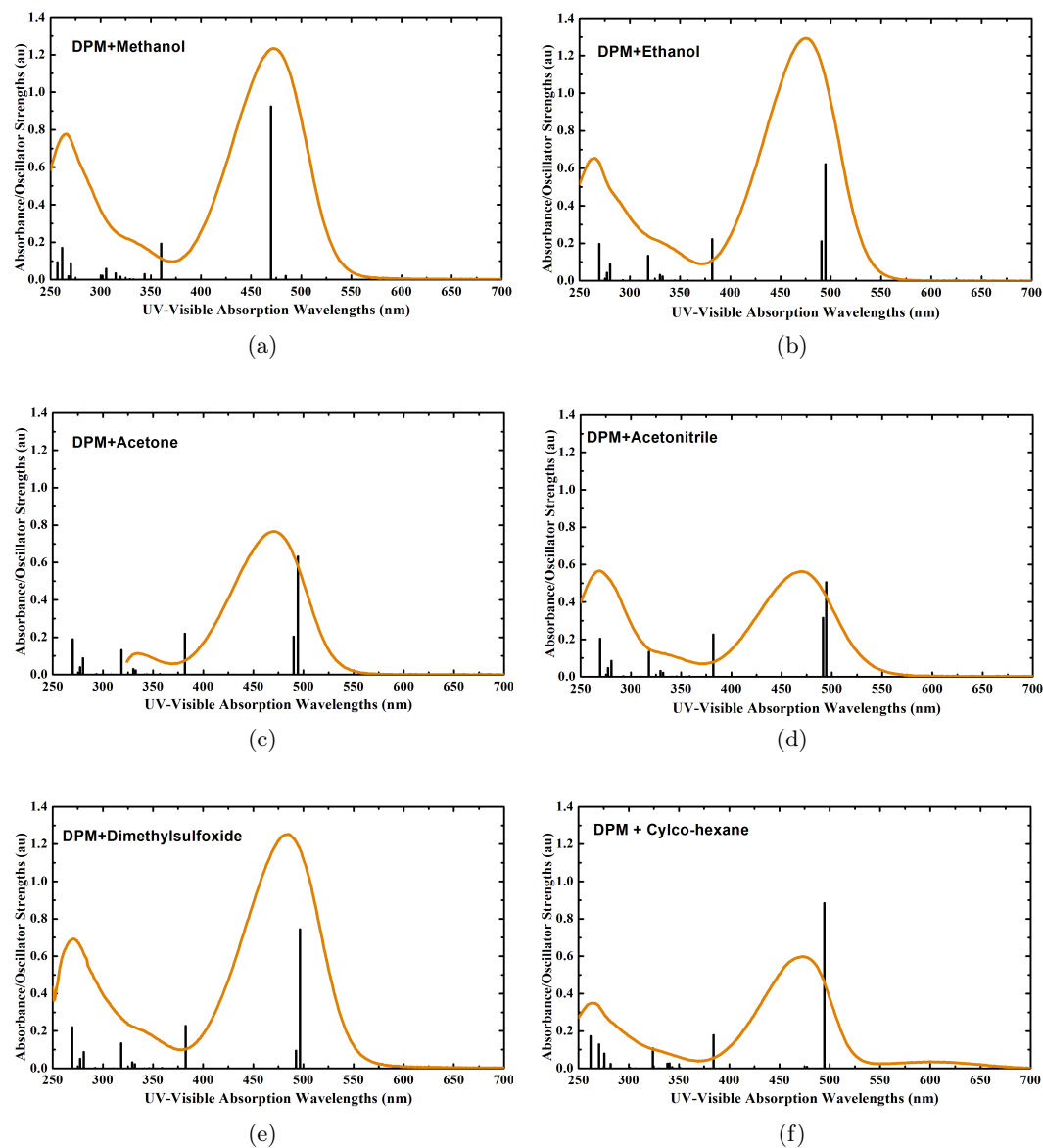


Figure 4.8: Experimental (curves) and Calculated (lines) Electronic Spectra of DPM Orange Isomer in (a) Methanol, (b) Ethanol, (c) Acetone, (d) Acetonitrile, (e) Dimethylsulfoxide and (f) Cyclo-hexane.

4. The B3LYP/CEP-31G combination, as implemented in Gaussian, gives the best approximation of the absorption spectra. This is attributed to the fact that the hybrid functional B3LYP tends to balance the errors associated with LDA and GGA functionals.
5. Of all the solvents used, methanol (polar protic) and dichloromethane (polar aprotic) show excellent agreement between the experiment and calculation. Hence, these are good solvents for DPM.
6. The concentration of DPM in polar protic solvents is high and thus they are characterised by high absorbance. Moreover, the polar aprotic solvents show low absorbance but DMSO shows an exceptionally high absorbance and is bathochromic (around 20 nm) when compared to that of DCM.

Chapter 5

Structural Optimisation of Electronically-altered Mercury Dithizonates

We shall now use what we have learnt in the last two chapters to study another set of molecules. In this chapter, we present the ground state properties of the electronically altered mercury dithizonates.

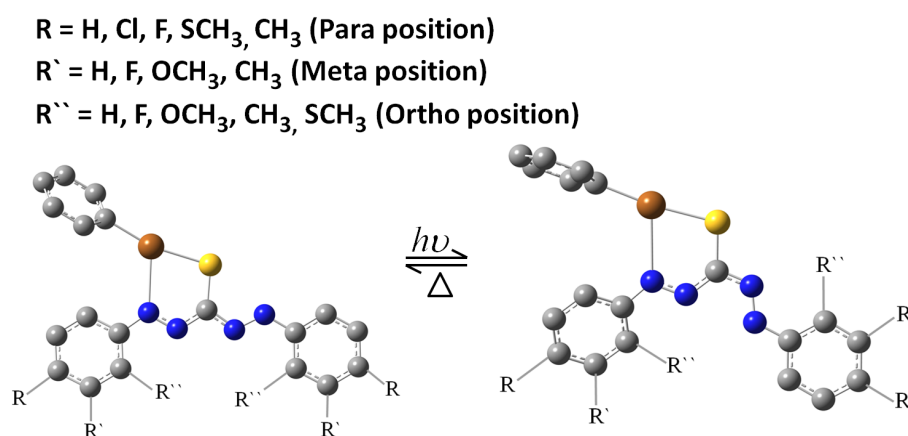


Figure 5.1: Schematic Structures of Substituted DPM Isomers. {Key: Orange: Hg; Yellow: S; Blue: N; and Dark Gray: C.}

5.1 Geometry Optimisation

To see how the atoms are labelled, we have painstakingly arranged and presented all the labellings, according to different positions of the substituents (see Figure 5.2). In Appendix A, the geometrical data of the selected optimised structures of the para-, meta- and ortho-substituted DPMs are presented in Tables A.2, A.3 and A.4, respectively. These molecules are also in two isomeric forms just as in non-substituted DPM. In essence, the properties investigated for DPM are also studied

here. Since these molecules were recently synthesized ¹, their X-ray crystallographic structural data are not available. Thus, in order to investigate the effects of the substituents on the dithizonato π -conjugated system, we compared our optimised data with their typical bond parameter values in literature ².

The process of optimisation of these molecules are of the same procedure as those of DPM and formalimine. We used the solvent, dichloromethane, for all the molecules considered in this chapter. As were listed in Chapter 1, we considered some electronic alterations to the dithizonato phenyl rings by substituting one of the hydrogen atoms at the para, meta and ortho positions of these phenyl rings.

In order to compare the combination, B3LYP/CEP-31G, we tried the two GGA functional, PW91 and OLYP with the same basis set, for the electronically altered molecules, but the former was again more accurate with regards to the absorption spectra and the potential energy surface scans presented in the next chapter. Thus, in the following, we present only the structural optimisations done by B3LYP/CEP-31G.

In DPM isomers, the root mean square deviations of the calculated optimised structure from the X-ray orange crystal structure were compared without the inclusion of the hydrogen atoms. This is acceptable because the dynamical effects – absorption spectra and isomerisation reactions – on the molecular orbitals of the mercury dithizonates, both substituted and non-substituted, solely border on the N-phenyl conjugated bonds which are mainly around the Ph-N-N-C-N-N-Ph dithizonato backbones of the molecules [2]. A close study of the overlaps between the phenyl- π orbitals and the p-orbitals of the nitrogen atoms directly attached to the phenyl rings shows that the former has a major effect on either retarding or allowing a free flow of the *cis-trans* isomerisation around C1-N3 double bond, which is situated at the chromophores of these molecules [2].

Thus, the most important geometry parameters are the bond lengths, C1-N3 and N3-N4, and the bond angle, S1-C1-N3. For all the substituents considered, these parameters stayed in the same range (See Tables A.2 – A.4). This tells us that the dihedral rotation in DPM is similar to those of the substituted DPMs.

As was reported in Ref. [2], the typical single and double bond lengths of C-N are 1.47 and 1.29 Å and for N-N, these are 1.45 and 1.25 Å, respectively. Our calculations here show a fair approximation in comparison to these values. For example, all our C-N single bond lengths fall within the range of 1.400 – 1.417 Å compared to the typical value of 1.47 Å. The double bond length values for C-N are within the range of 1.337 – 1.345 Å compared to the typical value of 1.29 Å. The N-N double bond lengths in our calculation fall between 1.305 – 1.310 Å compared to a typical value of 1.25 Å and the single bond lengths of the same are within 1.360 – 1.371 Å compared to a typical value of 1.425 Å. The fact that we have longer bond lengths in C=N and N=N than in C-N and N-N suggests that there is increased delocalisation of the π -electrons in our molecules.

Another interesting bond length in our molecules is the Hg-N bond. This bond is otherwise interpreted as a dative covalent bond; the lone pair electrons in the sp-

¹The crystalline forms of these molecules are being prepared by Dr. Karel von Eschwege of Chemistry Department, University of Free State, South Africa.

²The typical values are the norms for bond lengths or bond angles among the atoms in a molecule.

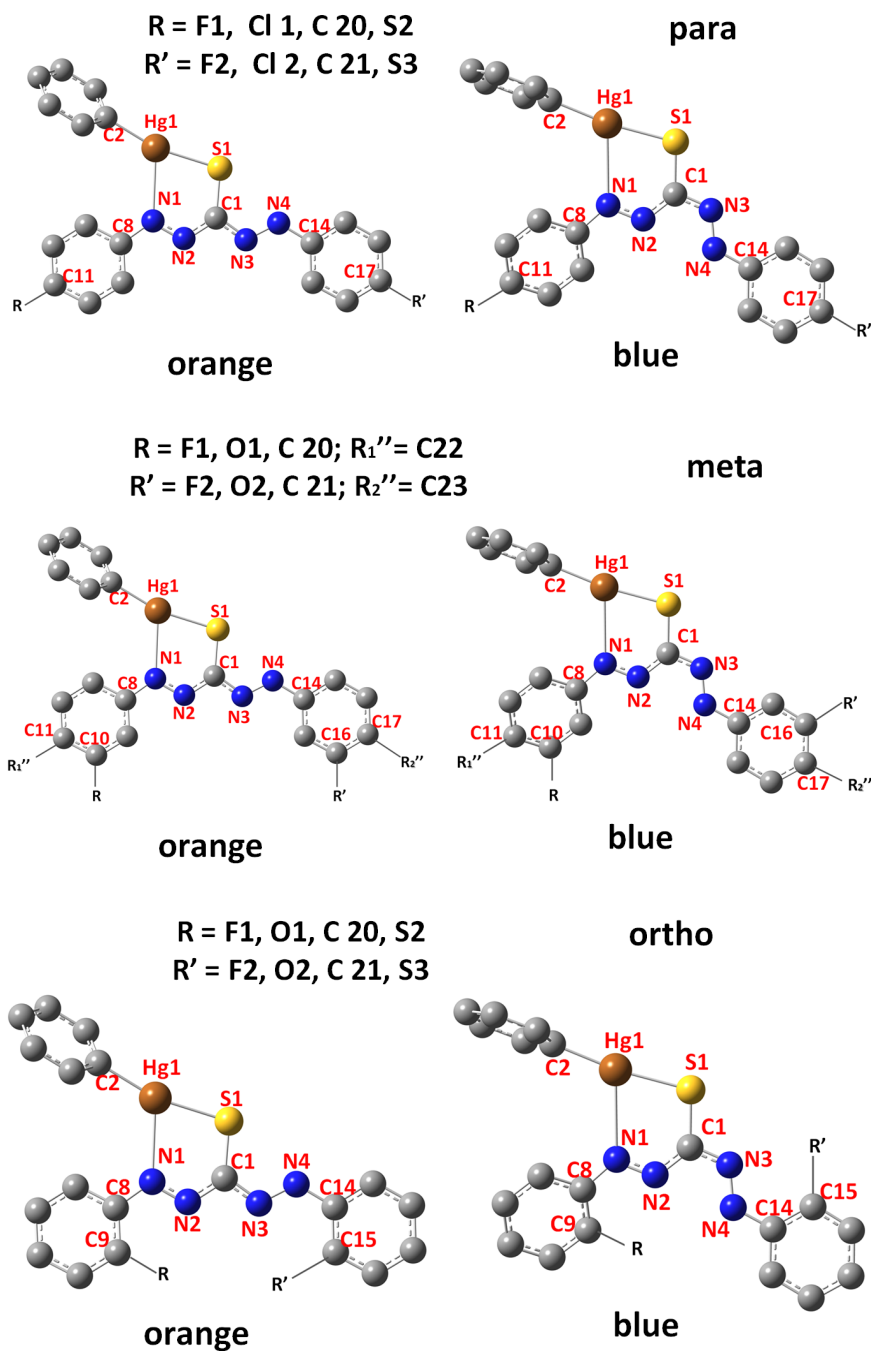


Figure 5.2: Structural Labelling of the Substituted Dithizonatophenylmercury II Isomers. {Key: Orange: Hg; Yellow: S; Blue: N; Gray: C.}

hybridized orbitals of the nitrogen atom could be deposited into an empty d-orbital of mercury. Calculated values of these bond lengths fall between 2.701 – 2.979 Å compared to a typical value of 2.651 Å. This gives an elongation of about 0.32 Å. The difference between the DFT calculated Optimised geometry parameters (bond lengths and angles) and X-ray crystal optimised structures have been attributed to the packing effects, restriction of movements among these bonds and the fact that DFT measurements are gas phase calculations [2].

Now, let us look at the bond lengths and bond angles between the phenyl rings and the substituted derivatives.

The first and foremost is the phenyl-fluorine bond lengths. This has been extensively studied [54, 55], especially with respect to the delocalized π -electrons along the phenyl rings and the possibility of hydrogen bonding with the fluorine atoms when they are very close (See Figure 5.2). The radius of an atom is one of the major factors that determines the bond length of the atom to other atoms. Fluorine has the highest electronegative value and a van der Waals' radius of 1.47 Å in contrast to 1.75 Å for chlorine [55]. As reported in Ref. [54], the typical values of phenyl-fluorine bond lengths are within the range of 1.332 – 1.349 Å and this compared fairly with our calculations which are in the range of 1.408 – 1.421 Å.

The phenyl-chlorine bond lengths which fall in the range 1.837 – 1.845 Å are longer than the fluorine counterpart as expected due to their longer van der Waals' radii. The carbon-sulphur bonds at the ortho and para positions are similar to the one attached to the central carbon atom (C1). The last is the carbon-oxygen bond lengths and these are in the range of 1.395 – 1.416 Å. The C-O-C and C-S-C bond angles are also reported in Tables A.2 – A.4.

The dihedral angles, S1-C1-N3-N4 (See Figure 5.2), are reported for all the molecules in the ground and the excited states. These angles typically show the *cis-trans* transformation from the orange to the blue isomers in our molecules. The dihedral angles for all our molecules are varied between 0 and 180° or –180 and 0°.

5.2 Energetic Details

The geometry optimisation of these molecules led to their electronic orange and blue ground states energy minima. The energy convergences obtained for the isomers of these molecules are similar to the ones we showed in Chapter 3 for formalimine and the DPM isomers (See Figures 3.6 and 3.7). Hence, we shall not present them here. However, we have listed in Table 5.1 the relative energy minima of the electronically altered DPM isomers. The energy differences between the orange and the blue ground states influence the stability of the different isomers (if the potential wells in between the isomers along all coordinates are similar); the higher the difference, the less stable the blue isomers and vice-versa. A close look at these energy minima shows that the typical energy difference between the orange and the blue isomers is ≤ 0.25 eV.

The fluorine-, sulphur-methyl- and methoxyl-substituted DPM isomers do show a level of stability in their blue isomers. This is attributed to the energy gaps between these isomers. We shall discuss this in more detail under the potential energy surface scans analysis presented in the next chapter.

Table 5.1: Ground State Energies of the Electronically-altered Blue Isomers Relative to Those of the Orange Isomers. R = Substituents.

Method/Basis Set	B3LYP/CEP-31G			
	para-substituents			
<i>R</i> -DPM	p-F	p-Cl	p-CH ₃	p-SCH ₃
SCF Energy (eV)	0.23	0.23	0.21	0.21
	meta-substituents			
<i>R</i> -DPM	m-F	m-CH ₃	m-OCH ₃	m-p-(CH ₃) ₂
SCF Energy (eV)	0.22	0.21	0.25	0.20
	ortho-substituents			
<i>R</i> -DPM	o-F	o-CH ₃	o-OCH ₃	o-SCH ₃
SCF Energy (eV)	0.04	0.20	0.06	0.05

5.3 Summary

In this chapter, we have presented the structurally optimised data obtained via B3LYP/CEP-31G combination for the electronically altered DPMs.

1. The most important bond lengths and bond angle that influence the dynamics of our molecules are C1-N3, N3-N4 and S1-C1-N3. These compare well with their respective typical values.
2. The influence of the substituents on the bond lengths and bond angles in our molecules are revealed through the longer bond parameters around the Ph-N-N-C-N-N-Ph dithizonato ligands' backbones due to the high degree of electron delocalisation.
3. The X-ray crystal structure of our molecules are not available. Based on the absorption spectra and the potential energy scans presented in the next chapter, the geometries used are valid because they give a close approximation to the experimental data.
4. The energy minima recorded here represent the orange and the blue isomers' ground states, and these point to the energy gaps between the two states.

We shall now present the results of the absorption spectra and potential energy surface scans for these molecules.

Chapter 6

Absorption Spectra and Potential Energies of Electronically-altered Mercury Dithizonates

Having done the structural optimisations of substituted DPM derivatives, the next thing is to investigate their active absorption regions through the DFT model and then compare the results with their steady state absorption spectra obtainable through UV-VIS spectroscopy. I shall also present the potential energy surface calculations of the molecules. Before going into the analysis of the results, I shall present some fundamental factors that will aid the understanding and the interpretation of the results.

6.1 Electro-chemistry, Hammett Constants and Absorption Spectra of Substituted DPM Molecules

For a proper understanding of the UV-VIS spectroscopy of these molecules, there are number of factors that should be considered. The first of these is the electro-chemistry property. For most of our substituted DPM molecules, these have been characterised in terms of first oxidation potentials, electron-donating groups (EDG) and electron-withdrawing groups (EWG). It was found that their first oxidation potentials decrease from the EWG (the substituents with fluorine (F) and chlorine (Cl)) to the EDG (other substituents) [59]:

o-F (917 mV) > m-F (765 mV) > p-F (723 mV) > o-Me (700 mV) > H (639 mV) > p-Me (638 mV) > m-OMe (613 mV) > m-Me (577 mV) > m-p-diMe (524 mV) > o-OMe (473 mV).

These oxidation potentials are results of cyclic voltammetry and we see that the o-F has the most electron withdrawing effect and o-OMe (ortho-methoxyl) the most electron donating effect [59]. The other molecules in our study that are not listed here are sandwiched into this trend based on their absorption spectra.

With respect to this, it is expected that the effects of the EDG on our molecules should present opposite absorption features when compared to those of the EWG. Considering the EWG, the depletion of electron density (delocalised π -electrons)

from the molecular orbitals of these molecules should increase their absorption energies or decrease their wavelengths. In contrast, the injection of electron density into the orbitals by the EDG should lower the energy and therefore increase the absorption wavelengths. These analyses should act as a rule of thumb for the interpretation of the electronically altered DPM excitation energies.

Another factor to consider are the Hammett constants obtained from the extended Hammett equations¹. A comprehensive table of values obtained from different authors over the years were compiled in Ref. [56]. Hammett constants of almost all the common substituents or substituents known in nature for the different positions on a benzylic (or a phenyl) ring have been suggested to be an aid to the interpretation of the π -conjugation strengths, the influence of the electron-donating and the electron-withdrawing substituents, and steric and resonance effects on any molecular orbital that is directly connected to phenyl or benzylic rings [56, 57, 58]. Of these properties, we are mainly interested in conjugation strengths of the orbitals of our molecules for they have major influence on their absorption wavelengths [51]. Any interested reader should look into Ref. [56] and other long lists of references given in the journal.

The effects of the substituents on molecular orbitals associated with phenyl rings have often been categorised according to the position of the substituents on the rings [56]. Particularly, it was reported in Ref. [57] that the substituents placed at the *para* and *ortho* positions should have a greater influence than the ones placed at the *meta* position. Just in line with this prediction, we found out that the shifts in the absorption wavelengths are much more pronounced for *para* and *ortho* substituents than for *meta* substituents (see Table 6.4.) The Hammett constants for these substituents have been categorised as a combination of "para & ortho" and "meta"; indicating that the effects observed from *para*-substituted radicals could also be used for *ortho*-substituted radicals [56, 57].

Another report on the effects of the substituents on the phenyl (or benzene) π -conjugation stated that the EWG have no influence on the position of the secondary band of the molecules but that the EDG always effect an increase in the wavelengths [51].

For the purpose of our study, we have ranked the substituents' positions separately. The EDG and EWG are also ranked separately. Based on the oscillator strengths, only some selected calculated absorption wavelengths of the molecules along with the corresponding experimental data are presented.

In the light of the above analysis, we see that different authors who have studied organic molecules in relation to UV-Vis spectroscopy, especially with substituted phenyl derivatives, have different views with regards to the interpretation of the absorption bands observed in organic molecules. We also observed a fluctuation if we should compare the absorption spectra of the molecules with the first oxidation potentials. Therefore, I shall interpret the following results in terms of wavelength shifts. The three main regions, the trough (minima), the primary and the secondary bands for the calculations and the experiments, are essentially analysed and com-

¹The Hammett constants are calculated as [56]: $\sigma_X = \log K_X - \log K_H$, where K_X is the ionisation constant for benzoic acid in water at 25°C and K_H is the corresponding constant for a *meta*- or *para*-substituted benzoic acid.

pared.

6.1.1 Analysis of the Para-substituted DPMs Absorption Spectra

In the following analysis, p-F is the most electron-withdrawing while p-SMe is the most electron-donating. The UV-VIS characterisations of the para-substituted isomers are given in Figure 6.1.

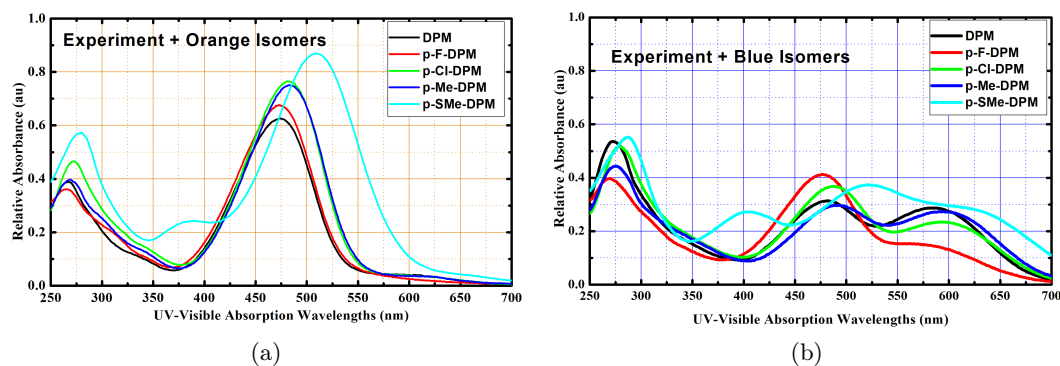


Figure 6.1: UV-Visible Absorption Spectra of (a) Orange and (b) Blue Isomers of the Para-substituted DPMs in Dichloromethane.

Let us analyse the orange isomers. With reference to the absorption bands of DPM, no shift was observed for the secondary and primary bands of p-F-DPM. It is however hypochromic in the primary band. There are slight red shifts of about 9 nm and 11 nm in the secondary bands as we move to p-Cl-DPM and p-Me-DPM, respectively, indicating more electron density in the delocalised π -conjugated system. Both of these appear to stay on top of each other (see Figure 6.1a). The primary absorption bands of p-Cl-DPM and p-SMe-DPM are red-shifted while others lie on top of one another. When more electrons are injected into the system, as we have in p-SMe-DPM, a huge red shift of about 37 nm is observed in the secondary band. At the shoulders of these absorption bands (near 375 nm), all the para-substituted DPMs ranked with that of DPM except for the p-SMe-DPM, which showed an active absorption peak around this region.

In the blue isomers (see Figure 6.1b), the primary bands (near 275 nm) of all the para-substituted DPM matched with that of DPM, except for p-SMe-DPM which shows a slight red shift. The shoulders (near 400 nm) of p-Me-DPM and p-Cl-DPM matched with that of DPM; p-F-DPM is blue shifted and p-SMe-DPM shows an absorption band around this region. The secondary bands of these molecules are all red-shifted compared to that of DPM. Again, p-SMe-DPM recorded the greatest red shift of about 26 nm from that of DPM. Of all the blue isomers, p-F-DPM and p-SMe-DPM revealed a quick conversion of their blue isomers into the orange isomers (see Figure 6.1b). These results show that the more electron-rich a substituent attached to the phenyl rings at the para position is, the longer the delocalised π -electrons and the longer is the wavelength into the visible spectrum.

We calculated these absorption spectra through solvent phase TD-DFT. The main active absorption regions of the calculated with a corresponding UV-VIS spectra are presented in Table 6.1. The first rows in the orange and the blue isomers show the secondary bands of the molecules. The plots of these bands (calculated vs. experimental) for the orange and the blue isomers are as shown in Figure 6.2. Starting with DPM isomers in the middle of this figure, we saw an accurate prediction. As we move from the electron-donating and electron-withdrawing groups, no regular pattern is observed but it is interesting to note that there are similar trends (i.e. treating EDG and EWG separately) for both the experiment and the calculation. These deviations are attributed to the errors associated with the approximations of the exchange-correlation functional and other models available in DFT.

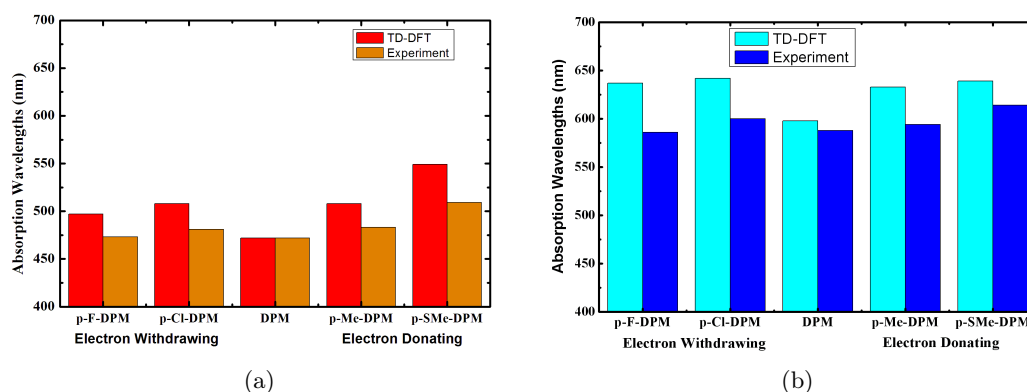


Figure 6.2: Experimental vs. Solvent (Dichloromethane) Phase TD-DFT Central Wavelengths of (a) Orange and (b) Blue Isomers of the Para-substituted DPM.

In the overall analysis, the spectra of the orange and the blue isomers of para-substituted DPM confirm that the more the number of electrons in our delocalised system, the longer the wavelength and vice-versa.

Table 6.1: Selected Singlet Excitations of the Para-substituted DPM Isomers. f: oscillator strength, λ : absorption wavelength, A: relative absorbance, Solvent: dichloromethane ($\epsilon = 8.9$), G09: Gaussian 09.

G09/B3LYP/CEP-31G															
Electron-withdrawing								Electron-donating							
p-F-DPM				p-Cl-DPM				p-CH ₃ -DPM				p-SCH ₃ -DPM			
Experiment		TD-DFT		Experiment		TD-DFT		Experiment		TD-DFT		Experiment		TD-DFT	
Orange Isomers															
λ (nm)	A	λ (nm)	f (au)	λ (nm)	A	λ (nm)	f (au)	λ (nm)	A	λ (nm)	f (au)	λ (nm)	A	λ (nm)	f (au)
473	0.677	497	0.814	481	1.529	508	0.888	483	0.781	508	1.008	509	0.490	549	1.115
ca. 374	0.071	385	0.250	375	0.081	393	0.279	377	0.066	385	0.150	381	0.245	409	0.224
ca. 322	0.160	322	0.139	333	0.150	333	0.171	341	0.128	341	0.151				
265	0.361	269	0.248	272	0.462	273	0.361	269	0.398	285	0.101	279	0.575	282	0.258
Blue Isomers															
λ (nm)	A	λ (nm)	f (au)	λ (nm)	A	λ (nm)	f (au)	λ (nm)	A	λ (nm)	f (au)	λ (nm)	A	λ (nm)	f (au)
586	0.150	637	0.394	600	0.466	642	0.440	595	0.274	633	0.511	614	0.579	639	0.563
ca. 340	0.143	340	0.164	399	0.206	393	0.018	352	0.167	352	0.160	400	0.282	390	0.082
270	0.398	281	0.378	279	1.032	285	0.251	277	0.443	285	0.208	285	0.541	296	0.256

6.1.2 Analysis of the Meta-substituted DPMs Absorption Spectra

Similarly, in the following: m-F is the most electron-withdrawing and m-p-dimethyl is the most electron-donating. The UV-VIS characterisations of the absorption spectra of orange and blue isomers of the meta-substituted DPMs are shown in Figure 6.3.

Starting with the orange isomers, m-F-DPM does not show any deviation in either the primary (near 275 nm) or the secondary (473 nm) bands when compared to that of DPM. The EDG, m-Me-DPM and m-OMe-DPM and m-p-diMe-DPM shows slight deviations and the most red-shifted is m-p-diMe-DPM, which is about 16 nm from that of DPM. All the orange isomers also ranked the same at the shoulders (near 375 nm). These meta-substituted orange spectra confirm that meta substituents do not have much effect on phenyl π -conjugated systems as proposed in Ref. [57, 51]. There is, however, a monotonic increase in their absorption wavelengths as we move from m-F-DPM to m-p-diMe-DPM (see Figure 6.3a and Table 6.2).

In the blue isomers (see Figure 6.3b), there was a quick conversion of the product into the reactant of m-Me-DPM and this was revealed in a very low absorbance of its secondary band. Comparing all the blue spectra with that of DPM, there are slight deviations (red shifts) in their secondary bands and m-Me-DPM recorded the highest red shift (about 22 nm from DPM). At the shoulders (near 400 nm), m-F-DPM and m-OMe-DPM ranked together with DPM; m-Me-DPM is blue-shifted and m-p-diMe-DPM is red-shifted (see Figure 6.3b).

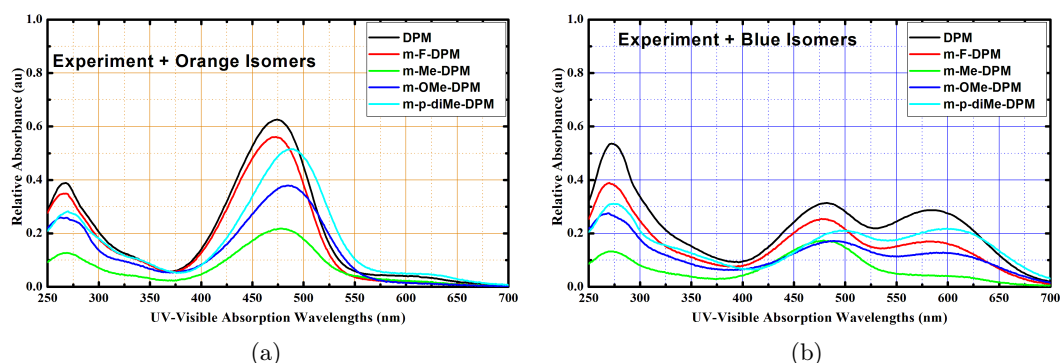


Figure 6.3: UV-Visible Absorption Spectra of (a) Orange and (b) Blue Isomers of the Meta-substituted DPMs in Dichloromethane.

Once again, we calculated these orange and blue spectra through our TD-DFT model. The selected calculated active absorption regions with their corresponding experimental values are shown in Table 6.2. The calculated orange spectra deviate from the experimental values as we move away from DPM, both towards the EWG and the EDG as shown in Figure 6.4a. However, similar trends are observed (monotonic increase in the absorption wavelengths) for both the experimental and calculated orange spectra. In the same vein, the calculated blue spectra also deviate from the experimental values but all are within the approximation errors of TD-DFT calculations (see Figure 6.4b and Table 6.2).

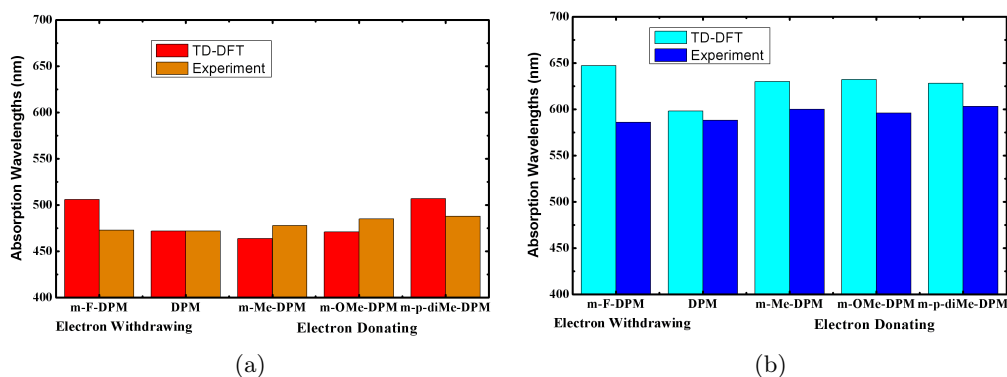


Figure 6.4: Experimental vs. Solvent (Dichloromethane) Phase TD-DFT Central Wavelengths of (a) Orange and (b) Blue Isomers of the Meta-substituted DPMs.

The overall observation revealed that the meta-substituted radicals do not have much influence on the spectra of DPM isomers. From the experimental data of the meta-substituted DPM isomers, we observed that the deviations in wavelengths from those of DPM isomers recorded are much shorter when compared to those of the para-substituted-DPMs.

Table 6.2: Selected Singlet Excitation Wavelengths of the Meta-substituted DPM Isomers. f : oscillator strength, λ : absorption wavelength, A : relative absorbance, Solvent: dichloromethane ($\epsilon = 8.9$), G09: Gaussian 09.

G09/B3LYP/CEP-31G															
Electron-withdrawing				Electron-donating											
m-F-DPM				m-CH ₃ -DPM				m-OCH ₃ -DPM				m-p-(CH ₃) ₂ -DPM			
Experiment		TD-DFT		Experiment		TD-DFT		Experiment		TD-DFT		Experiment		TD-DFT	
Orange Isomers															
λ (nm)	A	λ (nm)	f (au)	λ (nm)	A	λ (nm)	f (au)	λ (nm)	A	λ (nm)	f (au)	λ (nm)	A	λ (nm)	f (au)
473	0.561	506	0.634	478	0.218	464	0.804	485	0.379	471	0.739	488	0.516	507	1.023
		489	0.123												
ca. 374	0.057	394	0.309	364	0.025	365	0.155	371	0.055	371	0.146	382	0.054	381	0.135
ca. 317	0.129	317	0.143	349	0.032	349	0.115					339	0.102	339	0.167
268	0.349	267	0.145					263	0.259	272	0.111	270	0.283	279	0.103
Blue Isomers															
λ (nm)	A	λ (nm)	f (au)	λ (nm)	A	λ (nm)	f (au)	λ (nm)	A	λ (nm)	f (au)	λ (nm)	A	λ (nm)	f (au)
586	0.170	647	0.362	610	0.038	630	0.452	596	0.128	632	0.454	600	0.217	628	0.543
ca. 392	0.076	400	0.037	370	0.028	343	0.251	394	0.064	408	0.058	415	0.066	427	0.185
272	0.384	279	0.197	269	0.126	279	0.098	266	0.273	281	0.122	275	0.310	287	0.041

6.1.3 Analysis of the Ortho-substituted DPMs Absorption Spectra

Finally, we present the absorption spectra of the ortho-substituted DPM isomers. Here, o-F is the most electron-withdrawing group while o-OMe is the most electron-donating. The UV-VIS characterisations of these isomers are given in Figure 6.5.

Just as in para and meta, the spectrum of the orange isomer of the fluorine-substituted DPM, o-F-DPM, shows no deviation in its primary and secondary absorption bands when compared to those of DPM. In the orange EDGs, o-Me-DPM

is blue shifted (about 6 nm) from DPM. We observed red shifts of about 19 nm and 26 nm for *o*-SMe-DPM and *o*-OMe-DPM, respectively. At the troughs (near 375 nm), they appear to rank together with the exception of *o*-Me-DPM that is blue-shifted around this region. More so, *o*-OMe-DPM shows an active absorption wavelength near 650 nm.

In the blue isomers (see Figure 6.5b), *o*-F-DPM again absorbs at a close range to DPM. Both *o*-Me-DPM and *o*-SMe-DPM record slight red shifts in their secondary bands with a decreased absorbance. This is attributed to the fast back reaction from the products to their reactants. It is interesting to note that *o*-OMe-DPM, which is the most red shifted, shows an almost perfect spectrum of the blue isomer with no appearance of the orange isomer's. The troughs (near 400 nm) of all the ortho-substituted blue isomers ranked together.

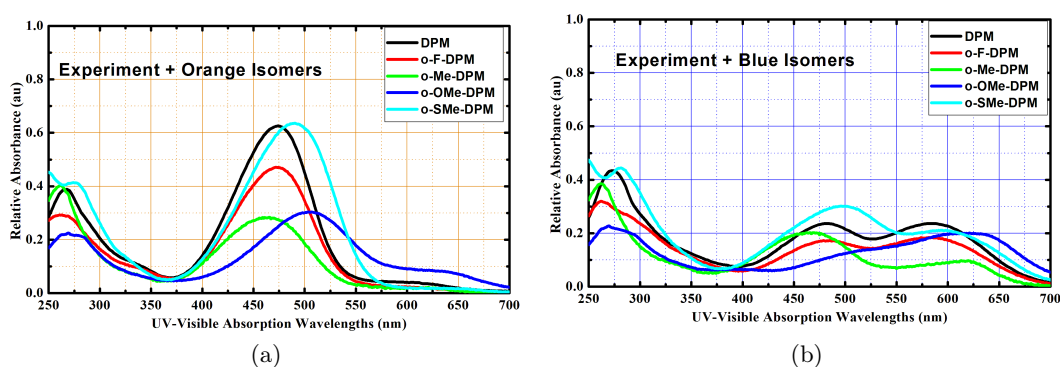


Figure 6.5: UV-Visible Absorption Spectra of the (a) Orange and the (b) Blue Isomers of Ortho-substituted DPM in Dichloromethane

We also calculated the spectra of the ortho-substituted DPM isomers. In the calculated orange spectra (See Figure 6.6a), starting from DPM, as we moved along the EDGs, I expected that the injection of more electron density into our delocalised system would lower the energy (or increase the wavelengths into visible spectrum). This was the case for *o*-Me-DPM and *o*-SMe-DPM but the rule failed for *o*-OMe-DPM. The comparison of the experimental and calculated spectra did rank well for *o*-Me-DPM and *o*-SMe-DPM but failed to show a similar trend for *o*-OMe-DPM. In Figure 6.6b, the calculated spectra of the blue isomers reveal a better approximation to the experimental data, as compared to those in the para and meta positions. Except for *o*-F-DPM and *o*-SMe-DPM that showed high deviations, the calculated blue spectra of *o*-Me-DPM and *o*-OMe-DPM are within a few nanometers from the experimental data. The data for the calculated active absorption regions of all the ortho-substituted isomers with their corresponding experimental values are given in Table 6.3.

The overall analysis of these spectra, both in the orange and the blue isomers, show better approximations compared to what we obtained at the para and meta positions.

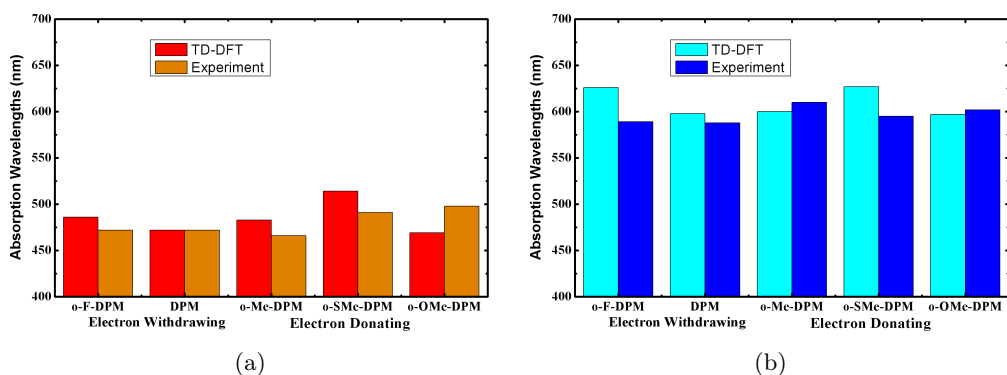


Figure 6.6: Experimental vs. Solvent (Dichloromethane) Phase TD-DFT Central Wavelengths of (a) Orange and (b) Blue Isomers of the Ortho-substituted DPMs.

Table 6.3: Selected Singlet Excitation Wavelengths of the Ortho-substituted DPM Isomers. f : oscillator strength, λ : absorption wavelength, A : relative absorbance, Solvent: dichloromethane ($\epsilon = 8.9$), G09: Gaussian 09.

G09/B3LYP/CEP-31G															
Electron-withdrawing				Electron-donating											
o-F-DPM				o-CH ₃ -DPM				o-OCH ₃ -DPM				o-SCH ₃ -DPM			
Experiment		TD-DFT		Experiment		TD-DFT		Experiment		TD-DFT		Experiment		TD-DFT	
Orange Isomers															
λ (nm)	A	λ (nm)	f (au)	λ (nm)	A	λ (nm)	f (au)	λ (nm)	A	λ (nm)	f (au)	λ (nm)	A	λ (nm)	f (au)
472	0.471	486	0.834	466	0.142	483	0.625	498	0.301	469	0.793	491	0.636	514	0.516
<i>ca.</i> 375	0.056	375	0.317	366	0.023	368	0.164	369	0.049	378	0.108	369	0.051	368	0.226
265	0.291	266	0.457	312	0.052	310	0.105	351	0.055	353	0.103	274	0.414	278	0.214
262		262	0.400	274		274	0.075	269		272	0.102	274		278	0.214
Blue Isomers															
λ (nm)	A	λ (nm)	f (au)	λ (nm)	A	λ (nm)	f (au)	λ (nm)	A	λ (nm)	f (au)	λ (nm)	A	λ (nm)	f (au)
589	0.184	626	0.384	610	0.047	600	0.473	602	0.199	597	0.427	595	0.211	627	0.447
<i>ca.</i> 400	0.059	416	0.282	352	0.030	357	0.036	397	0.065	395	0.095	377	0.068	377	0.051
268	0.313	280	0.495	262	0.193	285	0.061	274	0.220	297	0.039	282	0.444	289	0.251

Generally, we present the central absorption wavelengths (secondary bands) of the calculated and the steady state absorption spectra together with the Hammett constants of our molecules in Table 6.4. Comparing the calculated spectra with those of the experiment, we observed that the trend is similar for most of them: A decrease (blue-shifted) in the wavelengths of the calculated spectra corresponds to a decrease in the experimental spectra; an increase (red-shifted) in the wavelengths of calculated spectra also corresponds to an increase in the experimental spectra. The Hammett constants [56] also show this trend. Unfortunately, the Hammett constants for some of the radicals are not available in literature.

6.2 Broken Symmetry Calculation and Ground State Potential Energy Surface

As we mentioned in Chapter 4, the potential energy surface calculations are accessed through restricted closed shell and unrestricted open shell calculations. The com-

Table 6.4: Central Absorption Wavelengths and Hammett Constants [56] of the Electronically-altered DPMs.

Isomers R-DPM	Orange		Blue		Hammett Constants (σ)	
	Calculated (nm)	Experiment (nm)	Calculated (nm)	Experiment (nm)	Aqueous	Gas Phase
No substituent						
H	472	472	598	588	0	0
Para-substituents						
p-F	497	473	637	586	0.12	0.38
p-Cl	508	481	642	600	0.46	0.58
p-Methyl	508	483	633	594	-0.34	-0.14
p-S-Methyl	549	509	639	614	0	-
Meta-substituents						
m-F	506	473	647	586	0.68	0.50
m-Methoxyl	471	485	632	596	0.24	0.06
m-Methyl	464	478	630	610	-0.14	-0.10
m-p-di-Methyl	507	488	628	600	-0.96	-
Ortho-substituents						
o-F	486	472	626	589	-	-
o-Methyl	483	466	600	610	-	-
o-S-Methyl	514	491	627	595	-	-
o-Methoxyl	469	498	597	602	-	-

bination of these two methods essentially leads to the smoothness of the potential energy surface at maximum. The potential energy barriers are estimated as the difference between the energy minima at 0° and 90° dihedral angles. These barriers are presented in Table 6.5 and Figure 6.11.

6.2.1 Ground State Potential Energy Surface of the Para-substituted DPMs

The potential energy surface calculations in terms of SCF energies and dihedral angles obtained for the para-substituted DPMs are given in Table D.2 and Figure 6.7. The energies given in Figure 6.7 are relative to the minimum energies at 0° dihedral angles and these are -9994.30 eV, -9490.43 eV, -9084.60 eV and -9635.01 eV for p-F-DPM, p-Cl-DPM, p-Me-DPM and p-SMe-DPM, respectively.

Of these PES calculations, p-Cl-DPM, which is electron-withdrawing with a potential barrier of 1.38 eV was stable around its orthogonal geometry. As a result, a spin restricted closed shell calculation was sufficient for all its dihedral angles. The PES calculations of p-F-DPM, p-Me-DPM and p-SMe-DPM involved the use of broken symmetry (unrestricted open shell) for the dihedral angles between $70 - 120^\circ$, while other angles are stable with the restricted closed shell calculations. The potential barriers recorded for them are 1.21 eV, 1.20 eV and 1.18 eV, respectively. These are in the same range of value as that of non-substituted DPM.

As shown in Figure 6.7, except for p-Cl-DPM, the potential energy calculations of all the para-substituted DPM lie on top of that of DPM, with slight deviations around the orthogonal geometry. As expected, p-SMe-DPM, which has the most electron-donating substituent, has the lowest potential barrier. This expectation stems from our rule of thumb: the longer the delocalised π -electrons, the lower the energy needed for excitation. We expect that p-F-DPM would give us the highest barrier, but it is interesting to note that it only deviates from that of DPM by 10 meV. However, we are not totally surprised because the absorption spectra for all the fluorine-substituted DPM showed little or no deviation from that of DPM.

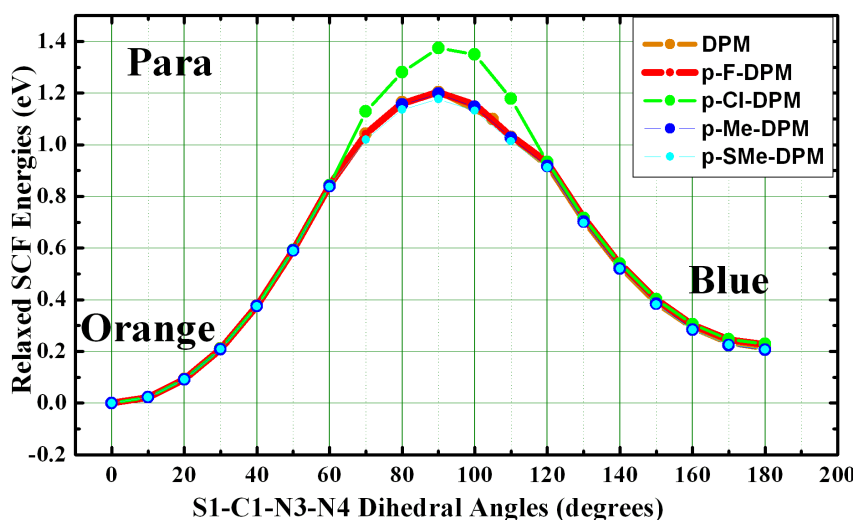


Figure 6.7: Relaxed Ground State Potential Energy Surfaces of Para-substituted DPM. Method: G09/B3LYP/CEP-31G.

In contrast to this, p-Cl-DPM shows the highest barrier, to the tune of an 0.2 eV increase when compared to that of DPM. For p-Methyl-DPM, its stability failed at a 70° dihedral angle, showing no deviation. No trend was observed for the potential barriers of the para-substituted DPMs, (see Figure 6.11a).

The overall analysis of these para-substituted DPMs potential energy curves reveals an absolute smoothness at the orthogonal geometry and the differences² between the orange ground states and the blue ground states of all the para-substituted DPM rank between 210 – 230 meV.

6.2.2 Ground State Potential Energy Surface of the Meta-substituted DPMs

The same procedure as above was performed in calculating the ground state PES of the meta-substituted DPM molecules. It was, however, more difficult to obtain these calculations than it was for the para-substituted DPM molecules. The steric effects associated with dihedral rotations seemed to be more pronounced on the phenyl ring attached to the mercury atom. The dihedral angles near the orthogonal geometries of the meta-substituted molecules appeared to require much energy in order to stay at the orientations enforced for their calculations. As such, we observed different influences on their potential energy barriers when compared to the non-substituted DPM. For all the calculations here, we used a broken symmetry calculation for the dihedral angles, 70–120°. The results are presented in Table D.3 and Figure 6.8. The energies given in Figure 6.8 are also relative to the minimum energies at 0° dihedral angles. These are –9994.31 eV, –9951.80 eV, –9084.61 eV and –9457.33 eV for m-F-DPM, m-OMe-DPM, m-Me-DPM and m-p-diMe-DPM, respectively.

²This is estimated as the difference between the energy minima at 0° and 180°.

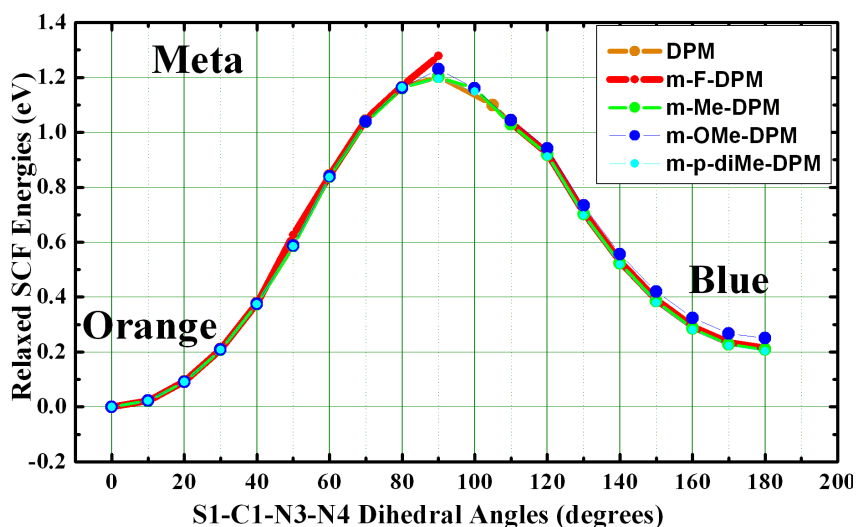


Figure 6.8: Relaxed Ground State Potential Energy Surfaces of Meta-substituted DPM. Method: G09/B3LYP/CEP-31G.

The most troublesome meta-substituted DPM is m-F-DPM. The orientations of the molecule at dihedral angles 90° and 100° appeared (during optimisation) to favour in-plane inversions rather than twisting rotations. As such, local minima were obtained. Several repetitions of geometry optimisation resulted in the convergence of 90° dihedral orientation but it failed at 100° . The barrier recorded for m-F-DPM is 1.28 eV, indicating an increase of about 80 meV from that of DPM.

For the EDGs, m-OMe-DPM, m-Me-DPM and m-p-diMe-DPM, we recorded potential barriers of 1.23 eV, 1.21 eV and 1.19 eV, respectively. Comparing these barriers to that obtained for DPM, we observed a slight barrier shift, ranging from 10 – 30 meV, as we move from m-p-diMe-DPM to m-OMe-DPM. As expected, m-p-diMe-DPM gives the lowest barrier while m-F-DPM gives the highest barrier.

The overall analysis for these meta-substituted DPM molecules shows a monotonic decrease in the potential barriers as we move from m-F-DPM to m-p-diMe-DPM, (see Figure 6.11b). The potential energy surfaces of the meta-substituted DPMs appear less smooth, and this is mainly revealed in m-F-DPM. The energy gaps between the orange ground states and the blue ground states is around 200–250 meV.

6.2.3 Ground State Potential Energy Surface of the Ortho-substituted DPMs

Finally, let us consider the potential energy surface calculations of the ortho-substituted DPMs. Broken symmetry calculation was used for all the $70 - 120^\circ$ dihedral angles. The results obtained here are given in Table D.4 and Figure 6.10. Again, the energies given in Figure 6.10 are relative to the minimum energies at 0° dihedral angles and these are -9993.65 eV, -9084.33 eV, -9951.09 eV and -9634.53 eV for o-F-DPM, o-Me-DPM, o-OMe-DPM and o-SMe-DPM, respectively.

The calculations here portrayed the highest level of complexity and this is attributed to the close contact of the hydrogen atom attached to N4 in the ortho-

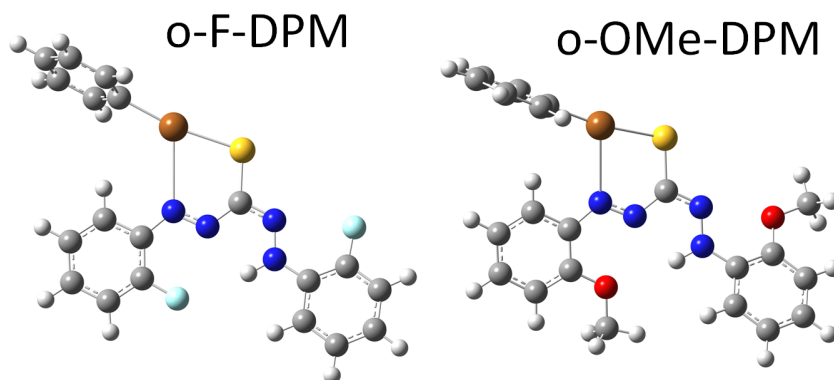


Figure 6.9: The Blue Isomers of o-F-DPM and o-OMe-DPM. {Key: Orange: Hg; Yellow: S; Blue: N; Dark Gray: C; Light Gray: H; Cyan: F; Red: O.}

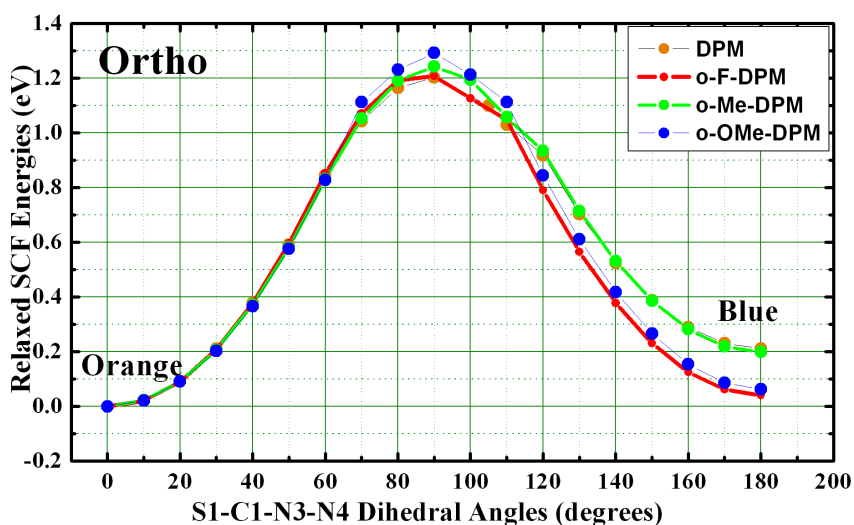


Figure 6.10: Relaxed Ground State Potential Energy Surfaces of Ortho-substituted DPM. Method: G09/B3LYP/CEP-31G.

substituted DPM blue isomer configurations (See Figures 6.9).

Of these, there is a possibility of a new bond formation between the fluorine and hydrogen in the blue isomer of o-F-DPM, and also between oxygen and hydrogen in the blue isomer of o-OMe-DPM. More so, we found that the more electron density we inject into our delocalised system, the more difficult it is for the twisting rotation, especially at the ortho position. Due to this difficulty, we could not get the true energy minima at 80 and 90° dihedral angles of the o-SMe-DPM as shown in Table D.4. In essence, the broken symmetry calculations for o-SMe-DPM did not result in true minima; its geometries around the orthogonal region returned to their initial optimisations. Hence, we could not calculate the barrier and this is why it was left out of the plots shown in Figure 6.10.

The EDG, o-F-DPM gave a potential barrier of 1.21 eV, indicating an increase

of 40 meV as compared to that of DPM. For the EWG, o-Me-DPM gave a barrier of 1.24 eV, which is about 40 meV more than that of DPM. Moving to o-OMe-DPM, the potential barrier increases to 1.29 eV.

The overall analysis shows that the potential energy barrier increases monotonically as we move from the o-F-DPM to the o-OMe-DPM. This is contrary to the rule of more electrons, more energy, for the barrier increases when more and more electrons are donated to our delocalised system. Moreover, it is interesting to note that o-F-DPM, o-SMe-DPM and o-OMe-DPM almost closed the energy gaps between their reactants and products to the tune of 40 meV, 50 meV and 60 meV, respectively. The energy gap between the reactant and the product of o-Me-DPM stands at 200 meV. The smoothness around the orthogonal geometries of the ortho-substituted DPMs are better than those with meta-substituents.

In conclusion, the relative stability of the products of all the substituted DPMs could be inferred from the difference in their energies. The barriers between the reactants and the products affect the rate at which the high energy conformation inter-converts to the lower energy one. If the barrier to convert the lower energy one is high, the life-time of the higher energy conformation as a meta-stable state increases. However, their excited state properties in connection to the model of Figure 4.2 are difficult to analyse and no simple rule could be applied to understand their behaviour during de-excitations. We predict that the life times of the ortho-substituted DPM molecules in the blue excited states should be the greatest when compared to those in para and meta positions based on the values given in Table 6.5. The conical intersections in these molecules act as funnels for ultrafast transfer from the excited to the ground state potential energy surfaces [60, 61].

Table 6.5: Potential Energy Barriers of the Non-substituted and Substituted DPMs. O:Orange and B:Blue.

R-DPM	Barrier Energies (eV)	Δ (O-B) (eV)
H	1.20	0.22
p-F	1.21	0.23
p-Cl	1.38	0.23
p-Methyl	1.20	0.21
p-S-Methyl	1.18	0.21
m-F	1.28	0.22
m-Methoxyl	1.23	0.25
m-Methyl	1.21	0.21
m-p-Dimethyl	1.19	0.20
o-F	1.21	0.04
o-Methyl	1.24	0.20
o-Methoxyl	1.29	0.06
o-S-Methyl	-	0.05

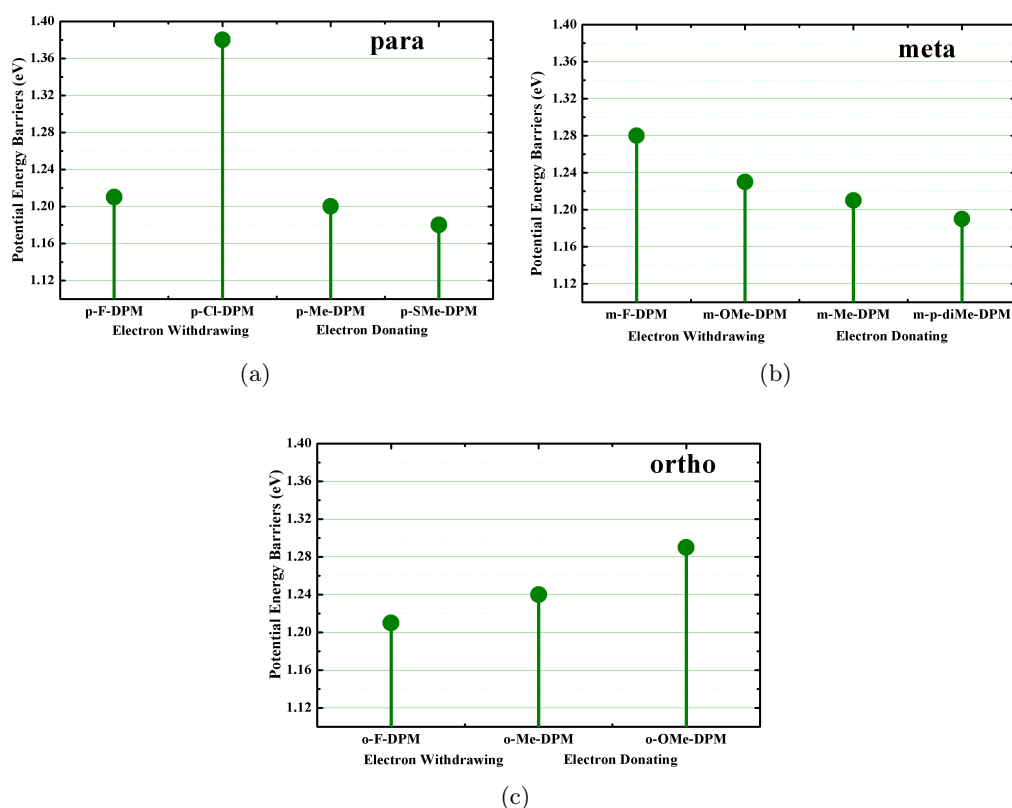


Figure 6.11: Ground State (S_0) Potential Energy Barrier Plots for the (a) Para-, (b) Meta- and (c) Ortho-Substituted DPMs.

6.3 Summary

We have presented the absorption spectra and the ground state potential energy surface calculations of the electronically altered DPM isomers in this chapter.

1. The absorption spectra of our molecules are analysed in terms of the shifts observed and this could be either bathochromic (red shift) or hypsochromic (blue shift).
2. The spectra observed experimentally and those calculated for para, meta and ortho positions showed similar trends (wavelength shifts); they increased or decreased simultaneously as shown in Table 6.4.
3. The potential energy calculations are obtained via broken symmetry (spin restricted open shell) and spin unrestricted closed shell calculations. Of the three positions considered: para, meta and ortho; the difficulties experienced in accessing true minimum energy for the PES calculations increased from para to ortho positions.
4. The potential energy barrier increases monotonically for the ortho substituents, from EWG to EDG; it decreases monotonically for the meta's and no trend

was observed for the para's.

5. In the overall analysis, we found that the more electron-rich the substituents at the para and ortho positions are, the longer the wavelengths of our molecules, and vice versa. For the meta positions, the radicals have little or no influence.

Chapter 7

Conclusion and Outlook

A set of photochromic molecules, dithizonatophenylmercury II and its derivatives have been studied. Starting from their kernel molecule, formalimine, a systematic study of the structural optimisations, the absorption spectra and the ground state potential energy curves of these molecules was carried out through numerical simulations afforded by density functional calculations and experimental analysis via UV-Vis spectroscopy. Through the concept of electron density proposed by Hohenberg and Kohn and a convenient matrix equation for easy computer codes provided by Kohn and Sham, the rather difficult Schrödinger electronic Hamiltonian was iteratively solved. Of all the DFT methods used in this study, the functional, B3LYP, combined with the basis sets, CEP-31G and 6-31G(d), gave the overall best approximations to the experimentally observed data. It was emphasized that the structural optimisations of these molecules essentially led to the estimation of their ground state energy minima. From these energy minima, both the absorption spectra and the potential energy surface scans could be accessed. The absorption spectra (singlet-singlet excitations), treated in terms of absorption wavelengths and oscillator strengths, were obtained from time-dependent density functional calculation (TD-DFT) and these were compared to the steady states spectra obtained from the UV-Vis spectroscopy experiments. Moreover, the potential energy calculations, treated in terms of dihedral angles and self consistent field (SCF) energies, were obtained through the use of spin restricted closed shell and the spin unrestricted open shell (otherwise known as broken symmetry) calculations.

First, we found that the structural optimisations of formalimine were in good agreement with previous calculations and thus, its ground state energy minimum led to calculated absorption spectra; emphasizing the lowest excitation energy of 5.0 – 5.4 eV, which was also found in literature. It was found that the absorption wavelengths with maximum oscillator strengths in formalimine ranged from 80 – 84 nm and as such, it could not be accessed through femto second experiments. The potential energy barrier of formalimine was found to be 2.32 eV (double that of DPM) using the rigid scan method and this also compared with what was found in literature.

Furthermore, the structural optimisation of DPM isomers gave a convincing agreement with X-ray crystal data and a previous calculation. This then led to an excellent approximation of the orange spectra with respect to the experiment centered

at 472 nm, and the calculated spectra of the blue isomer centered at 598 nm only deviated by 10 nm from the experiment's. This was found to be in good agreement with previous calculations. Using the relaxed scan method, DPM, in both methanol and dichloromethane (DCM), gave a potential barrier of 1.20 eV, indicating no dependence on solvents.

In the study of solvent dependence of the DPM orange isomers, the overall analysis showed a bathochromic effect (red-shifted) as we moved from DCM to dimethylsulfoxide (DMSO). This is attributed to a higher dielectric constant and dipole moment of DMSO. DPM dissolved in polar aprotic (except for DMSO) and non-polar solvents generally gave low absorbance while it gave high absorbance when dissolved in polar protic solvents. Methanol and DCM were found to be the best solvents for DPM due to the excellent agreement between the calculation and experiment.

Through the injection (or depletion) of electrons, which elongates (or shortens) the delocalised π -conjugation along the Ph-N1-N2-C1-N3-N4-Ph molecular orbitals of the electronically altered DPM isomers, we found that regardless of the position and the nature of the substituents, the optimised bond lengths and angles did not show significant deviations when compared to those of non-substituted DPM isomers. However, other bond lengths and angles, especially across the dithizonato ligand's backbone, were either shortened or elongated. The calculated absorption spectra of the electronically altered DPM molecules were found to have similar trends to the experiments for the para and meta substituted DPM isomers while there were fluctuations in the wavelength shifts for those of the ortho-substituted DPM isomers.

From the most EWR, o-F-DPM, to the most EDR, p-S-Methyl-DPM, the experimental orange absorption spectra generally revealed primary bands around 250 – 275 nm and the secondary bands around 463 – 508 nm against the calculated primary bands around 250 – 275 nm and secondary bands around 469 – 548 nm. The blue isomers gave an experimental spectral range of 250 – 275 nm (primary bands) and 586 – 610 nm (secondary bands) against the calculated spectral ranges of 250 – 275 nm and 597 – 647 nm, for the primary and the secondary bands, respectively. Due to the inability to transform all the *orange specie* to the *blue specie*, the secondary bands of the *orange* appeared in the *blue* spectra.

Finally, we observed a monotonic increase in the potential energy barrier of the ortho-substituted DPMS, from EWR to EDR. In the meta substituents, the barrier decreased monotonically as we moved from the EWR to the EDR. No trend was observed for the para substituents. The energy difference between the orange and the blue isomers ranged between 0.2 – 0.25 eV; except in o-F-DPM, o-OMe-DPM and o-SMe-DPM for which we recorded 40 meV, 60 meV and 50 meV, respectively. The difficulty experienced in potential energy surface scans of the DPM derivatives grew from para to ortho positions. There are chances that the forbidden crossing region of the conical intersection will be avoided in these molecules due to the associated fast back reactions. In overall comparison, the results obtained from DFT calculations deviated from experimental values but the errors are within the margin of DFT approximations.

A current outlook is on the extensive study of vibrational modes (frequencies) (accessible through DFT model) and the excited state potential energy surfaces calculation of these molecules (not accessible through DFT but may be possible within another model).

Appendices

Appendix A

Photochromism and Geometrical Data of Substituted DPMs

A.1 Photochromic Effects

Only p-SMe-DPM and o-OMe-DPM have different colours in their ground states.

Table A.1: Colour Changes in our Molecules

Molecule	Ground States	Excited States
DPM	Orange	Blue
p-F-DPM	Orange	Blue
p-Cl-DPM	Orange	Blue
p-Me-DPM	Orange	Blue
p-SMe-DPM	Red	Blue
m-F-DPM	Orange	Blue
m-Me-DPM	Orange	Blue
m-OMe-DPM	Orange	Blue
m-p-diMe-DPM	Orange	Blue
o-F-DPM	Orange	Blue
o-Me-DPM	Orange	Blue
o-SMe-DPM	Orange	Blue
o-OMe-DPM	Red	Blue

A.2 Geometrical Data of the Substituted DPM Isomers.

Table A.2: Optimised Structures of Para-substituted Dithizonatophenylmercury II Isomers. R = Substituents.

Bond Lengths Å								
<i>R</i> -DPM	Orange Isomer				Blue Isomer			
Method	p-F	p-Cl	p-CH ₃	p-SCH ₃	p-F	p-Cl	p-CH ₃	p-SCH ₃
Basis Set	B3LYP	B3LYP	B3LYP	B3LYP	B3LYP	B3LYP	B3LYP	B3LYP
	CEP-31G	CEP-31G	CEP-31G	CEP-31G	CEP-31G	CEP-31G	CEP-31G	CEP-31G
Hg1 – S1	2.563	2.565	2.552	2.563	2.537	2.518	2.527	2.525
Hg1 – C2	2.138	2.142	2.141	2.143	2.142	2.140	2.142	2.139
Hg1 – N1	2.831	2.767	2.752	2.760	2.838	2.910	2.832	2.898
N1 – N2	1.305	1.306	1.308	1.309	1.307	1.306	1.309	1.308
N1 – C8	1.440	1.442	1.440	1.438	1.436	1.435	1.433	1.430
N2 – C1	1.409	1.409	1.407	1.406	1.406	1.407	1.403	1.408
C1 – S1	1.847	1.845	1.851	1.850	1.849	1.851	1.851	1.854
C1 – N3	1.341	1.341	1.342	1.342	1.340	1.340	1.340	1.339
N3 – N4	1.360	1.360	1.359	1.359	1.364	1.365	1.363	1.369
N4 – C14	1.422	1.420	1.424	1.422	1.419	1.417	1.421	1.415
C11 – F1	1.416	-	-	-	1.414	-	-	-
C17 – F2	1.421	-	-	-	1.421	-	-	-
C11 – Cl 1	-	1.840	-	-	-	1.837	-	-
C17 – Cl 2	-	1.845	-	-	-	1.845	-	-
C11 – C20	-	-	1.530	-	-	-	1.529	-
C17 – C21	-	-	1.532	-	-	-	1.532	-
C11 – S2	-	-	-	1.848	-	-	-	1.844
C17 – S3	-	-	-	1.857	-	-	-	1.863
Bond Angles (°)								
Hg1 – S1 – C1	106.2	104.5	104.3	104.4	105.3	105.8	105.2	106.3
S1 – Hg1 – N1	70.6	71.8	72.3	72.0	71.8	71.2	71.8	71.5
N1 – Hg1 – C2	122.5	120.1	122.5	120.4	118.3	117.0	118.6	116.6
Hg1 – N1 – N2	119.0	119.1	119.0	119.1	117.0	115.0	116.7	115.9
N1 – N2 – C1	117.6	117.9	118.1	118.1	118.5	118.6	118.4	118.7
N2 – C1 – S1	126.3	126.4	126.2	126.2	127.1	127.5	126.7	127.5
S1 – C1 – N3	122.5	121.5	122.1	122.2	115.4	115.1	115.4	115.0
C1 – N3 – N4	118.6	118.4	118.5	118.6	119.6	119.6	119.5	119.1
C11 – S2 – C20	-	-	-	103.4	-	-	-	103.5
C17 – S3 – C21	-	-	-	103.0	-	-	-	100.5
S1–C1–N3–N4	0.1	0.5	0.2	0.4	-179.4	-178.1	-178.4	-179.8

Table A.3: Selected Optimised Structures of Meta-substituted Dithi-
zonatophenylmercury II Isomers. R = Substituents.

Bond Lengths Å								
<i>R</i> -DPM	Orange Isomer				Blue Isomer			
	m-F	m-CH ₃	m-OCH ₃	m-p-(CH ₃) ₂	m-F	m-CH ₃	m-OCH ₃	m-p-(CH ₃) ₂
Method	B3LYP	B3LYP	B3LYP	B3LYP	B3LYP	B3LYP	B3LYP	B3LYP
Basis Set	CEP-31G	CEP-31G	CEP-31G	CEP-31G	CEP-31G	CEP-31G	CEP-31G	CEP-31G
Hg1 – S1	2.546	2.575	2.557	2.547	2.531	2.527	2.513	2.514
Hg1 – C2	2.142	2.143	2.141	2.139	2.142	2.142	2.139	2.140
Hg1 – N1	2.789	2.701	2.773	2.844	2.848	2.841	2.908	2.893
N1 – N2	1.305	1.306	1.304	1.307	1.306	1.308	1.308	1.309
N1 – C8	1.441	1.444	1.443	1.439	1.436	1.436	1.436	1.433
N2 – C1	1.410	1.408	1.411	1.407	1.407	1.404	1.406	1.404
C1 – S1	1.846	1.847	1.853	1.852	1.846	1.850	1.854	1.857
C1 – N3	1.340	1.341	1.338	1.341	1.339	1.340	1.339	1.340
N3 – N4	1.360	1.357	1.358	1.359	1.364	1.363	1.364	1.364
N4 – C14	1.419	1.424	1.424	1.424	1.416	1.420	1.419	1.421
C10 – F1	1.419	-	-	-	1.418	-	-	-
C16 – F2	1.419	-	-	-	1.420	-	-	-
C10 – C20	-	1.532	-	1.532	-	1.532	-	1.532
C16 – C21	-	1.532	-	1.532	-	1.533	-	1.532
C10 – O1	-	-	1.406	-	-	-	1.405	-
C16 – O2	-	-	1.408	-	-	-	1.407	-
C11 – C22	-	-	-	1.530	-	-	-	1.529
C17 – C23	-	-	-	1.531	-	-	-	1.532
C20 – O1	-	-	1.473	-	-	-	1.473	-
C21 – O2	-	-	1.471	-	-	-	1.472	-
Bond Angles (°)								
Hg1 – S1 – C1	104.4	102.6	103.7	106.5	105.6	105.3	105.7	105.5
S1 – Hg1 – N1	71.4	72.4	71.9	70.8	71.3	71.6	71.4	71.6
N1 – Hg1 – C2	124.0	128.0	118.9	123.1	118.4	118.5	117.2	117.0
Hg1 – N1 – N2	118.0	119.3	118.0	118.4	117.0	116.7	114.8	115.0
N1 – N2 – C1	117.5	118.0	117.9	117.9	118.6	118.4	118.7	118.8
N2 – C1 – S1	126.0	125.8	126.2	126.3	126.7	126.7	127.4	127.3
S1 – C1 – N3	122.6	123.0	123.0	121.9	115.6	115.4	114.8	114.9
C1 – N3 – N4	118.3	118.8	119.5	118.7	119.7	119.5	119.8	119.4
C10 – O1 – C20	-	-	118.2	-	-	-	118.3	-
C16 – O2 – C21	-	-	118.4	-	-	-	118.2	-
S1–C1–N3–N4	2.0	1.2	0.8	0.2	-177.9	-178.1	-178.0	-178.4

Table A.4: Selected Optimised Structures of Ortho-substituted Dithi-
zonatophenylmercury II Isomers. R = Substituents.

Bond Lengths Å								
<i>R</i> -DPM	Orange Isomer				Blue Isomer			
	o-F	o-CH ₃	o-OCH ₃	o-SCH ₃	o-F	o-CH ₃	o-OCH ₃	o-SCH ₃
Method	B3LYP	B3LYP	B3LYP	B3LYP	B3LYP	B3LYP	B3LYP	B3LYP
Basis Set	CEP-31G	CEP-31G	CEP-31G	CEP-31G	CEP-31G	CEP-31G	CEP-31G	CEP-31G
Hg1 – S1	2.537	2.532	2.536	2.544	2.530	2.521	2.522	2.523
Hg1 – C2	2.136	2.138	2.138	2.138	2.145	2.142	2.143	2.141
Hg1 – N1	2.896	2.886	2.979	2.974	2.931	2.966	2.878	2.928
N1 – N2	1.307	1.308	1.306	1.306	1.308	1.310	1.307	1.310
N1 – C8	1.434	1.440	1.432	1.429	1.429	1.435	1.428	1.425
N2 – C1	1.411	1.409	1.417	1.415	1.400	1.403	1.400	1.403
C1 – S1	1.850	1.855	1.862	1.864	1.848	1.854	1.854	1.854
C1 – N3	1.342	1.342	1.338	1.337	1.345	1.342	1.345	1.341
N3 – N4	1.363	1.360	1.365	1.361	1.366	1.364	1.371	1.364
N4 – C14	1.416	1.426	1.423	1.422	1.412	1.423	1.423	1.419
C9 – F1	1.408	-	-	-	1.413	-	-	-
C15 – F2	1.413	-	-	-	1.413	-	-	-
C9 – C20	-	1.529	-	-	-	1.528	-	-
C15 – C21	-	1.531	-	-	-	1.531	-	-
C9 – O1	-	-	1.395	-	-	-	1.399	-
C15 – O2	-	-	1.416	-	-	-	1.403	-
C9 – S2	-	-	-	1.851	-	-	-	1.850
C15 – S3	-	-	-	1.862	-	-	-	1.864
C20 – O1	-	-	1.476	-	-	-	1.478	-
C21 – O2	-	-	1.484	-	-	-	1.472	-
Bond Angles (°)								
Hg1 – S1 – C1	107.7	107.2	105.4	105.2	106.0	107.1	103.0	106.8
S1 – Hg1 – N1	70.0	70.6	68.6	68.4	71.4	70.5	72.0	71.0
N1 – Hg1 – C2	122.8	122.8	121.8	118.5	118.1	120.9	116.2	118.5
Hg1 – N1 – N2	118.3	117.6	114.2	114.2	114.2	114.3	112.5	115.2
N1 – N2 – C1	117.1	117.8	116.7	117.0	119.7	119.0	119.8	118.9
N2 – C1 – S1	126.8	126.7	126.3	125.8	128.1	127.7	127.0	127.6
S1 – C1 – N3	121.8	121.6	122.0	122.5	115.4	114.6	116.5	114.8
C1 – N3 – N4	117.5	118.1	118.4	118.6	118.2	118.9	117.3	119.2
C9 – O1 – C20	-	-	118.8	-	-	-	118.5	-
C15 – O2 – C21	-	-	115.8	-	-	-	118.3	-
C9 – S2 – C20	-	-	-	102.1	-	-	-	103.1
C15 – S3 – C21	-	-	-	102.6	-	-	-	101.8
S1–C1–N3–N4	-0.2	0.1	3.5	4.1	-179.0	-178.1	-176.3	-177.9

Appendix B

Codes

The codes below were used in this study for Gaussian calculations. We submitted them to CHPC super cluster.

B.1 Geometry Optimisation and Frequency Calculation

Frequencies could be generated along the geometry Optimisation. However, we can leave it out by removing "Freq" from the job route section.

```
%chk=DPM_b3lyp-opt.chk                                     ### checkpoint file
# B3LYP/CEP-31G Opt Freq SCRF=(Solvent=Dichloromethane)   ### Job route
Dithizonatophenylmercury II Relaxed Potential Energy Surface Scan
                                                            ### A space between the route and the name of the job
O 1                                                         ### The name of the job
S                                                           ### A space between the job's name and the molecule specification
S    0.044112000    0.065417000    0.579946000           ### Charge and Multiplicity, respectively
C    1.805428000    0.031972000    0.290923000           ### Input: Cartesian Coordinates of the atoms in the molecule
N    2.493506000    1.152968000    0.123312000
N    1.627363000    2.268103000    0.178480000
...                                                         ### Continues down to the last atom

*****
#/bin/csh
###These lines are for Moab
#MSUB -l nodes=4:ppn=8
###MSUB -l partition=ALL
#MSUB -l walltime=3:00:00
#MSUB -m be
###MSUB -V
#MSUB -o /export/home/oopeyemi/scratch/PESS/DPM-b3lyp-opt.out
#MSUB -e /export/home/oopeyemi/scratch/PESS/DPM-b3lyp-opt.err
#MSUB -d /export/home/oopeyemi/scratch/PESS
#MSUB -mb
#MSUB -M olaoye@sun.ac.za

##### Running commands
source /opt/gridware/gaussian/g09/g09setup
g09 < DPM-b3lyp-pess_opt.com > DPM-b3lyp-pess_opt.log
*****
```

B.2 Singlet Excitation Calculation

Below is the time-dependent calculation codes for singlet-singlet excitation energies.

```
%chk=DPM_b3lyp-exci.chk
# B3LYP/CEP-31G TD=NStates=15 SCRF=(Solvent=Dichloromethane)

Dithizonatophenylmercury II Singlet-Singlet Excitation

O 1
S 0.044112000 0.065417000 0.579946000
C 1.805428000 0.031972000 0.290923000
N 2.493506000 1.152968000 0.123312000
N 1.827363000 2.288103000 0.178480000
...

#####
#/bin/csh
###These lines are for Moab
#MSUB -l nodes=4:ppn=8
###MSUB -l partition=ALL
#MSUB -l walltime=3:00:00
#MSUB -m be
###MSUB -V
#MSUB -o /export/home/oopeyemi/scratch/Excitation/DPM-b3lyp-exci.out
#MSUB -e /export/home/oopeyemi/scratch/Excitation/DPM-b3lyp-exci.err
#MSUB -d /export/home/oopeyemi/scratch/Excitation
#MSUB -mb
#MSUB -M oiaoye@sun.ac.za

##### Running commands
source /opt/gridware/gaussian/g09/g09setup
g09 < DPM-b3lyp-exci.com > DPM-b3lyp-exci.log
#####
```

B.3 Ground State Potential Energy Calculation

Below is the code for ground state potential energy calculation (closed shell). For open shell calculations, a stable calculation is first done on the Optimised geometry of the specified dihedral angle and this is achieved by replacing "opt=modredun" with "stable=opt" at the route section. Then, for broken symmetry, "B3LYP" is replaced by "UB3LYP", and "geom=checkpoint" and "guess=checkpoint" are added to the job route section: "checkpoint" is read from the one generated by a stable calculation and **no input is needed**.

```
%chk=DPM_b3lyp.chk                                     ### checkpoint file
#P B3LYP/CEP-31G opt=modredun scf=(conver=8)           ### Job route
Dithizonatophenylmercury II Relaxed Potential Energy Surface Scan
                                                         ### A space between the route and the name of the job
O 1                                                     ### The name of the job
S 0.044112000 0.065417000 0.579946000                ### A space between the job's name and the molecule specification
C 1.805428000 0.031972000 0.290923000                ### Charge and Multiplicity, respectively
N 2.493506000 1.152968000 0.123312000                ### Input: Cartesian Coordinates of the atoms in the molecule
N 1.827363000 2.288103000 0.178480000
...
D 1 2 3 4 0.0 S 18 10.0                                ### Continues down to the last atom
                                                         ### A space between the coordinates and the job
                                                         ### Job: Rotate the molecule through dihedral angle from 0 to 180 degrees

*****
#/bin/csh
###These lines are for Moab
#MSUB -l nodes=4:ppn=8
###MSUB -l partition=ALL
#MSUB -l walltime=3:00:00
#MSUB -m be
###MSUB -v
#MSUB -o /export/home/oopeyemi/scratch/PESS/DPM-b3lyp-pess_lt.out
#MSUB -e /export/home/oopeyemi/scratch/PESS/DPM-b3lyp-pess_lt.err
#MSUB -d /export/home/oopeyemi/scratch/PESS
#MSUB -mb
#MSUB -M olaoye@sun.ac.za

##### Running commands
source /opt/gridware/gaussian/g09/g09setup
g09 < DPM-b3lyp-pess_lt.com > DPM-b3lyp-pess_lt.log
*****
```

Appendix C

Acronyms and Interchangeable Terms

C.1 Acronyms

DPM: Dithizonatophenylmercury II

Me: Methyl

OMe: Methoxyl

SMe: Sulphur Methyl

p: para

m: meta

o: ortho

ca.: approximately

DCM: Dichloromethane

DMSO: DimethylSulfoxide

DFT: Density Functional Theory

ADF: Amsterdam Density Functional, 2010 version

G09: Gaussian, 2009 version

EDG: Electron Donating Groups

EWG: Electron Withdrawing Groups

CCDC: Cambridge Crystallographic Data Centre

C.2 Interchangeable Terms

The following terms mean the same thing in this study.

- Groups/Substituents
- Central Absorption Wavelengths/Secondary Bands
- Troughs/Minima
- First Peaks/Primary Bands
- Hypsochromic/Blue Shift

- Bathochromic/Red Shift
- Hypochromic/Decrease in Absorbance or Intensity
- Hyperchromic/Increase in Absorbance or Intensity

Appendix D

Calculated Ground State Potential Energies

D.1 Conversion of Units

The following conversion rates are taken from Chemcraft software.

1. $1 \text{ eV} \approx 23.06 \text{ kcal/mol}$ and $1 \text{ kJ/mol} \approx 2625.50 \text{ Hartrees}$
2. $27.2116 \text{ Hartrees} \approx 1 \text{ eV}$
3. $0.124 \text{ nm} \approx 1 \text{ eV}$

Table D.1: Ground State Potential Energies at Different Dihedral Angles for Formaldimine and DPM.

G09/B3LYP/6-31G(d)		G09/B3LYP/CEP-31G	
Dichloromethane			
Rigid-Formaldimine		Relaxed-DPM	
Barrier Energy: 2.32 eV		Barrier Energy: 1.20 eV	
Angles (°)	Energies (eV)	Angles (°)	Energies (eV)
0	-2574.90	0	-8711.83
10	-2574.86	10	-8711.80
20	-2574.73	20	-8711.73
30	-2574.52	30	-8711.61
40	-2574.24	40	-8711.45
50	-2573.89	50	-8711.24
60	-2573.50	60	-8710.98
70	-2573.10	70	-8710.78
80	-2572.77	80	-8710.66
90	-2572.64	90	-8710.62
100	-2572.79	105	-8710.73
110	-2573.13	110	-8710.80
120	-2573.54	120	-8710.91
130	-2573.93	130	8711.12
140	-2574.29	140	-8711.30
150	-2574.57	150	-8711.44
160	-2574.78	160	-8711.54
170	-2574.91	170	-8711.60
180	-2574.96	180	-8711.61

Table D.2: Ground State Relaxed Potential Energies at Different Dihedral Angles for the Para-substituted DPM.

G09/B3LYP/CEP-31G							
Electron-withdrawing				Electron-donating			
p-F-DPM		p-Cl-DPM		p-CH ₃ -DPM		p-SCH ₃ -DPM	
Barrier Energy: 1.21 eV		Barrier Energy: 1.38 eV		Barrier Energy: 1.20 eV		Barrier Energy: 1.18 eV	
Angles (°)	Energies (eV)						
0	-9994.30	0	-9490.43	0	-9084.60	0	-9635.01
10	-9994.27	10	-9490.40	10	-9084.57	10	-9634.99
20	-9994.20	20	-9490.33	20	-9084.50	20	-9634.92
30	-9994.09	30	-9490.22	30	-9084.39	30	-9634.80
40	-9993.92	40	-9490.05	40	-9084.22	40	-9634.64
50	-9993.70	50	-9489.83	50	-9084.00	50	-9634.42
60	-9993.75	60	-9489.58	60	-9083.76	60	-9634.17
70	-9993.25	70	-9489.30	70	-	70	-9633.99
80	-9993.13	80	-9489.14	80	-9083.44	80	-9633.87
90	-9993.09	90	-9489.05	90	-9083.40	90	-9633.83
100	-9993.14	100	-9489.08	100	-9083.45	100	-9633.88
110	-9993.26	110	-9489.25	110	-9083.57	110	-9634.00
120	-9993.36	120	-9489.49	120	-9083.68	120	-9634.10
130	-9993.58	130	-9489.71	130	-9083.89	130	-9634.31
140	-9993.76	140	-9489.89	140	-9084.07	140	-9634.49
150	-9993.89	150	-9490.02	150	-9084.21	150	-9634.63
160	-9993.99	160	-9490.12	160	-9084.31	160	-9634.73
170	-9994.05	170	-9490.18	170	-9084.37	170	-9634.78
180	-9994.07	180	-9490.20	180	-9084.39	180	-9634.80

Table D.3: Ground State Relaxed Potential Energies at Different Dihedral Angles for the Meta-substituted DPM.

G09/B3LYP/CEP-31G							
Electron-withdrawing		Electron-donating					
m-F-DPM		m-OCH ₃ -DPM		m-CH ₃ -DPM		m-p-(CH ₃) ₂ -DPM	
Barrier Energy: 1.28 eV		Barrier Energy: 1.23 eV		Barrier Energy: 1.21 eV		Barrier Energy: 1.19 eV	
Angles (°)	Energies (eV)	Angles (°)	Energies (eV)	Angles (°)	Energies (eV)	Angles (°)	Energies (eV)
0	-9994.31	0	-9951.80	0	-9084.61	0	-9457.33
10	-9994.29	10	-9951.77	10	-9084.58	10	-9457.31
20	-9994.22	20	-9951.70	20	-9084.52	20	-9457.24
30	-9994.10	30	-9951.59	30	-9084.40	30	-9457.12
40	-9993.93	40	-9951.42	40	-9084.23	40	-9456.96
50	-9993.68	50	-9951.21	50	-9084.02	50	-9456.75
60	-9993.47	60	-9950.96	60	-9083.77	60	-9456.49
70	-9993.26	70	-9950.76	70	-9083.57	70	-9456.21
80	-9993.14	80	-9950.63	80	-9083.45	80	-9456.17
90	-9993.03	90	-9950.57	90	-9083.40	90	-9456.14
100	-	100	-9950.64	100	-9083.45	100	-9456.18
110	-9993.27	110	-9950.75	110	-9083.58	110	-
120	-9993.38	120	-9950.85	120	-9083.69	120	-9456.42
130	-9993.60	130	-9951.06	130	-9083.90	130	-9456.63
140	-9993.78	140	-9951.24	140	-9084.08	140	-9456.81
150	-9993.92	150	-9951.38	150	-9084.22	150	-9456.95
160	-9994.02	160	-9951.47	160	-9084.32	160	-9457.05
170	-9994.07	170	-9951.53	170	-9084.38	170	-9457.11
180	-9994.09	180	-9951.55	180	-9084.40	180	-9457.13

Table D.4: Ground State Relaxed Potential Energies at Different Dihedral Angles for the Ortho-substituted DPM.

G09/B3LYP/CEP-31G							
Electron-withdrawing		Electron-donating					
o-F-DPM		o-CH ₃ -DPM		o-OCH ₃ -DPM		o-SCH ₃ -DPM	
Barrier Energy: 1.21 eV		Barrier Energy: 1.24 eV		Barrier Energy: 1.29 eV		Barrier Energy: -	
Angles (°)	Energies (eV)						
0	-9993.65	0	-9084.33	0	-9951.09	0	-9634.53
10	-9993.63	10	-9084.31	10	-9951.07	10	-9634.50
20	-9993.56	20	-9084.24	20	-9951.00	20	-9634.43
30	-9993.44	30	-9084.12	30	-9950.89	30	-9634.31
40	-9993.27	40	-9083.96	40	-9950.73	40	-9634.15
50	-9993.05	50	-9083.75	50	-9950.52	50	-9633.93
60	-9992.80	60	-9083.50	60	-9950.26	60	-9633.68
70	-9992.58	70	-9083.22	70	-9949.98	70	-9633.39
80	-9992.46	80	-9083.14	80	-9949.86	80	-
90	-9992.44	90	-9083.09	90	-9949.80	90	-
100	-9992.52	100	-9083.13	100	-9949.88	100	-9633.36
110	-9992.60	110	-9083.17	110	-9949.98	110	-9633.48
120	-9992.86	120	-9083.39	120	-9950.25	120	-9633.74
130	-9993.08	130	-9083.62	130	-9950.48	130	-9633.97
140	-9993.27	140	-9083.80	140	-9950.67	140	-9634.15
150	-9993.42	150	-9083.94	150	-9950.83	150	-9634.30
160	-9993.52	160	-9084.05	160	-9950.94	160	-9634.40
170	-9993.59	170	-9084.11	170	-9951.01	170	-9634.46
180	-9993.61	180	-9084.13	180	-9951.03	180	-9634.48

List of References

- [1] P. Kukura, D. W. McCamant, S. Yoon, D. B. Wandschneider and R. A. Mathies. *Structural Observation of the Primary Isomerisation in Vision with Femtosecond-Stimulated Raman*. *Science*, **310**, 1006–1009, 2005.
- [2] K. G. von Eschwege, J. Conradie and J. C. Swarts. *A DFT Perspective on the Structures and Electronic Spectra of the Orange and Blue Isomers of Photochromic Dithizonatophenylmercury(II)*. *J. Phys. Chem.*, **112**, 2211–2218, 2008.
- [3] M. Klessinger and J. Michl. *Excited States and Photochemistry of Organic Molecules*. VCH Publishers, 1995.
- [4] C. Jiang, R. Xie, F. Li and R. Allen. *Tran-to-cis Isomerisation of Stilbene Following an Ultrafast Laser Pulse*. *Chemical Physics Letters*, **474**, 263–267, 2009.
- [5] J. Wachtveitl, T. Nggele, B. Ike11, W. Ninth, M. Kruger, S. Rudolph-Btihner, D. Oesterhelt and L. Moroder. *Ultrafast Photoisomerization of Azobenzene Compounds*. *Journal of Photochemistry and Photobiology A: Chemistry*, **105**, 283–288, 1997.
- [6] M. A. Ratner and G. C. Schatz. *Introduction to Quantum Mechanics in Chemistry*. Prentice-Hall Inc., 2001.
- [7] H. Haken and H.C. Wolf. *Molecular Physics and Elements of Quantum Chemistry – Introduction to Experiments and Theory*. Second Edition, Springer, 2004.
- [8] O. O. Olaoye. *Evolution of Wave Packets in a Harmonic Potential*. Postgraduate Diploma Essay in Mathematical Sciences, African Insitute for Mathematical Sciences, 2010.
- [9] H. Schwoerer, R. Pausch, M. Heid, V. Engel and W. Kiefer. *Femtosecond time-resolved two photon ionization spectroscopy of K₂*. *Chemical Physics*, 9749–9754, 1997.
- [10] O. Kenji. *Wave-Packet and Coherent Dynamics*. *Annual Review of Physical Chemistry*, **60**, 487–511, 2009.
- [11] T. Buyana. *Molecular Physics*. World Scientific Publishing Co. Pte. Ltd., 170–171, 1997.
- [12] G. te Velde, F.M. Bickelhaupt, S.J.A. van Gisbergen, C. Fonseca Guerra, E.J. Baerends, J.G. Snijders and T. Ziegler. *Chemistry with ADF*. *Journal of Computational Chemistry*, **22**, 931, 2001.
- [13] C. Fonseca Guerra, J.G. Snijders, G. te Velde and E.J. Baerends. *Towards an order-N DFT method*. *Theoretical Chemistry Accounts*, **99**, 391, 1998.
- [14] ADF2010, SCM, Theoretical Chemistry, Vrije Universiteit, Amsterdam, The Netherlands, <http://www.scm.com>

- [15] M. J. Frisch, G. W. Trucks, H. B. Schlegel, G. E. Scuseria, M. A. Robb, J. R. Cheeseman, G. Scalmani, V. Barone, B. Mennucci, G. A. Petersson, H. Nakatsuji, M. Caricato, X. Li, H. P. Hratchian, A. F. Izmaylov, J. Bloino, G. Zheng, J. L. Sonnenberg, M. Hada, M. Ehara, K. Toyota, R. Fukuda, J. Hasegawa, M. Ishida, T. Nakajima, Y. Honda, O. Kitao, H. Nakai, T. Vreven, J. A. Montgomery, Jr., J. E. Peralta, F. Ogliaro, M. Bearpark, J. J. Heyd, E. Brothers, K. N. Kudin, V. N. Staroverov, R. Kobayashi, J. Normand, K. Raghavachari, A. Rendell, J. C. Burant, S. S. Iyengar, J. Tomasi, M. Cossi, N. Rega, J. M. Millam, M. Klene, J. E. Knox, J. B. Cross, V. Bakken, C. Adamo, J. Jaramillo, R. Gomperts, R. E. Stratmann, O. Yazyev, A. J. Austin, R. Cammi, C. Pomelli, J. W. Ochterski, R. L. Martin, K. Morokuma, V. G. Zakrzewski, G. A. Voth, P. Salvador, J. J. Dannenberg, S. Dapprich, A. D. Daniels, O. Farkas, J. B. Foresman, J. V. Ortiz, J. Cioslowski, and D. J. Fox. *Gaussian 09, Revision A.02*, Gaussian, Inc., Wallingford CT, 2009.
- [16] V. Bonačić-Koutecký and J. Michl. *Photochemical syn-anti isomerisation of a Schiff base: A two-dimensional description of a conical intersection in formaldehyde*. *Theoretical Chimica*, **68**, 40–45, 1985.
- [17] H. Hirai and O. Sugino. *A time-dependent density-functional approach to nonadiabatic electron-nucleus dynamics: formulation and photochemical application*. *Phy. Chem. Chem. Phys.*, **11**, 4570–4578, 2009.
- [18] W. Koch and M. C. Holthausen. *A Chemist's Guide to Density Functional Theory*. Wiley-VCH Verlag GmbH, 2001.
- [19] A. H. Zewail. *Femtochemistry: Atomic-Scale Dynamics of the Chemical Bond Using Ultrafast Lasers*. Nobel Foundation, Stockholm, 1–17, 2000.
- [20] R. G. Parr and W. Yang. *Density Functional Theory of Atoms and Molecules*. Oxford University Press, 1989.
- [21] D. Joubert. *African School on Electronic Structure Methods and Applications: Density Functional Theory Basics*. Proceedings, July, 2010.
- [22] P. W. Atkins and R. S. Friedman. *Molecular Quantum Mechanics*. Oxford University Press Inc., New York, 1997.
- [23] R. O. Jones. *Introduction to Density Functional Theory and Exchange-Correlation Energy Functionals*. *Computational Nanoscience*, **31**, 45–70, 2006.
- [24] D. R. Hartree. *Mathematical Proceedings of the Cambridge Philosophical Society*. **24**, 89–110, 1928.
- [25] P. Hohenberg and W. Kohn. *Inhomogeneous Electron Gas*. *Physical Review*, **136**, 3B, B865–B871, 1964.
- [26] J. C. Slater. *A Simplification of the Hartree-Fock Method*. *Physical Review*, **81**, 385–390, 1951.
- [27] W. Kohn and L. J. Sham. *Self Consistent Equations Including Exchange and Correlation Effects*. *Physical Review*, **140**, 4A, A1133–A1138, 1965.
- [28] F. Schautz, F. Buda and C. Filippi. *Excitations in photoactive molecules from quantum Monte Carlo*. *arXiv:cond-mat/040450*, **1**, 1–9, 2008.
- [29] C. C. Roothaan. *Restricted Open Hartree-Fock Method*. *Rev. Mod. Phys.*, **32**, 179, 1960.

- [30] C. Molteni, I. Frank and M. Parrinello. *An Excited State Density Functional Theory Study of the Rhodopsin Chromophore*. J. Am. Chem. Soc., **121**, 12177–12183, 1999.
- [31] T. Ziegler, A. Rauk and E. J. Baerends. *On the Calculation of Multiplet Energies by the Hatree-Fock-Slater Method* Theor. Chim. Acta, **43**, 261–271, 1977.
- [32] M. Schulte and I. Frank. *Restricted open-shell Kohn-Sham theory: N unpaired electrons*. Chemical Physics, **373**, 283–288, 2010.
- [33] E. Runge and E. K. U. Gross. *Density-Functional Theory for Time-Dependent Systems*. Physical Review Letters, **52**, 12, 997–1000, 1984.
- [34] L. S. Meriwether, E. C. Breitner and C. L. Sloan. *The Photochromism of Metal Dithizonates* J. Am. Chem. Soc., **87**, 4441–4448, 1965.
- [35] M. Jerry. *Advanced Organic Chemistry reactions, mechanisms and structure*. New York : John Wiley & Sons, Inc., (3rd ed.), 1985.
- [36] H. M. N. H. Irving, G. Andrew and E. J. Risdon. J. Chem. Soc., 541, 1949.
- [37] J. F. Reith and K. W. Gerritsma. Recl. Trav. Chim., Pays-Bas, **64**, 41, 1945.
- [38] W. Yang. *Direct Calculation of Electron Density in Density-Functional Theory*. Physical Review Letter, **66**, 11, 1438–1441 1991.
- [39] E. V. Lenthe and E. J. Baerends. *Optimized Slater-Type Basis Sets for the Elements 1–118*. Wiley Periodicals, Inc., J. Comput. Chem., **24**, 1142–1156, 2003.
- [40] C. C. J. Roothaan. *New Development in Molecular Orbital Theory*. Review of Modern Physics, **2**, 2, 75–78, 1951.
- [41] R. Ditchfield, W. J. Hehre and J. A. Pople. J. Chem. Phys., **54**, 724, 1971.
- [42] V. A. Rassolov, M. A. Ratner, J. A. Pople, P. C. Redfern and L. A. Curtiss. J. Comp. Chem., **22**, 976, 2001.
- [43] W. Stevens, H. Basch and J. Krauss. J. Chem. Phys., **81**, 6026, 1984.
- [44] W. J. Stevens, M. Krauss, H. Basch and P. G. Jasien. Can. J. Chem., **70**, 612, 1992.
- [45] T. R. Cundari and W. J. Stevens. J. Chem. Phys., **98**, 5555 1993.
- [46] R. Sumathi. *Dissociation and isomerization reactions of formalimine on the ground and excited state surface*. Journal of Molecular Structure (Theochem), **364**, 97–106, 1996.
- [47] W. J. Hehre. *A Guide to Molecular Mechanisms and Quantum Chemical Calculations*. Wavefunction Inc.: Irvine, CA, **181**, 153, 2003.
- [48] A. T. Hutton, H. M. N. H. Irving and L. R. Nassimbeni. Acta Crystallogr., B36, 2064, 1980.
- [49] N. L. Doltsinis. *Time-Dependent Density Functional Theory*. Computational Nanoscience, **31**, 357–373, 2006.
- [50] S. C. Althorpe and G. A. Worth. *Quantum Dynamics at Conical Intersections*. Collaborative Computational Project on Molecular Quantum Dynamics (CCP6), Daresbury Laboratory, Daresbury, Warrington, WA4 A4D, United Kingdom, 2004.

- [51] S. Kumar. Spectroscopy of Organic Compounds. Department of Chemistry, Guru Nanak Dev University, Amritsar-143005, 2006.
- [52] J. L. Dela Cruz and G. J. Blanchard. The Influence of Chromophore Structure on Intermolecular Interactions. A Study of Selected Rhodamines in Polar Protic and Aprotic Solvents. *J. Phys. Chem. A*, **106**, 10718–10724, 2002.
- [53] F. F. Jian, P. S. Zhao and H. B. Ma. *Theoretical and Experimental Studies on a Metal-organic Complex of (Isopropylxanthato)(Phenyl)Mercury(I) [Hg(I)(C₆H₅)(C₄H₇OS₂)].* Structural Chemistry, **16**, No. 5, 469–474, 2005.
- [54] K. G. von Eschwege and A. Kuhn. *Low-temperature redetermination of 1,3-bis(pentafluorophenyl)triazene.* Acta Cryst., **E66**, o3177, 2010.
- [55] B. E. Smart. *Fluorine substituent effects (on bioactivity).* Journal of Fluorine Chemistry, **109**, 3–11, 2001.
- [56] C. Hansch, A. Leo and R. W. Taft. *A Survey of Hammett Substituent Constants and Resonance and Field Parameters.* Chem. Rev., **97**, 165–195, 1991.
- [57] I. Fernandez and G. Frenking. *Correlation between Hammett Substituent Constants and Directly Calculated π -Conjugation Strength.* J. Org. Chem, **71**, 6, 2251–2256, 2006.
- [58] M. A. Fox and R. C. Owen. *The Possibility of π -Electron Donation by the Electron-Withdrawing Substituents CN, CHO, CF₃ and ⁺NH₃.* J. Am. Chem. Soc., **102**, 6561–6563, 1980.
- [59] E. Botha. Quantum computational, structural and electrochemical properties of substituted dithizones and photochromic dithizonato phenylmercury complexes. Master's Dissertation, University of Free States, 2011.
- [60] A. Nenov, P. Kölle, M. A. Robb, and R. de Vivie-Riedle. *Beyond the van der Lugt/Oosterhoff Model: When the Conical Intersection Seam and the S₁ Minimum Energy Path Do Not Cross.* J. Org. Chem., **75**, 123–129, 2010.
- [61] H. Schwoerer, K. G. von Eschwege, G. Bosman, P. Krok, J. Conradie. *Ultrafast Photochemistry of Dithizonatophenylmercury (II).* ChemPhysChem, **12**, 2653–2658, 2011.